1-1-2005

Kinetics and morphology of electric field-induced patterning in thin polymer films.

Kathryn Amanda Leach
University of Massachusetts Amherst

KINETICS AND MORPHOLOGY OF ELECTRIC FIELD-INDUCED PATTERNING IN THIN POLYMER FILMS

A Dissertation Presented

by

KATHRYN AMANDA LEACH

Submitted to the Graduate School of the
University of Massachusetts in partial fulfillment of the
degree requirements for the degree of

DOCTOR OF PHILOSOPHY

September 2005

Polymer Science and Engineering

KINETICS AND MORPHOLOGY OF ELECTRIC
FIELD-INDUCED PATTERNING IN THIN POLYMER FILMS

A Dissertation Presented

by

KATHRYN AMANDA LEACH

Approved as to style and content by:

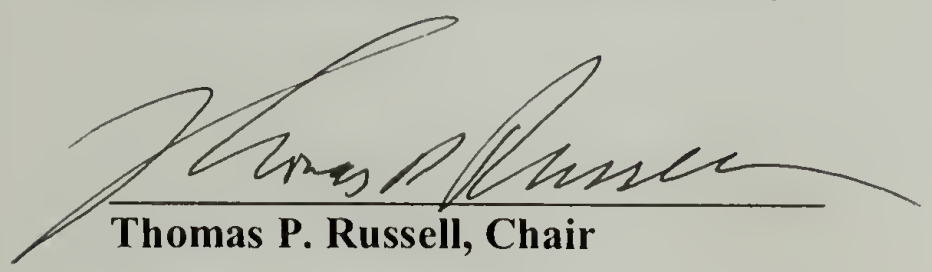

Thomas P. Russell, Chair

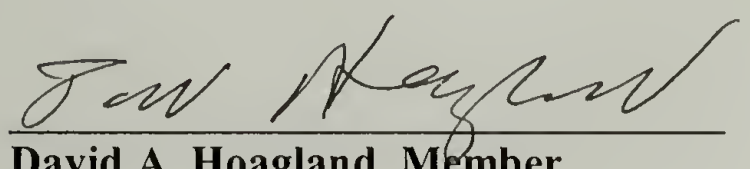

David A. Hoagland, Member

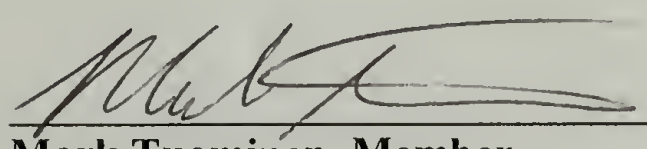

Mark Tuominen, Member

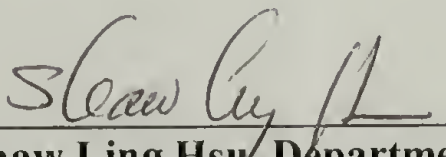

Shaw Ling Hsu, Department Head
Polymer Science and Engineering

To my Parents

ACKNOWLEDGEMENTS

For enabling this project, thanks go to Prof. Tom Russell, to whom I will always be indebted for his patient and insightful advisorship. Tom has an inspiring passion for science and dedication to the scientific enterprise, and it has been an honor to work in his group. Thanks are also deserved by the other members of my thesis committee, Prof. David Hoagland and Prof. Mark Tuominen. Their many contributions to the educational experience of writing and defending my proposal, prospectus, and dissertation were very valuable to my growth as a science researcher. I sincerely appreciate their helpful advice and comments.

This work would not have been possible without the contributions of several talented graduate students with whom I collaborated. Zhiqun Lin was a generous resource during the beginning of my work, initiated the use of PDMS for *in situ* studies, and continued to offer his valuable help and advice during the course of the research. Suresh Gupta at UMass Amherst and Michael Dickey at UT Austin provided another component of helpful experimental work and insights for the experiments on electric field induced dewetting and thiol-ene photocurable materials. Particularly, Michael took all of the SEM images shown in Chapter 4, without which the results would have been very difficult to interpret. It has been a delightful experience to work with Zhiqun, Suresh, and Michael, whom I will always respect and value as scientists and friends.

I am thankful for all of the Russell Group members, past and present, who taught me about polymer science, international relations, and camaraderie. In particular, Irene Tsai and Ting Xu, my classmates in joining the PSE department and the Russell Group, have been supportive and caring, and I treasure my friendships with them. I am also

extremely grateful for vital encouragement from Kris Lavery and Matt Misner during the final year of my graduate school life. Matt has shown unfailing dedication in his support for my aspirations but also provided many necessary reality-checks along the way to the completion of my work.

My development as a researcher has benefited greatly from the guidance and assistance of professors, visiting researchers and postdocs in the Polymer Science and Engineering Department, including Tobias Kerle, Kevin Cavicchi, Duyeol Ryu, Kyusoon Shin, and Amiya Tripathy. I'm especially grateful for the advice of Prof. Shenda Baker to apply to the Polymer Science and Engineering program, and for her mentorship and support during my graduate career. Specific words of advice from Hocheol Kim, Masahiro Kimura, Linda Molnar, Prof. Dave Hoagland and Prof. Bryan Coughlin were extremely important in encouraging me to persevere in my academic pursuits. I also enjoyed participating in the work of Dr. Greg Dabkowski in outreach programs to schools and the Research Experience for Undergraduates program.

I would never have been able to reach this level of achievement without the love of my family, which has given me support and encouragement in all aspects of my life. They inspire me to always strive to do the most I am capable of and to take pride in my work. Their care and love for me is my source of strength and personal conviction.

ABSTRACT

KINETICS AND MORPHOLOGY OF ELECTRIC

FIELD-INDUCED PATTERNING IN THIN POLYMER FILMS

SEPTEMBER 2005

KATHRYN AMANDA LEACH, B.S. HARVEY MUDD COLLEGE

M.S., UNIVERSITY OF MASSACHUSETTS AMHERST

Ph.D., UNIVERSITY OF MASSACHUSETTS AMHERST

Directed by: Professor Thomas P. Russell

Electrohydrodynamic instabilities in thin liquid polymer films are generated when electrostatic pressure overcomes surface tension, leading to amplification of fluctuations at the polymer surface. The growth kinetics of these fluctuations are, in principle, similar to the growth in size of domains during phase separation of polymer mixtures. Consequently, an exponential dependence of fluctuation height on time, characterized by a time constant, can be predicted from the strength of the electric field and the characteristics of the polymer. Results for in situ measurements of fluctuation growth in polydimethylsiloxane show good agreement with theory at early stages and divergence from theory at later stages. At the early stages, the measured time constants shoe quantitative agreement with theory, using no adjustable parameters. Furthermore, a significant reduction in the rate of amplification was observed when a low-viscosity thiol-

ene mixture was used. To preserve the fluctuations and patterned structures, the low molecular weight liquid could be polymerized using ultraviolet light.

In situ observation of the growth and decay of electrohydrodynamic instabilities in varying electric fields showed that, since the time scales are predictable, they can be manipulated by varying the electric field. When the electric field was cycled between low and high, growth and decay of fluctuations in the varying electric fields was observed.

Electric fields were also used to generate patterns in polymer/polymer/air trilayers with a PS film sandwiched between a silicon substrate and a layer of PMMA. The degree to which the viscosity of the polymer film at the substrate is smaller than that of the upper layer has a strong effect on the morphology of structure formation. Several unique three-dimensional microstructures are made possible by tuning electric-field induced fluctuations in concert with dewetting. The kinetics of structure formation were enhanced by this configuration resulting in much faster patterning than achieved in prior studies.

External electric fields were also used to amplify fluctuations in bilayers with block copolymers added to reduce interfacial tension. A significant reduction in characteristic length scale for the instabilities was observed. This process shows promise for application to nanometer-scale lithography.

TABLE OF CONTENTS

LIST OF TABLES

LIST OF FIGURES

Figure

CHAPTER 1

BACKGROUND

1.1 Previous Work

The effect of an applied electric field on thin polymer films is an area of active research[1-13]. In most thin film applications, minimization of instabilities is necessary to maintain the long term integrity of the film. However, several recent studies suggest that understanding and controlling instabilities due to an applied electric field may have significant technological value[1-6,8,9]. The behavior of electrohydrodynamic instabilities in small molecule liquids has long been observed and studied with great interest [14]. However, studies undertaken regarding this phenomenon in polymer liquids have only emerged relatively recently.

Several important theoretical developments and experimental systems have generated interest in the application of electrohydrodynamic instabilities to patterning in thin polymer films. First, Schäffer et al. used an electric field applied perpendicular to a polymer/air interface to generate electrostatic pressure from the gradient in dielectric constant between air and the polymer. The polymer film was coated onto a silicon wafer which was then mounted parallel to another silicon wafer, leaving a small air gap between the film and the uncoated wafer. A DC voltage was applied between the two silicon wafers at a temperature above the glass transition temperature of the polymer, causing the film to break up into an array of polymer pillars which were regular in size and spacing. That work showed that changing the magnitude of the applied electric field offered a simple way to control the length scale of the structures formed in the polymer film.

That length scale could be predicted using an electric field-induced instability model in which perturbations in the film were modeled as sine waves of very small amplitude and a wide range of wavelengths. The amplification and supression of such surface waves was shown to be governed by the balance between the electrostatic pressure and the Laplace pressure at the polymer/air interface. According to this principle, when electrostatic pressure overcomes surface tension, fluctuations having wavelengths longer than a critical wavelength are amplified. Eventually, the peaks of the fluctuations contact the opposite electrode. Columns of polymer are formed, with a characteristic center-to-center distance corresponding to the wavelength of the fastest growing fluctuation. This process is shown schematically in Figure 1.1. Under a patterned electrode, the polymer film may replicate either the topographic patterning or chemical patterning of the electrodes down to a length scale of ~140 nm.

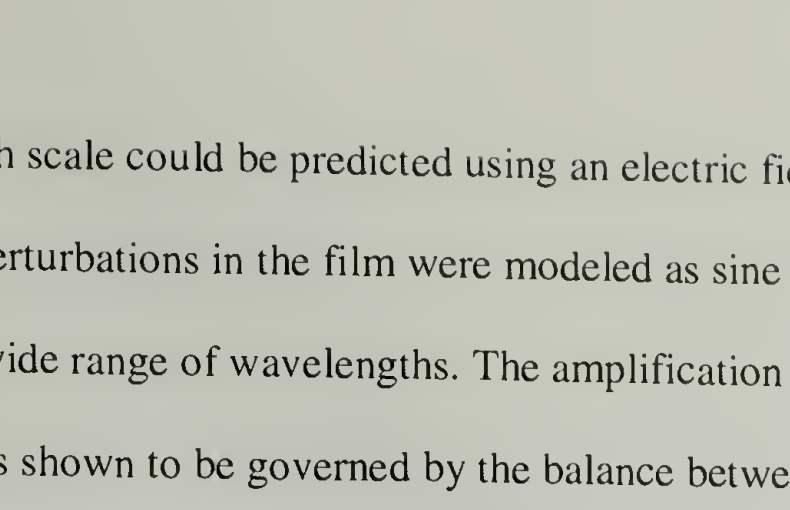

Figure 1.1. Schematic showing the growth of fluctuations in a thin polymer film between two electrodes.

Using linearized instability analysis, Lin et al.[4,5] extended the model of Schäffer et al.[1,2] to the polymer-polymer bilayer case and conducted experiments on this case. They showed that by filling the air gap with another liquid, the interfacial tension was decreased, and the characteristic spacing decreased, in reasonable agreement with calculations using the extended theory. Further experiments demonstrated that the

extended theory captured the important experimental parameters so well that the bilayer and single layer data could be collapsed onto a single master curve using reduced variables[5]. The agreement between the experimentally measured size scale and those predicted analytically was quite good.

Besides achieving agreement between theory and experiment, the work discussed above suggested great promise for use in new patterning technologies. These may be, on one hand, free from the acids and solvents required for photolithography, and on the other hand, extended to nanometer length scales which are difficult to reach even by state-of-the-art photolithographic methods. For example, in more complex polymeric systems, such as diblock copolymers, a hierarchy of length scales is possible, which span the micrometer and nanometer regimes[13]. Further investigation of the nature of electrohydrodynamic instabilities is necessary to realize the potential technological benefits as well as to answer additional fundamental questions.

1.2 Overview of This Work

The fundamental areas which are addressed in this thesis include the kinetics of structure formation by electrohydrodynamic instabilities, the reduction of size scales by minimization of surface or interfacial tension, the morphology of the instabilities during their formation, and the interplay between dewetting and electric field-induced dewetting.

Until now, studies had not been designed to observe the exponential growth rates of electrohydrodynamic instabilities which are predicted in the theoretical models. A detailed study of kinetics at the early stages of structure formation using in situ imaging techniques will be discussed in Chapter 2.

An outcome of the bilayer experiments of Lin, et al., was the suggestion that, by reducing interfacial tension, the size scale of electric field-induced fluctuations could be reduced further. Block copolymers are well-known as compatiblizers in many polymer blends, due to the fact that they generally segregate to the interfaces of immiscible blends and reduce the interfacial free energy by mediating interactions. The use of block copolymers to modify the energies of polymer surfaces and interfaces will be shown for one bilayer system, polystyrene and polydimethylsiloxane. The effect of the reduction of interfacial tension on electrohydrodynamic instabilities will be discussed.

The influence of substrate-polymer dewetting on electric-field induced polymer-polymer dewetting is also treated. It has been shown that concentric structures can be generated in a polymer bilayer with an air gap, though these structures take above one week annealing times to grow and span between the electrodes[5,6]. This thesis will demonstrate what other microstructures that can be generated and whether altering substrate-polymer interactions can change the time scales for pattern formation.

In Chapter 5, electric field-induced patterning is applied to a low-molecular weight photocurable material which has a low viscosity, but can be cured to a crosslinked solid polymer within seconds of UV irradiation. The same photocurable system has been used for another non-photolithographic patterning method, imprint lithography, which has shown great promise for commercial application. Some unique features of the photocuring process and the advantages of using electric fields over imprint lithography are shown.

In Chapter 6, variation of the applied voltage is used to control on the amplification and decay of electric field-induced fluctuations in polydimethylsiloxane.

By periodically increasing and decreasing the applied voltage, the rates of electric field-driven growth and surface tension-driven decay can be manipulated for many cycles. This effect could have future applications in microfluidics as a pumping or mixing mechanism.

Suggestions for future work related to and extending from the topics of this thesis suggested in the final chapter. There are still many possibilities for investigating the fundamentals of electrohydrodynamic instabilities and even more for the creative application of electric field induced patterning to new materials and new electrode configurations.

1.3 References

1. Schäffer, E.; Thurn-Albrecht, T.; Russell, T. P.; Steiner, U. *Nature* **2000**, *403*, 874-877.

2. Schäffer, E.; Thurn-Albrecht, T.; Russell, T. P.; Steiner, U *Europhys. Lett.* **2001**, *53*, 518-524.

3. Lin, Z.; Kerle, T.; Baker, S. M.; Hoagland, D. A.; Schäffer, E.; Steiner, U. Russell, T. P. *J. Chem. Phys.* **2001**, *114*, 2377-2381.

4. Lin, Z.; Kerle, T.; Russell, T. P.; Schäffer, E.; Steiner, U. *Macromolecules* **2002**, *35*, 3971-3976.

5. Lin Z.; Kerle, T.; Russell, T. P. Schäffer, E.; Steiner, U. *Macromolecules* **2002**, *35*, 6255-6262.

6. Morariu, M. D.; Voicu, N. E.; Schäffer, E.; Lin, Z.; Russell, T. P.; Steiner, U. *Nature Materials* **2003**, *2*, 48-52.

7. Herminghaus, S. *Phys. Rev. Lett.* **1999**, *83*, 2359-2361.

8. Pease, L. F., III; Russell, W. B. *J. Non-Newtonian Fluid Mech.* **2002**, *102*, 233-250.

9. Pease, L. F., III; Russell, W. B. *Langmuir* **2004,** *20*, 795.

10. Morkved, T. L; Lu, M.; Urbas, A. M. ; Ehrichs, E. E. ; Jaeger, H. M. ; Mansky, P. ; Russell, T. P. *Science* **1996**, *273*, 931.

11. Thurn-Albrecht T.; DeRouchey, J.; Russell, T.P.; Jaeger, H.M. *Macromolecules* **2000** *33*, 3250-3253.

12. Xu, T.; Zvelindovsky, A. V.; Sevink, G. J. A.; Gang, O.; Ocko, B.; Zhu, Y.; Gido, S.

P.; Russell, T. P. *Macromolecules* **2004**, *37*, 6980-6984.

13. Xiang, H.Q.; Lin, Z.; Russell, T. P.; Macromolecules **2004**, *37*, 5358-5363.

14. Swan, J. W. *Proc. R. Soc. London* **1897**, *62*, 38-46

15. Lin, Zhiqun. University of Massachusetts Amherst, Amherst, MA. Unpublished Work, 2001.

16. Wu, S. Polymer Interface and Adhesion. (Marcel Dekker, 1982)

17. Oddershede, L.; Nagel, S. *Phys. Rev. Lett.* **2000**, *85*, 6.

18. Anastasiadis, S. H.; Gancarz, R.; Koberstein, J. T. ; *Macromolecules* **1989**, *22*, 1449.

19. Shull, K.; Kramer, E. *Macromolecules* **1990**, *23*, 4769-4779 and Shull, K.; Kramer, E.; Hadziioannou, G.; Tang, W. *Macromolecules* **1990**, *23*, 4780-4787.

20. Retsos, H. ; Margiolaki, I. ; Messaritaki, A.; Anastasiadis, S. H. *Macromolecules* **2001**, *34*, 5295-5305.

21. Mönch, W.; Herminghaus, S. *Europhys. Lett.* **2001**, *53*, 525-531.

22. Mowery, C. L.; Crosby, A. J.; Ahn, D.; Shull, K. R. *Langmuir* **1997**, *13*, 6101-6107.

23. Flanigan, C. M.; Shull, K. R. *Langmuir* **1999**, *15*, 4966-4974.

24. Saville, D. A. *Annu. Rev. Fluid Mech.* **1997**, *29*, 27-64.

CHAPTER 2

EARLY STAGES IN THE GROWTH OF ELECTRIC FIELD-INDUCED SURFACE FLUCTUATIONS

2.1. Introduction

The stability of thin polymer films and the control of structure and morphology in thin films are essential for the practical use of polymers in many applications. The static and dynamic aspects of thin film instabilities arising from polymer/substrate and polymer/air interactions, that result in characteristic dewetting patterns, have been thoroughly studied.[1-9] The influence of external electrostatic forces on the stability of a polymer surface has also been studied in detail, both experimentally and theoretically. The use of electrostatic pressure to destabilize polymer surfaces underpins electrospinning technology, by which submicron diameter polymer fibers can be readily produced. Studies have also appeared on the dynamics of the deformation of a polymer surface by an electric field, when free charges are present at the surface[10-15]. Such experiments are challenging, not only because of the high voltages required, but also because of the small length scales and extremely short time scales involved.

The effect of an applied electric field on thin polymer films, in the absence of free charges, is an area of active research. Schäffer et al. described electrohydrodynamic instabilities in polystyrene (PS), poly(methyl methacrylate) (PMMA), and poly(1-bromostyrene) (PSBr) films between parallel electrodes such that an air gap is left between the polymer film and opposite electrode.[16,17] Their results showed that changing the magnitude of the electric field offers a simple way to control the length scale of structures formed by a balance between the electrostatic pressure and the Laplace

pressure at the polymer/air interface. When electrostatic pressure overcomes surface tension, fluctuations of a range of wavelengths are amplified. The fastest growing fluctuation dominates the film and eventually the liquid spans between the electrodes, forming columns of polymer with a characteristic center-to-center distance corresponding to the wavelength of that fluctuation. Under a patterned electrode, the polymer film will replicate either the topographic patterning or chemical patterning of the electrodes down to a length scale of ~140 nm.

Chou and Zhuang developed a process, termed lithographically induced self assembly (LISA), where similar arrays of columns in PMMA films mounted between silicon wafers with an air gap can be produced.[18,19] Although no external field was applied, a qualitative dependence of column diameter and period on molecular weight was reported. Using this process, arrays of columns were produced under topographically patterned surfaces having triangular, rectangular, and square features. The quality of the lateral ordering of the columns depended on the commensurability of the characteristic spacing of the columns with the lateral pattern dimension. They suggested that image charges in the mask gave rise to a local electric field that caused structure formation. Subsequently, Deshpande, et al.[20] made *in situ* optical observations of LISA which showed that the initial formation of columns occurs at the corners of the pattern, then along the edges, and, finally, moving to the interior of the pattern.

Lin et al.[21] extended the model of Schaffer et al.[16,17] to the polymer-polymer bilayer case and conducted experiments with bilayer systems of oligomeric dimethyl siloxane (ODMS), poly(isoprene) (PI), and oligomeric styrene (OS). They showed that by filling the air gap with another liquid, the interfacial tension decreased, and the

characteristic spacing decreased in reasonable agreement with the decrease predicted from calculations using the extended theory. Further experiments demonstrated that the extended theory captured the important experimental parameters so well that the bilayer and single layer data could be reduced to a single master curve with dimensionless variables.[22] The agreement between the experimentally measured size scale and those predicted analytically was excellent. However, they could not explain the observed 50-fold decrease in time required to form columns. Pease and Russel[23] later compared experimental data available from Lin et al.[21,22], Schaffer et al.[16], and Chou et al.[18] for both single layer and bilayer systems and found that, in all but one case, the characteristic times predicted by theoretical models was much shorter than the reported experimental time.

Structure formation at a polymer-air interface in an electric field is analogous to phase separation in polymer blends. In the latter system, phase domains develop over time with a periodicity equal to the dominant wavelength of concentration fluctuations in the system. The wavelength of these fluctuations is dictated by a balance between thermodynamics and kinetics. Thermodynamics, which is governed by the interfacial energy resulting from the formation of phases, favors the growth of large domains, while diffusion kinetics favors the growth of smaller phases. The kinetics of phase separation in polymer blends, i.e. the rate at which fluctuations grow at early stages of the phase separation, is characterized by an exponential growth, in accordance with the linearized Cahn-Hilliard arguments. However, at later stages, deviations from this behavior are seen and hydrodynamics associated with the flow of the polymers must be considered. The growth of fluctuations at the air-polymer interface in an electric field should follow a

similar pattern, as it is similarly governed by a balance between surface tension and electrohydrodynamic flow. The linearized theory of Schäffer et al.[16, 17] assumes that the rate of growth in the amplitude of the dominant wavelength should be exponential. However, deviations from this should be expected as the flow of the polymer in the thin films becomes dominant.

Here, the early and intermediate stages of the growth of electrohydrodynamic instabilities in PDMS thin films is discussed. Using *in situ* laser scanning confocal microscopy, reflection interference fringes arising from film thickness fluctuations are investigated as a function of time, before columns are formed between the electrodes. Quantitative information on the growth rates of fluctuations was obtained that delineates a temporal regime in which the linearized theoretical arguments are applicable.

2.2. Experimental Methods

Linear polydimethysiloxane fluids were spin coated from 20% (w/w) solutions in toluene or heptane, onto silicon wafers. Three PDMS viscosities were used: 500 cSt, 1000cSt, and 10,000cSt, as specified by the manufacturer. GPC and rheometry measurements gave the molecular weights and zero shear rate viscosities as shown in Table 1. The dielectric constant of these fluids at 20 °C were measured to be 3.0 over a frequency range of 5 Hz-100 kHz [24], using a broadband impedance spectrometer (Novocontrol) equipped with a liquid cell (BDS 1308). Indium tin oxide (ITO) coated glass slides (Delta Technologies, Ltd) were mounted opposite the films, with a spacer of evaporated silicon oxide or with ultrasmooth polyimide films (Mictron, Toray Industries) separating the silicon substrate and glass slide, ensuring precise air gaps of three to ten

microns. The fill fraction, i.e. the ratio of film thickness to distance between silicon and glass, was varied from 0.1 to 0.5. Voltages ranging from 40 to 90V were applied from a DC power supply to the silicon wafer and ITO glass. A Filmetrics spectral reflectance instrument was used to measure film and gap thickness. A confocal laser scanning microscope (Leica TCS-SP2) was used to record reflection images of the film at a wavelength of 458 or 543 nm.

In previous experiments, we and others[20, 24] observed that structure growth is perturbed at the edges of the film, especially when the gap is smaller at one edge than another, creating a lateral gradient in electrostatic pressure. Careful attention was paid to the mounting of the ITO glass to make the electrodes as parallel as possible. The air gap was measured after mounting by spectral reflectance measurements and *in situ* observations of reflected light images were made at the same spot where the gap measurement was made. Even without a wedge-shaped gap, structure development may be affected by curvature of the electric field lines at the film's edge, so only regions near the center of the film were investigated. Perturbations arising from heterogeneities, such as dust particles in the film, also produce significant effects on structure formation. Sample preparation was therefore performed to minimize contaminants. Glass electrodes were cleaned by ultrasonication in aqueous ethanolamine solution, silicon wafers were cleaned in a sulfuric acid bath containing Nochromix® inorganic oxidizers, and polymer solutions were filtered using 0.2 μm PTFE filters.

Table 2.1. Physical properties of PDMS materials studied.

Viscosity from manufacturer (centistokes)	Viscosity by rheometry (Pascal seconds)	Weight Averaged Molecular Weight (g/mol)	PDI
500	0.494	36000	1.4
1000	1.071	67000	1.8
10000	10.25	146000	2.0

2.3 Results and Discussion

When the polymer film is above its glass transition temperature, a spectrum of capillary waves is present at the liquid-air interface due to thermal fluctuations. However, surface tension suppresses the amplification of these waves. Therefore, as shown by the interference optical micrograph in Figure 2.1(a), the film surface is initially featureless. Slight variations in the intensity over the field of view are possible due to positioning of the sample at a slight angle with respect to the imaging plane. If there is a significant gradient in the gap spacing, i.e. the gap is wedge-shaped, another set of fringes, parallel lines running perpendicular to the gradient, will be evident in the micrograph, even when the film is smooth.

When a voltage is applied between the substrate and opposite electrode, electrostatic pressure acts against the surface tension. If there is sufficient voltage and dielectric contrast at the interface, electrostatic pressure overcomes surface tension and causes a roughening of the film due to the amplification of surface waves. It should be noted that, rather than a pulsed laser, a continuous wave laser was employed to raster-scan the sample, so that no heat is expected to be generated across the sample. In other words, no temperature gradient induced instabilities would be expected.[25] Within seconds of application of electrostatic pressure to the PDMS-air interface, a lateral pattern of

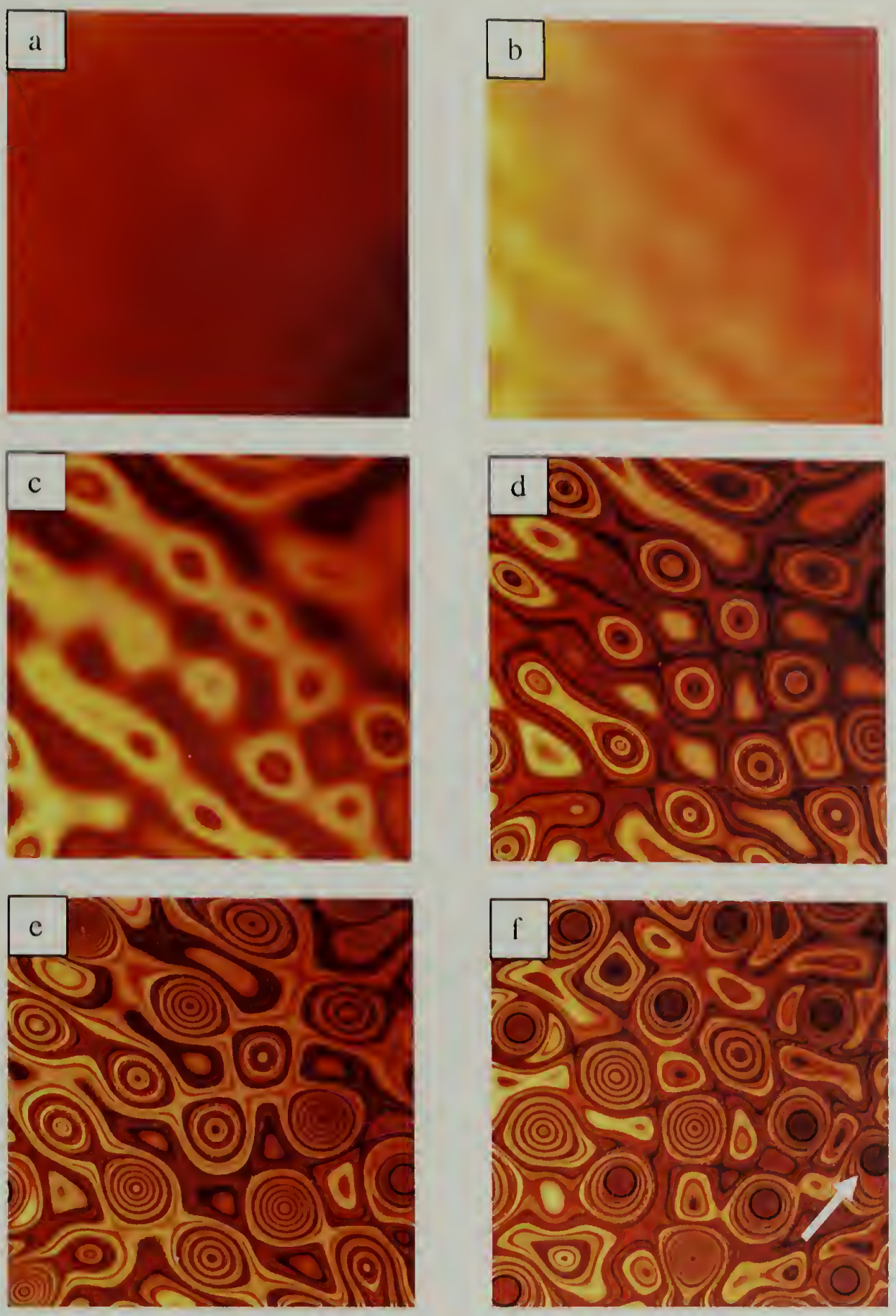

Figure 2.1. The various stages of structure development by electric field-amplified instability, as a function of time, of a PDMS film on silicon.
(a)[0.0 s] The film is initially featureless.
(b) [36.6 s] Fluctuations appear as lateral variations in intensity in the plane of the film.
(c) [75.8 s] Amplified peaks exhibit reflection interference fringes as height increases
(d) [109.7 s] Peaks are encircled by fringes as height increases further.
(e) [129.3 s] As peaks grow, the number of fringes around each peak increases.
(f) [144.1 s] When peaks span the two planar electrodes, cylindrical structures are formed. The arrow indicates a pillar which has shifted laterally after electrode contact. Laser scanning confocal micrographs were acquired by reflection imaging through a transparent electrode. Laser wavelength is 458 nm; image dimension is 740 x 740 μm^2.

intensity maxima are apparent in the confocal image, as shown in Figure 2.1(b). The interference of the reflected light is dependent on the refractive index of the film, n, and the incident wavelength, λ, such that the change in height, Δh, between intensity maxima or minima is given by $\Delta h = \lambda/2n$. For these experiments, Δh ranges from 160 nm to 200 nm. Thus, as the intensity increases from a minimum to a maximum in Figure 2.1(b), thickness variations are less than $\Delta h/2$, i.e. less than 80nm. The fluctuations have a typical spacing of one hundred microns or more in the plane of the film. Consequently, these fluctuations represent only minor height variations of the film surface and, as such, conform to the linearized theoretical framework, which assumes the lubrication flow approximation.

The amplitude of height variations increases with time due to the electrostatic pressure. The intensity of bright regions of Figure 2.1(b) is increased in Figure 2.1(c). However, in some areas the center of the bright spot is darkened due to destructive interference of reflected light, as the height approaches a thickness for which an intensity minimum is observed. Comparison of Figure 2.1(c) to Figure 2.1(f), in which the final column morphology is shown, confirms that the characteristic spacing of the final columnar morphology corresponds to the wavelength of the undulations observed at early times.

As the peak height continues to increase with time, the undulations in the film surface are characterized by rings of interference fringes, as shown in Figure 2.1(d). At the base of each feature, the fringes are noticeably broader and less axially symmetric than at the center. The base of the peak is quite sensitive to flow in the plane of the film, resulting from the mass transport from the surrounding fluctuating film and to the

smoothing effect of the Laplace pressure normal to the film surface. This micrograph illustrates that the characteristic distance between the growing peaks is determined by the competition between electrostatic and Laplace pressures. For example, in the lower left quadrant of Figure 2.1(d), a row of three peaks is visible, where the middle peak eventually decreases in height while the other two peaks grow, as seen in Figure 2.1(e). Figure 2.1(d) also shows that disparities in height between peaks which, though slight at first, become amplified with time as a result of the exponentially increasing growth rate.

When the amplitude of the fluctuations increases sufficiently to span the air gap between the film and upper electrode, the polymer fluid and the electrode come into contact. First, contact is made by the center of the peak, followed by an equilibration of the structure to a columnar shape. In Figure 2.1(f), the columns of PDMS appear as circular contacts between the film and the upper electrode. There is a strong driving force towards the alignment of air-polymer surfaces parallel to the electric field to minimize the electrostatic pressure. Furthermore, spreading of PDMS on the ITO-glass decreases the interfacial energy at the upper electrode. The same sequence of events is shown for another sample in Figure 2.2. In that figure, the change in amplitude occurs very slowly at first, but much more quickly at later times.

The thermodynamic factors of electrostatic pressure and surface energy minimization favor the coalescence of columns into one larger structure as the equilibrium state of this system. This was never observed, though coalescence of the columns was observed in some PDMS/air systems. Columns can coalesce as they grow in radius by drawing additional material from the fluid reservoir on the lower electrode.

Similar experiments with other polymers show this behavior only at high temperature.[24] Pattern replication occurs precisely by this coalescence mechanism, as shown by Lin.[24] The growth in amplitude of the surface waves was determined from the change in the film thickness determined from the interference fringes that encircle each peak. Since the period of the fringes is dictated by the slope of the film, they can be used to calculate the three dimensional shape of the surface fluctuations. Figure 2.3 shows an example of a surface topography cross-section calculated from interference fringes. The peak height was determined by fitting the resulting topographic profile to a Gaussian peak function, weighted with strictest fitting constraints at the center of the peak, so as to most accurately estimate the height in the center of the feature. Though not predicted theoretically, the Gaussian peak shape was found to describe the shape of the surface features at early times suitably.

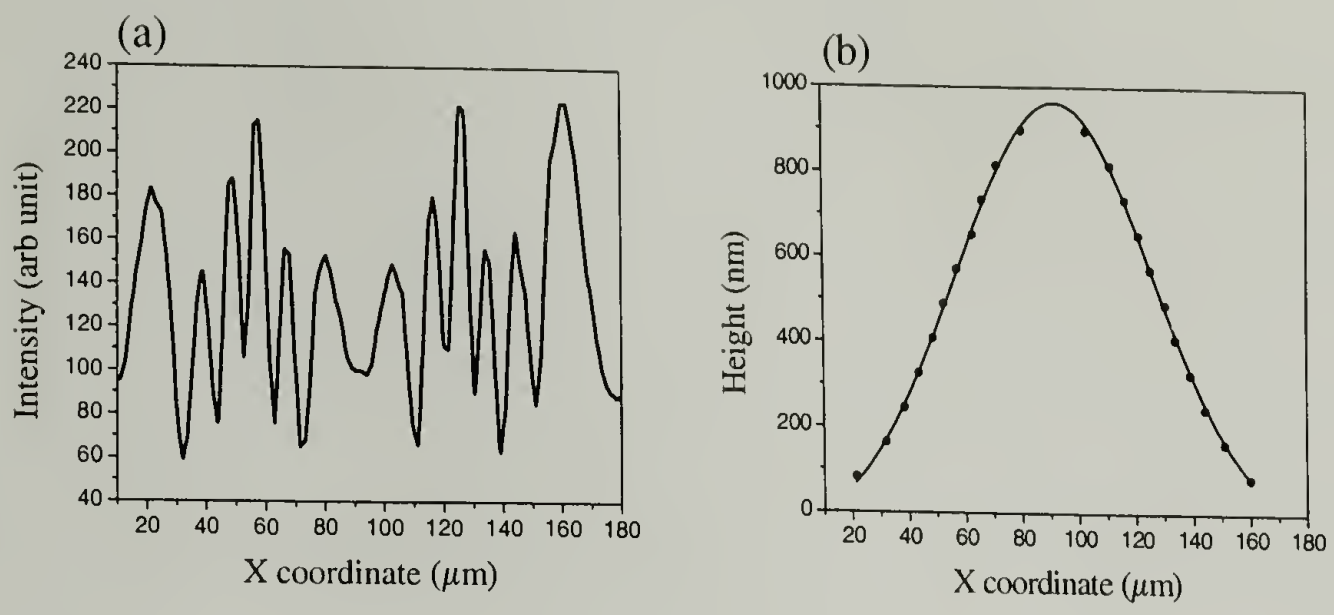

Figure 2.3. (a) Cross-sectional intensity profile of a peak showing interference fringes. (b) Calculation of peak shape from fringe spacing (squares) and Gaussian fit to points (line).

From a frame-by-frame calculation of peak height, the growth in the amplitude of the waves was found to depend exponentially on time. A typical growth curve is shown in Figure 2.4 in a semi-log plot. A single exponent could be used to describe the early stages of structure growth. However, the growth in some cases was found to accelerate towards the upper electrode at the final stages of structure growth and the rate became faster than the initial exponential dependence. The linearized theory takes into account the increased electrostatic pressure at the peaks, which is the reason for the initial stages of exponential growth. In the later stages, however, the shape of the fluctuations could not be described by a simple smooth function, since they became increasingly pointed. The electrostatic pressure at the peak is higher than elsewhere across the surface, and field lines are no longer parallel. The peak shape at these late stages could not be measured directly due to increasingly rapid changes in shape. In the final stages of pillar formation, the shape more closely resembles an electrohydrodynamic spout, as seen by

Oddershede and Nagel,[15] where a divergence in tip curvature was found as the liquid was drawn to the opposing electrode.

In all experiments, when the amplified waves grew and spanned the air gap to the opposite electrode, an array of polymer columns formed, where the center-to-center distance of the columns was identical to the lateral distance between the most rapidly growing fluctuations. However, not all of the fluctuations grew into columns simultaneously. Rather, slight differences in the initial height of the peaks were enhanced due to the exponential nature of the growth rate. As shown in Figures 2.1 and 2.2, the sequence in which pillars form seems to be stochastic. In some cases, the final formation of a pillar caused draining of the underlying 'reservoir' of material and, therefore, slowed the growth of adjacent features. This type of dynamic effect is not incorporated into the linear stability model, and resulted in deviations from predicted growth rates. Analysis of characteristic growth rates, therefore, focused on the fastest growing peaks, which are least perturbed by such effects, that could be described by a simple Gaussian function. The experimental data consistently show an exponential growth of the peak height with time (Figure 2.4). For thinner films and at lower fields, the exponent is smaller, corresponding to slower structure formation. For thicker films and higher fields, the exponent was larger, corresponding to faster structure formation. In the linearized stability analysis, the wave-like fluctuations at the film surface were modeled as changes

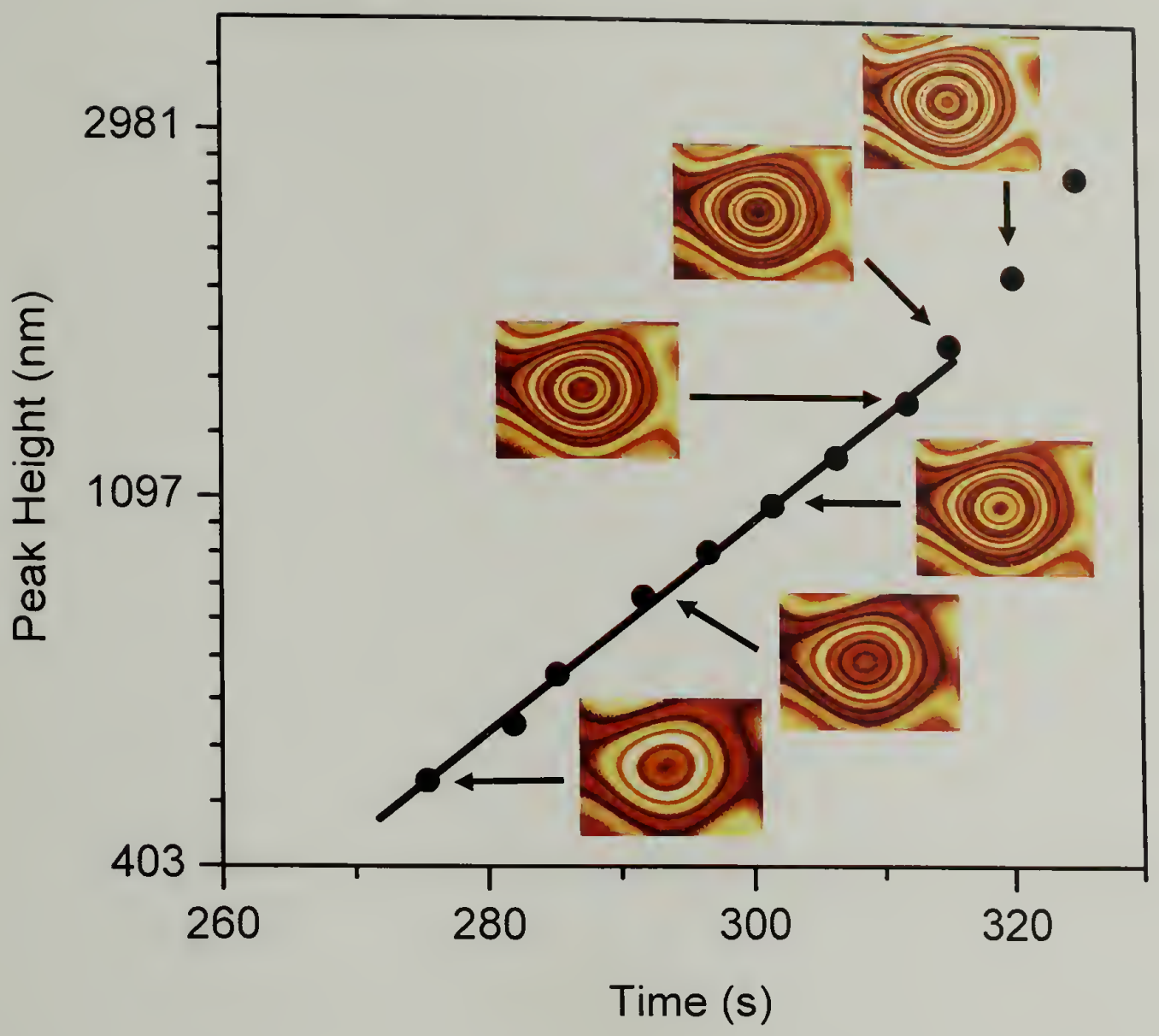

Figure 2.4. Development of peak height (natural log scale) with time for a typical feature. Line indicates best fit for data up to 320s. Image dimension is 198 x 384 μm^2.

in height, h, as a function of spatial coordinate, x, and time, t, along with parameters of amplitude, u, wavenumber, q, and growth time scale, τ: $h(x,t)=h_0+ue^{iqx+t/\tau}$. It is the characteristic growth rate, τ^{-1}, that is given by the slope of the line fit to a semi-logarithmic plot of the data at early times, as represented in Figure 2.4. To enable comparison between experiments, the electric field strength in the polymer, E_P, for each experiment was reduced to a dimensionless quantitity using the parameter E_0, the same field parameter used by Schäffer et al.[17], and the measured initial characteristic time from

each curve, τ_{meas}, was similarly reduced to a dimensionless characteristic time using the characteristic time scale, τ_0.

$$E_P = \frac{U}{\left(\varepsilon_P d - \left(\varepsilon_P - 1\right)h_0\right)} \tag{2.1}$$

$$E_0 = \frac{U}{\lambda_0} \tag{2.2}$$

$$\lambda = 2\pi\sqrt{\frac{\gamma U}{\varepsilon_0 \varepsilon_P \left(\varepsilon_P - 1\right)^2}} E_P^{-\frac{3}{2}} \tag{2.3}$$

$$\lambda_0 = \frac{\varepsilon_0 \varepsilon_P \left(\varepsilon_P - 1\right)^2 U^2}{\gamma} \tag{2.4}$$

$$\tau = \frac{3\gamma\eta}{\varepsilon_0{}^2 h_0{}^3 U^4}\left(\frac{\varepsilon_P}{\varepsilon_P - 1}d - h_0\right)^6\left(1 - \frac{1}{\varepsilon_P}\right)^2 \tag{2.5}$$

$$\tau_0 = \frac{3\gamma\eta U^8}{\pi^4 \varepsilon_0{}^2 h_0{}^3}\left(\frac{\varepsilon_0 \varepsilon_P \left(\varepsilon_P - 1\right)}{\gamma}\right)^6\left(1 - \frac{1}{\varepsilon_P}\right)^2 \tag{2.6}$$

$$\frac{\tau}{\tau_0} = \pi^4\left(\frac{E_P}{E_0}\right)^{-6} \tag{2.7}$$

In the above expressions, γ is the polymer surface tension, U is the applied voltage, η is the viscosity, h_0 is the initial polymer film thickness, d is the separation distance between the two electrodes, ε_0 is the dielectric permittivity in a vacuum, and ε_P is the polymer dielectric constant. These experimental parameters determine E_P, the electric field strength in the polymer, and E_0, λ_0, and τ_0, the characteristic parameters used to reduce experimental results to dimensionless values. Equations 2.1-2.4 and 2.7 were taken from reference 17, whereas eqs 2.5 and 2.6 were derived from the analysis therein. Equation 2.7 shows the expected relationship between the dimensionless values.

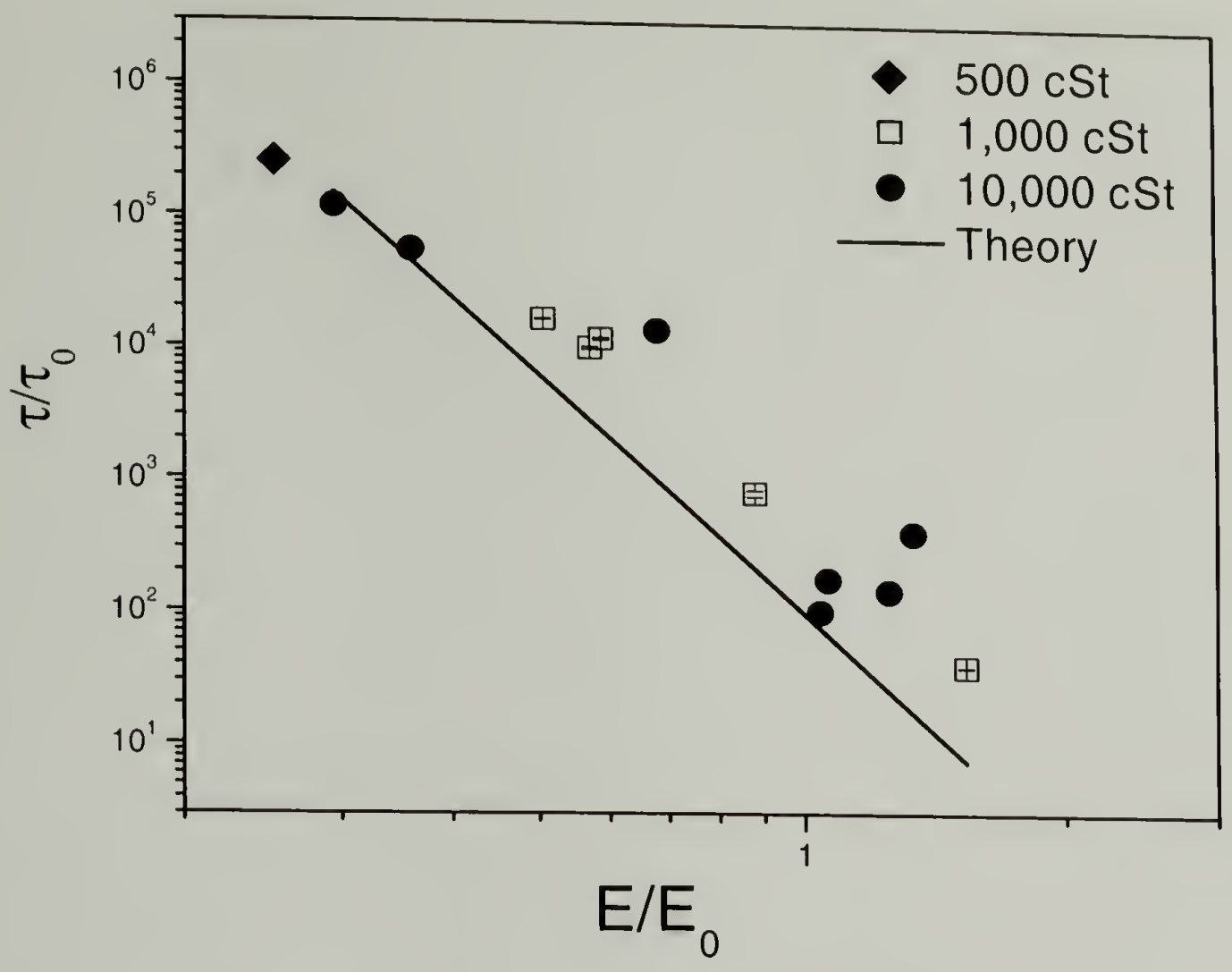

Figure 2.5. Variation of dimensionless characteristic time with dimensionless electric field and comparison with predicted values. Both axes have logarithmic scales.

A log-log plot of τ/τ_0 as a function of E_P/E_0 is shown in Figure 2.5, along with predicted values according to eqs 2.5 and 2.6. No fitting parameters were used to scale the data. The error bars due to the uncertainties in the exponential fit are smaller than the symbols in the figure. The scatter in the data, though, may arise from the uncertainty with which the fastest growing wavelength is chosen from within the field of view in the microscope. It is not possible to know which peak corresponds precisely to the fastest growing wave in the system. Although the growth rate of the first peak to reach the upper electrode is measured, we do not have sufficient resolution to obtain a statistical measurement of the growth rate of all peaks. We note that the values and trends of the experimental results, over four orders of magnitude in τ/τ_0, correspond remarkably well (within a factor of

two) to the predicted values for the three samples of PDMS with different viscosities that were studied. No systematic deviations from the predicted characteristic time values were seen as a function of viscosity. To within experimental errors a power law with an exponent of -6 was seen in the experimental data, as would be expected theoretically. Thus, if experiments are restricted to the very early stages of growth in the surface fluctuations, quantitative agreement between experiment and theory can be obtained. The accelerated growth at later times will, of course, give rise to marked departures from the linear approximation and, as such, pronounced disagreement with linearized predictions.

2.4 Conclusions

The evolution of electric field-induced instabilities in thin polymer films was shown to be characterized by an exponential growth in peak height with time at early times. At later stages of growth, an acceleration in the growth rate with time was observed. The characteristic time for growth during the early stages agrees very well with theoretical predictions using a simple linear instability analysis. Surface waves having a characteristic periodicity grew simultaneously across the film surface, in a manner akin to the early stages of spinodal phase separation. Future experiments could assess the changes in the shapes of the fluctuations prior to the formation of columns that span the gap to the upper electrode. In addition, by chemical modification of the surfaces of the film and electrode, the reversibility of the process is being examined. Finally, although the agreement of these measurements with theoretical predictions is excellent, methods with more statistical certainty, such as small angle light scattering or off-specular X-ray

reflectivity, could be pursued to provide confirmation of the microscope-based experiments.

2.5. References

1. Vrij, A. *Discuss. Farad. Soc.* **1966,** *423*, 23.

2. *Ann. Rev. Fluid Mech.*, **1979**, *11*, 371.;

3. deGennes, P. G. Wetting: Statics and Dynamics. *Rev. Mod. Phys.* **1985**, 57, 827.

4. Daillant, F., Brochard-Wyart, F. Drying of Solids Wetted by Thin Liquid Films. *Can. J. Phys.* **1990**, 68, 1084-1088.

5. Reiter, G. Dewetting of Thin Polymer Films. *Phys. Rev. Lett.* **1992**, *68*, 75-78.

6. Brochard-Wyart, F., Martin, P., Redon, C. Liquid-Liquid Dewetting. *Langmuir* **1993**, 3682-3690.

7. Jacobs, K; Herminghaus, S.; Mecke, K. Thin Liquid Polymer Films Rupture via Defects. *Langmuir* **1998**, *14*, 965-969.

8. Sharma, A.; Khanna, R. Pattern Formation in Unstable Liquid Films. *Phys. Rev. Lett.* **1998**, *81*, 3463-3466.

9. Kerle, T.; Yerushalmi-Rozen, R.; Klein, J.; Fetters, L.J. van der Waals Stable Thin Liquid Films: Correlated Undulations and Ultimate Dewetting. *Europhys. Lett.* **1998**, *44*, 484-490.

10. Swan, J. W. Stress and Other Effects Produced in Resin and in a Viscid Compound of Resin and Oil by Electrification. *Proc. R. Soc. London* **1897**, *62*, 38-46.

11. Doshi, J.; Reneker, D. H. Electrospinning Process and Applications of Electrospun Fibers. *J. Electrostat.* **1995**, *35*, 151-160.

12. Yarin, A.L., Koombhongse, S.; Reneker, D.H. Taylor Cone and Jetting From Liquid Droplets in Electrospinning of Nanofibers. *J. Appl. Phys.* **2001**, *90*, 4836-4846.

13. Shin Y. M.; Hohman, M. M.; Brenner, M. P.; Rutledge, G. C. Experimental Characterization of Electrospinning. *Polymer* **2001**, *42*, 9955-9967.

14. Shin Y. M.; Hohman, M. M.; Brenner, M. P.; Rutledge, G. C. Electrospinning: A Whipping Fluid Jet Generates Submicron Polymer Fibers. *Appl. Phys. Lett.* **2001**, *78*, 1149-1151.

15. Oddershede, L.; Nagel, S. Singularity During the Onset of an Electrohydrodynamic Spout. *Phys. Rev. Lett.* **2000**, *85*, 6, 1234-1237

16. Schäffer, E.; Thurn-Albrecht, T.; Russell, T. P.; Steiner, U. Electrically Induced Structure Formation and Pattern Transfer. *Nature* **2000**, *403*, 874-877.

17. Schäffer, E.; Thurn-Albrecht, T.; Russell, T. P.; Steiner, U. Electrohydrodynamic Instabilities in Polymer Films. *Europhys. Lett.* **2001**, *53*, 518-524.

18. Chou, S. Y.; Zhuang, L. Lithographically Induced Self-Assembly of Periodic Polymer Micropillar Arrays. *J. Vac. Sci. Technol., B* **1999**, *17*, 3197-3202.

19. Chou, S. Y.; Zhuang, L.; Guo, L. Lithographically Induced Self-Construction of Polymer Microstructures for Resistless Patterning. *Appl. Phys. Lett.* **1999**, *75*, 1004-1006.

20. Deshpande, P.; Sun, X.; Chou, S. Y. Observation of Dynamic Behavior of Lithographically Induced Self-Assembly of Supramolecular Periodic Pillar Arrays in a Homopolymer Film. *Appl. Phys. Lett.* **2001**, *79*, 1688-1690.

21. Lin, Z.; Kerle, T.; Baker, S. M.; Hoagland, D. A.; Schäffer, E.; Steiner, U. Russell, T. P. Electric Field Induced Instabilities at Liquid/Liquid Interfaces. *J. Chem. Phys.* **2001**, *114*, 2377-2381.

22. Lin, Z.; Kerle, T.; Russell, T. P.; Schäffer, E.; Steiner, U. Structure Formation at the Interface of a Liquid/Liquid Bilayer in Electric Field. *Macromolecules* **2002**, *35*, 3971-3976.

23. Pease, L. F., III; Russell, W. B. Limitations on Length Scales for Electrostatically Induced Submicron Pillars and Holes. *Langmuir* **2004,** *20*, 795-804.

24. Lin, Z. Surface and Interfacial Structures Induced By Electrohydrodynamic Instabilities. Ph.D. Dissertation, University of Massachusetts, Amherst, MA, 2003.

25. Schäffer, E.; Harkema, S.; Blossey, R.; Steiner, U. Temperature-Gradient-Induced Instability in Polymer Films *Europhys. Lett.* **2002**, *60*, 255-261.

CHAPTER 3

EFFECT OF BLOCK COPOLYMER ON ELECTROHYDRODYNAMIC INSTABILITIES AT LIQUID-LIQUID INTERFACES

3.1 Introduction

In the fabrication of high-strength polymer blends, one frequently-employed strategy for mediating interfacial interactions between immiscible polymer phases is the addition of copolymer compatibilizers.[1] In general, block copolymers reduce the interfacial energy and, therefore, it is less costly energetically to have smaller domain sizes.[2] The addition of a small amount of block copolymer, usually less than 1% by weight, results in a sharp decrease in interfacial tension. The interfacial tension continues to decrease with the addition of block copolymer until the interface is saturated.[3] Upon further addition, the block copolymers can form micelles, which themselves may segregate to the interface or become dispersed in the bulk homopolymer phases.[4] A number of theoretical models have been developed to predict the distribution of block copolymers and interfacial tension in an blend of two polymers which are immiscible.[5,6,7,8] Experimental studies of block copolymer segregation at interfaces have shown changes in droplet shape and size as a function of copolymer concentration, and changes in interfacial width in thin films.

The addition of a polystyrene-*b*-poly(dimethylsiloxane) (PS-*b*-PDMS) block copolymer to PS/PDMS bilayers was studied here, since it presents a model system where a large surface energy gradient can be used to drive surface segregation. X-ray reflectivity was used to characterize the distribution of block copolymer in the thin films

and bilayers before and after annealing. As predicted from the theoretical model of the linearized instability theory, the reduction of surface or interfacial free energy decreases the wavelength of electrohydrodynamic instability

3.2 Experimental Methods

3.2.1 Contact Angle and X-ray Reflectivity Experiments

A PS-*b*-PDMS block copolymer having a 34 kg/mol PS block and a 12.5 kg/mol PDMS block was added to solutions of 30 kg/mol PS in toluene, yielding an overall polymer concentration of 2% (wt/wt) and block copolymer concentrations from 0 to 10 % (wt/wt) of total polymer content. The polydispersity indices of the block copolymer and homopolymer used were 1.14 and 1.04, respectively. Films were spin-coated onto silicon wafers that had been freshly cleaned in concentrated sulfuric acid with added inorganic oxidizers. The thicknesses of the layers were determined using a Rudolph Research AutoEL-II optical ellipsometer equipped with a 632.8 nm HeNe laser at a 70° angle of incidence. The thicknesses of the PS/PS-*b*-PDMS films were in the range of 95-100 nm. For bilayer experiments, 18.2 kg/mol PDMS homopolymer with a PDI of 1.4 was used as the second layer. To make the bilayers, wafers that had been coated with PS/PS-*b*-PDMS films were spin coated with PDMS from 2% (wt/wt) heptane solution, yielding PDMS films 85-90 nm in thickness.

Advancing and receding contact angle measurements were made on thin PS/PS-*b*-PDMS films, containing varying amounts of block copolymer, after 0, 12, and 24 hours of annealing. X-ray reflectivity measurements were made on thin films and bilayers containing 0-5 % block copolymer in the PS layer after 0, 12, 24, and 48 hours of

annealing. A Panalytical Xpert system, equipped with a copper rotating anode X-ray generator, was used to measure intensity for specular reflections for incident angles ranging from 0.01 to 1.5°.

3.2.2. Electric Field Experiments

The same PS-*b*-PDMS block copolymer was added to solutions of 30 kg/mol PS in toluene, yielding overall polymer concentrations of 7% (wt/wt) and block copolymer concentrations from 0 to 10 % (wt/wt) of total polymer content. Films were spin-coated as described above onto freshly cleaned silicon wafers, and measured using optical ellipsometry. The thickness of the PS/PS-*b*-PDMS films was 300-500 nm. The films were heated for 24 hours under flowing nitrogen at 150°C, then spin coated with 65 cSt PDMS cast from bulk sample, or 500 cSt PDMS cast from 11-25% (wt/wt) heptane solution, resulting in PDMS films 400-4500 nm in thickness, as measured by spectral reflectance interferometry (F-10, Filmetrics, Inc.). In experiments on both single films and bilayers, the edges of the films, where thickness is nonuniform due to edge effects on flow during spin coating, were rinsed by partial dipping in solvent to remove polymer.

In the electric field experiments on thin single layer films, amorphous silicon oxide spacers, 500-800 nm thick, were thermally evaporated onto the edges of conductive ITO-coated glass. The wafer was mounted opposite the ITO electrode, with the silicon oxide spacer separating the wafer from the ITO-coated glass. A 30-50 V electric field was applied between the two electrodes and the sample was heated to 150°C under the electric field for 1 day. For the bilayers, the upper electrode, conductive ITO-coated glass, was placed directly in contact with the PDMS film and heated for 12 hours at

150°C under flowing nitrogen. Then, a 30-50 V field was applied and the sample heated to 150°C for 1 day. In both thin film and bilayer experiments, the polymer films were allowed to cool to room temperature in the electric field, and digitally photographed twice using optical microscopy: once through the ITO-glass electrode and a second time after removing the glass electrodes. The bilayers were immersed in heptane for several minutes and dried, to remove the upper PDMS layer. They were again photographed and measured by non-contact (TappingMode) atomic force microscopy(AFM) using a Digital Instruments D3100 scanning force microscope.

The wavelength of electrohydrodynamic instabilities was determined as a function of block copolymer content and electric field strength. It is expected that the PDMS blocks will segregate to the PS-air interface and modify the surface energy of the film. In addition, the influence of added PS-*b*-PDMS ton the interfacial tension of the PS/PDMS bilayer system was examined.

3.3. Results and Discussion

3.3.1. Contact Angle Measurements

Since PS has a surface tension of 31.4 mN/m at 150°C and PDMS has a surface tension of 14 mN/m[9], there is a strong surface energy gradient that drives PS-*b*-PDMS to segregate to the surface. Figure 3.1 shows the changes in water contact angle observed in PS films with PS-b-PDMS added, as a function of annealing time. The contact angle increase indicates that the concentration of PDMS chains is increasing. The maximum value of advancing contact angle, 110.8 (± 0.5) degrees, and the maximum value of receding contact angle 91.0 (± 0.6) degrees were reached after 24 hours for the films

containing 5 and 10 weight percent block copolymer. For films with 1 and 2 weight percent added, the angles were slightly less after 24 hours, but still significantly higher than the film with no added block copolymer.

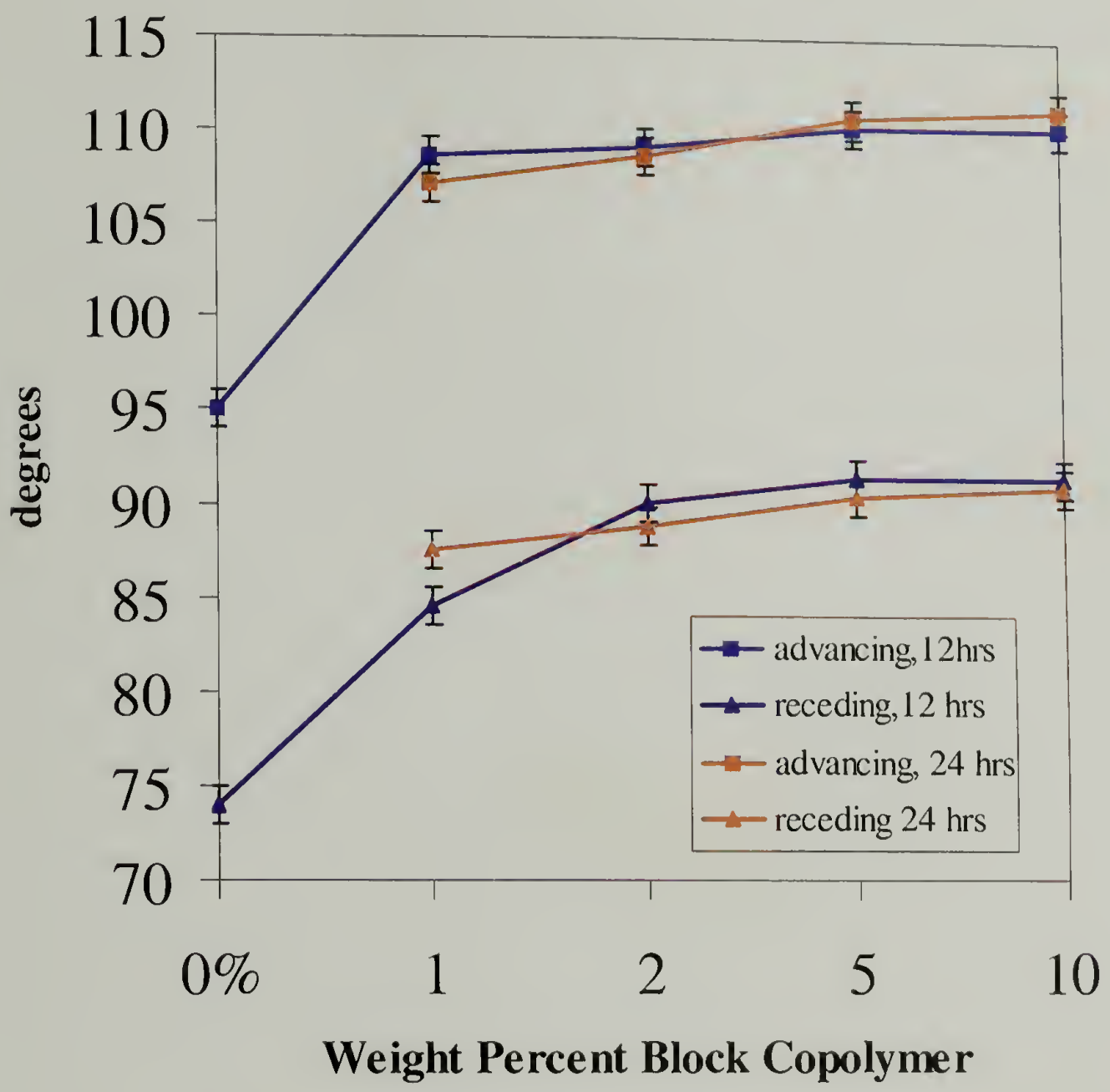

Figure 3.1 Contact angle of water droplets on PS films containing PS-*b*-PDMS block copolymer after annealing for 12 and 24 hours at 150°C.

Similar to these results, blends of PS-*b*-PDMS with bulk PS, even just after dip coating from toluene solution, with as little as one or two weight percent of block copolymer, had much lower surface tension than homopolymer PS films, and that surface concentration increased even after only 5 hours of annealing.[10] For the thin film system

studied here, it appears PS-b-PDMS surface concentration increases over time, even after 24 hours when annealed at 150°C.

3.3.2. Electric Field Experiments with Modified PS/Air

Since PS-b-PDMS segregates to the PS-air interface, the surface tension should be reduced to values similar to PDMS, that is ~14 mN/m. Figure 3.2 shows a 357 nm PS film that contains 2 wt % PS-*b*-PDMS, that has been annealed 24 hours at 150°C, then another 24 hours with 35 V applied between the silicon substrate and ITO glass having spacers to create a 750 nm air gap. The average center-to-center spacing of the features is not significantly lower than the theoretical value for the PS/air system without block copolymer. However, the expected change in spacing is a reduction by 2 μm, which is less than the error in the experimental measurements. Due to the size of the change relative to the error bars, it was not possible to observe the effect of PS-*b*-PDMS on electrohydrodynamic instabilities at the PS-air interface.

It is also possible to modify the PS-air interface simply by spin coating a thin layer of PDMS on top of the PS film. A 50 nm film of PDMS on a 373 nm PS film, annealed at 150°C for 1 day with a 1350 nm air gap and 35 V applied gave the structures shown in Fig. 3.3. Due to the low surface tension of PDMS, the pillars migrated laterally within the sample so that it was not possible to produce an ordered array. The characteristic center-to-center spacing calculated from the image shown was larger than the theoretical value calculated assuming a surface tension of 14 mN/m.

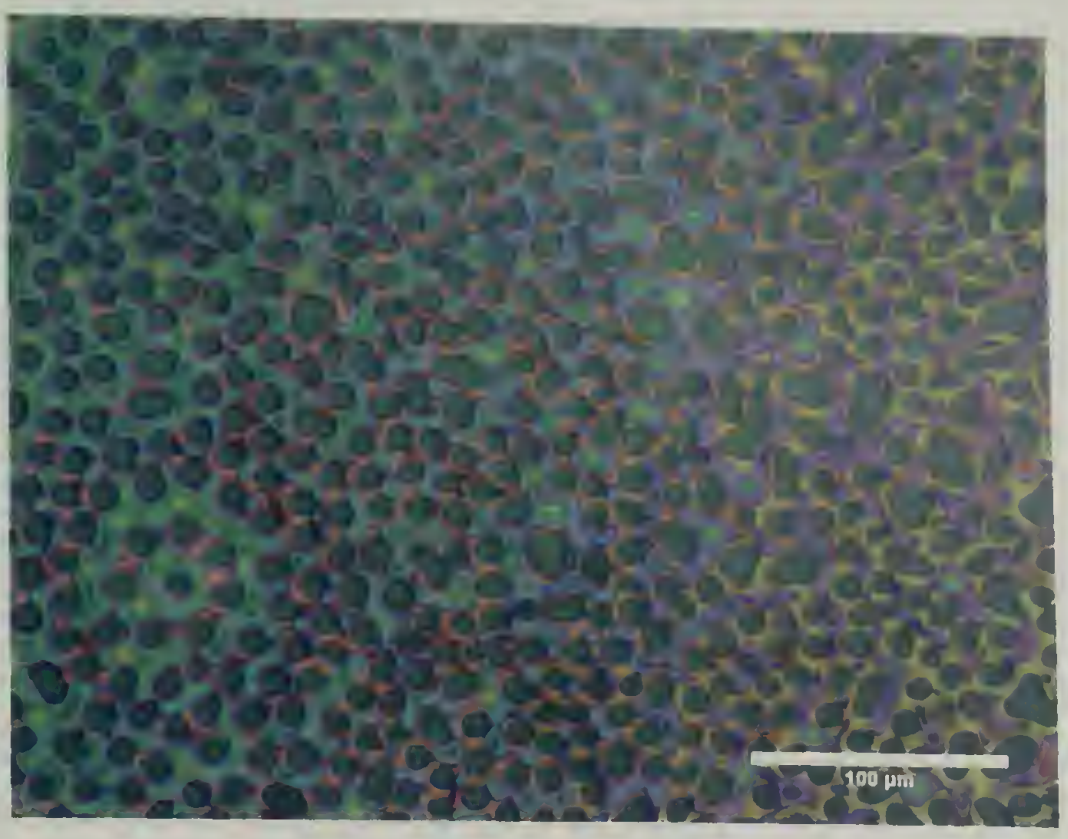

Figure 3.2 357 nm PS film with 2 wt % PS-*b*-PDMS added, annealed 24 hrs at 150°C, then another 24 hrs at 150°C with 35 V applied and a 750 nm air gap. Image dimension is 400 x 300 μm^2.

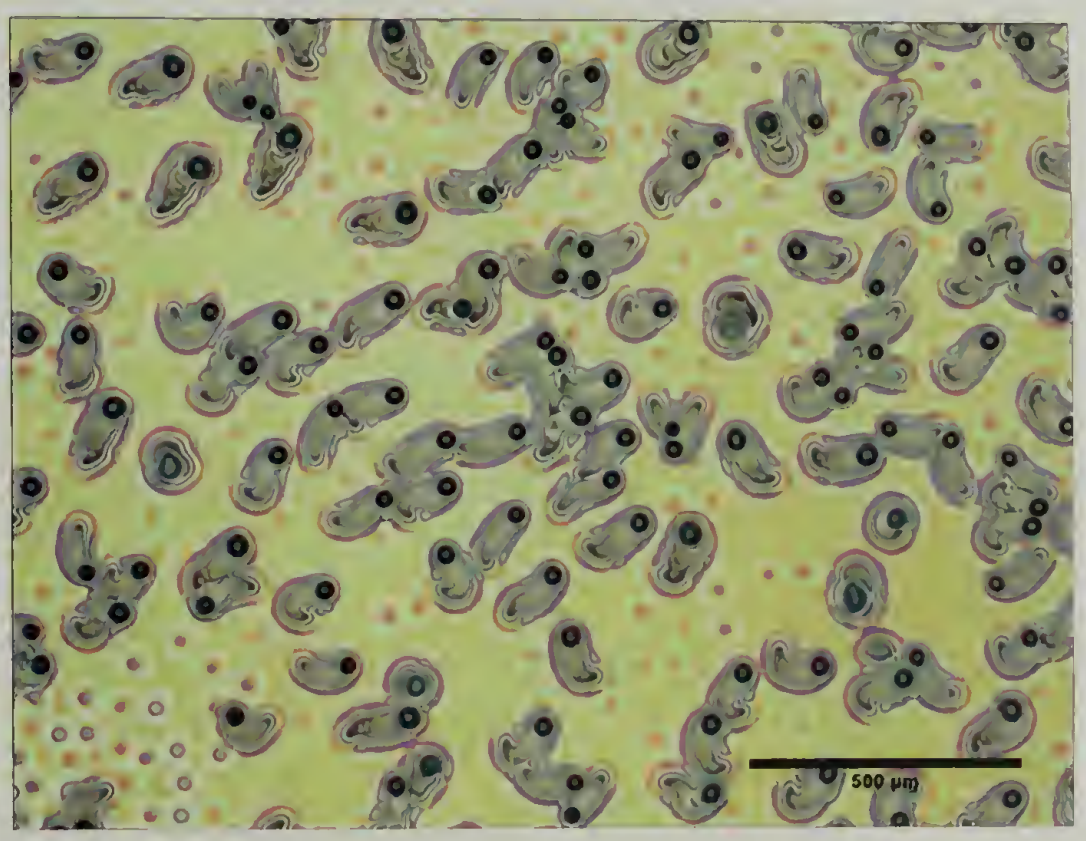

Figure 3.3. 371 nm PS film covered with 50 nm PDMS, annealed 24 hrs at 150°C with 35 V applied and a 1350 nm air gap. Image dimension is 1.9 x 1.4 mm^2.

3.3.3 Electric Field Experiments on Bilayers with Block Copolymer

Table 3.1 summarizes the results of the electric field experiments described in 3.3.2 and several experiments where PS was annealed with various amounts of PS-*b*-PDMS added. The interfacial tension between PS and PDMS at 150°C is 6.1 mN/m. Since PS and PDMS are strongly segregated, the interfacial tension between the homopolymer layers can theoretically be reduced to zero when block copolymer concentration at the interface is maximized. However, the equilibrium state of saturation of the interface is impossible to achieve in experiment, especially in the case of PS-b-PDMS, which has a critical micelle concentration of less than 0.01%. The maximum decrease in interfacial tension, observed by Hu et al., for the addition 0.02% PS-b-PDMS to the PS/PDMS interface, was 85%, to a value of 0.09 mN/m.[11] However, when the

Table 3.1. Experiments on PS/PS-*b*-PDMS films annealed in electric fields.

Sample	PS Layer	PDMS Layer	PS-*b*-PDMS weight percent	Voltage	Characteristic Spacing	
					Predicted	Observed
1	412 nm	275 nm	1	13	25	16 ± 3
2	365 nm	2300 nm	2	22	120	9 ± 1
3	463 nm	4500 nm	2	19	68	18 ± 2
4	1177 nm	850 nm	10	23	56	20 ± 5
5	357 nm	750 nm air gap	2	35	11	12 ± 4
6	373 nm	50 nm + 1350 nm air gap	0	35	23	40 ± 10

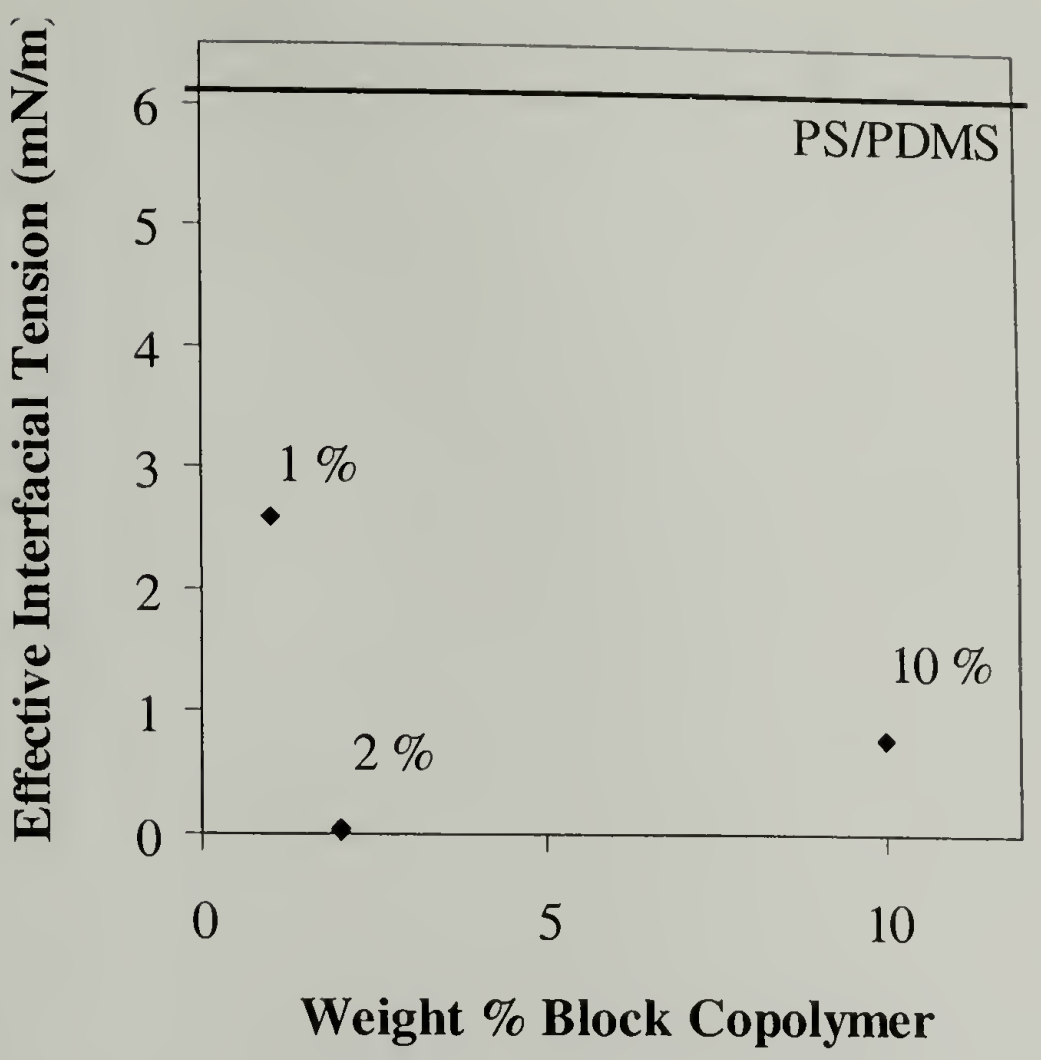

Figure 3.4. Effect of added block copolymer to interfacial tension in PS/PDMS bilayers, deduced from the resulting characteristic spacing of electrohydrodynamic instabilities at the polymer/polymer interface. The horizontal line represents the literature value of 6.1 mN/m for the PS/PDMS homopolymer/homopolymer interface.

block copolymer was added to the PS phase instead of the PDMS phase of the same system, the maximum reduction of interfacial tension was more limited, just 29% for 1% copolymer.

The effective value for interfacial tension can be deduced from the characteristic spacing of the electrohydrodynamic instabilities, shown in Figure 3.4. The minimum effective interfacial tension was found for the two samples with 2 wt % block copolymer, which gave an average of 0.025 mN/m. Surprisingly, the effective interfacial tension goes up for the highest amount of block copolymer added, 10 wt %. One possible explanation might be that micelles formed in the homopolymer phase of PS, causing a change in the

dielectric contrast at the polymer/polymer interface. If the effective interfacial tension were the same in the 10% PS-b-PDMS film as in the film with 2 % block copolymer, about 0.025 mN/m, then an increase in effective dielectric constant for the PS film from 2.46 to 2.55 is necessary for the observed characteristic spacing. If all of the block copolymer were emulsified in the PS film as micelles, then weighted average of the PS and PDMS components would raise the dielectric constant only slightly, to 2.47. The electrostatic pressure at the interface would be weakened as a consequence, shifting the characteristic wavelength of the instability to higher values, but wouldn't account for the change observed in the characteristic spacing.

The reduction in characteristic wavelength is a factor of 2 for the film with 1 wt % PS-b-PDMS, factors of 13 and 20 for the films with 2 % added, and a factor of 4 for the film with 10 % added block copolymer. The relative significance of these values is shown in Figure 3.5 in terms of the dimensionless parameters, λ/λ_0 and $E_1E_2/(E_P)^2$, calculated according to the same equations used by Lin et al.[12]:

$$\lambda_0 = \frac{\varepsilon_0(\varepsilon_1 - \varepsilon_2)^2 U^2}{\gamma_{12}(\varepsilon_1\varepsilon_2)^{1/2}} \tag{3.1}$$

$$E_1 = \frac{\varepsilon_2 U}{(\varepsilon_1 h_2 + \varepsilon_2 h_1)} \tag{3.2}$$

$$E_2 = \frac{\varepsilon_1 U}{(\varepsilon_2 h_1 + \varepsilon_1 h_2)} \tag{3.3}$$

$$E_0 = \frac{U}{\lambda_0} = \frac{\gamma_{12}(\varepsilon_1\varepsilon_2)^{1/2}}{\varepsilon_0 U(\varepsilon_1 - \varepsilon_2)^2} \tag{3.4}$$

In the above expressions, γ_{12} is the interfacial tension, U is the applied voltage, h_1 and h_2 are the initial polymer film thicknesses, ε_0 is the permittivity in a vacuum, and ε_1 and ε_2 are the dielectric constants. E_1 and E_2 are the electric field strength in the polymer films. The difference is significant for all four samples, though the decrease in characteristic spacing is less for the 10 wt % block copolymer sample, than for 2 %, as discussed above.

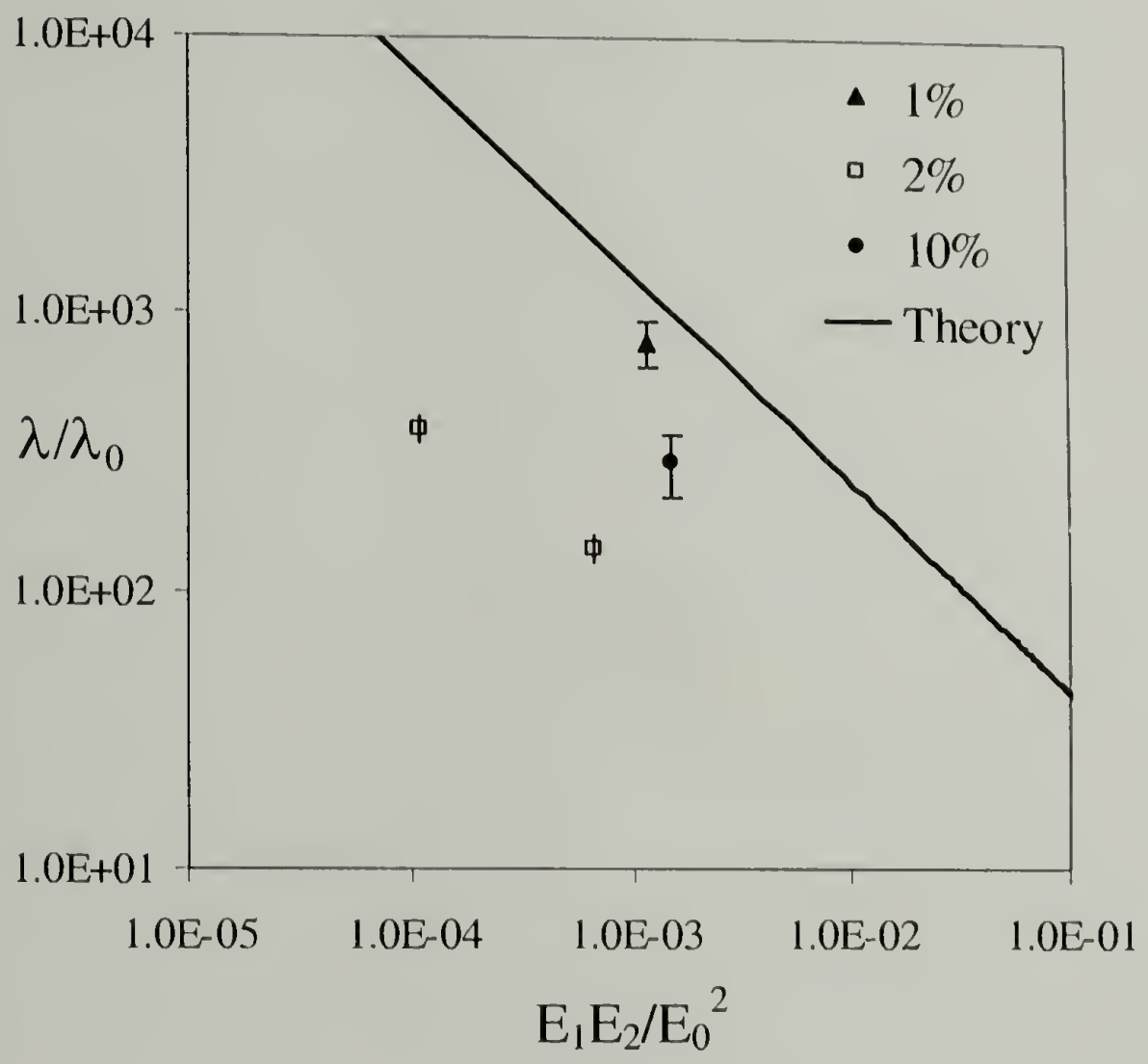

Figure 3.5. Comparison of measured characteristic spacing with theoretical values for PS/PDMS with various amounts of PS-*b*-PDMS added. The line corresponds to calculations with the interfacial tension set to a value of 6.1 mN/m.

3.3.4. X-ray Reflectivity

In the reflectivity profiles shown in Figure 3.6, there is a beat frequency due to interference between the reflections from the PS and PDMS surfaces. This relative

amplitude of the peaks and the overall intensity decay could be used to quantify the interfacial width, if there is enough contrast between the polymer layers. Unfortunately, the contrast for these two polymers and the resolution of the instrument were not high enough to enable fitting and quantification of interfacial width. As such, these experiments allow a qualitative observation of the increase in interfacial roughness when block copolymer is added to the bilayer. Another experimental problem with this approach is that the PDMS films roughen significantly during annealing, due to contamination with dust particles from the laboratory environment. After 48 hours, the beating pattern arising from the two frequencies, characteristic of the the thicknesses of the two layers was completely washed out.

It is necessary to increase the contrast between the two polymers to quantify the interfacial width of PS/PDMS bilayers, possibly by deuterating the PDMS or PS component and using neutron reflectivity rather than x-ray. Furthermore, neutron reflectivity experiments with deuterated block copolymer would could be used to study the distribution of the copolymer in the bilayer. It would be interesting, for example, to know whether the degree to which block copolymer segregates to the substrate/polymer interface relative to the amount at the polymer/polymer interface. Neutron scattering could also be used to characterize the size and distribution of the micelles that may be present in the homopolymer layers. Finally, a high intensity source would be useful for reducing the amount of time necessary to make the reflectivity measurement and, therefore, the amount of time over which the PDMS film is subject to contamination from dust particles. A clean, closed sample chamber would also help to prevent the detrimental effect of roughening of the PDMS-air interface on the reflectivity profile.

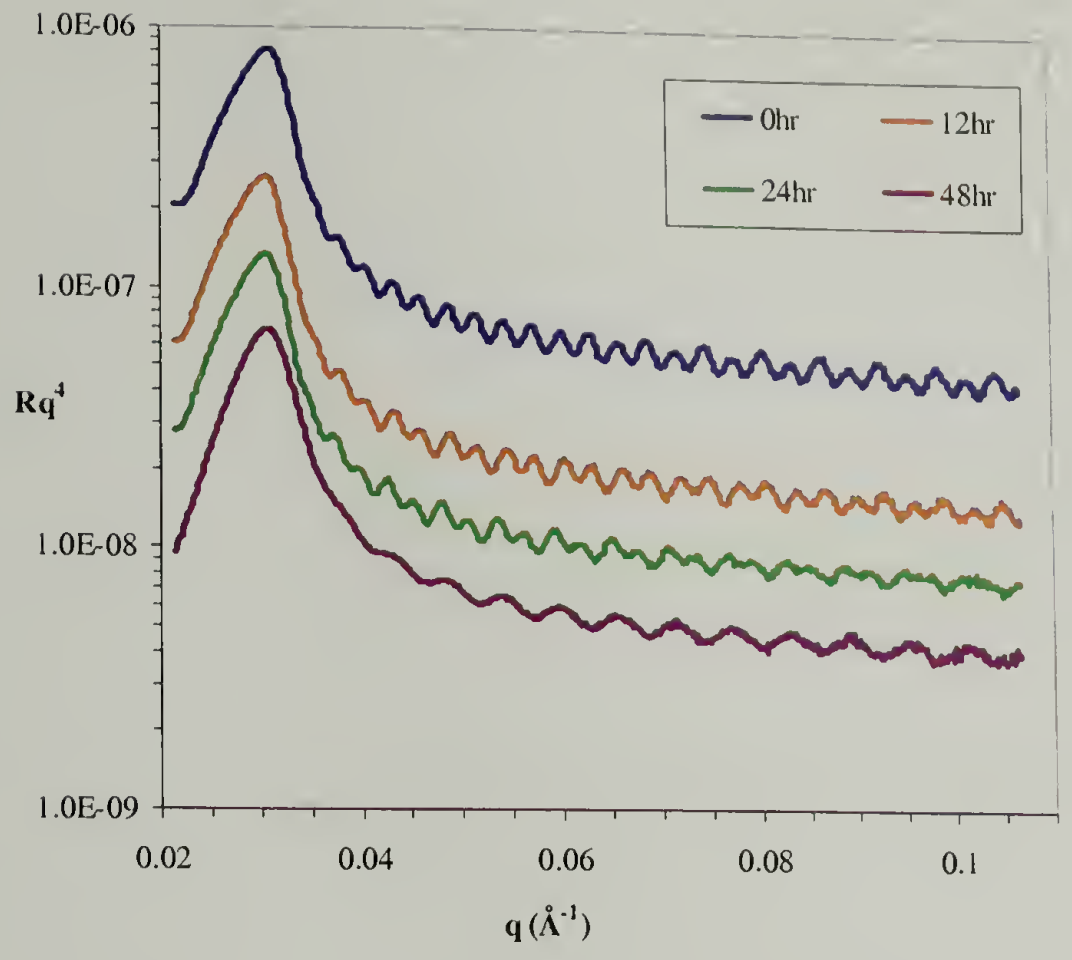

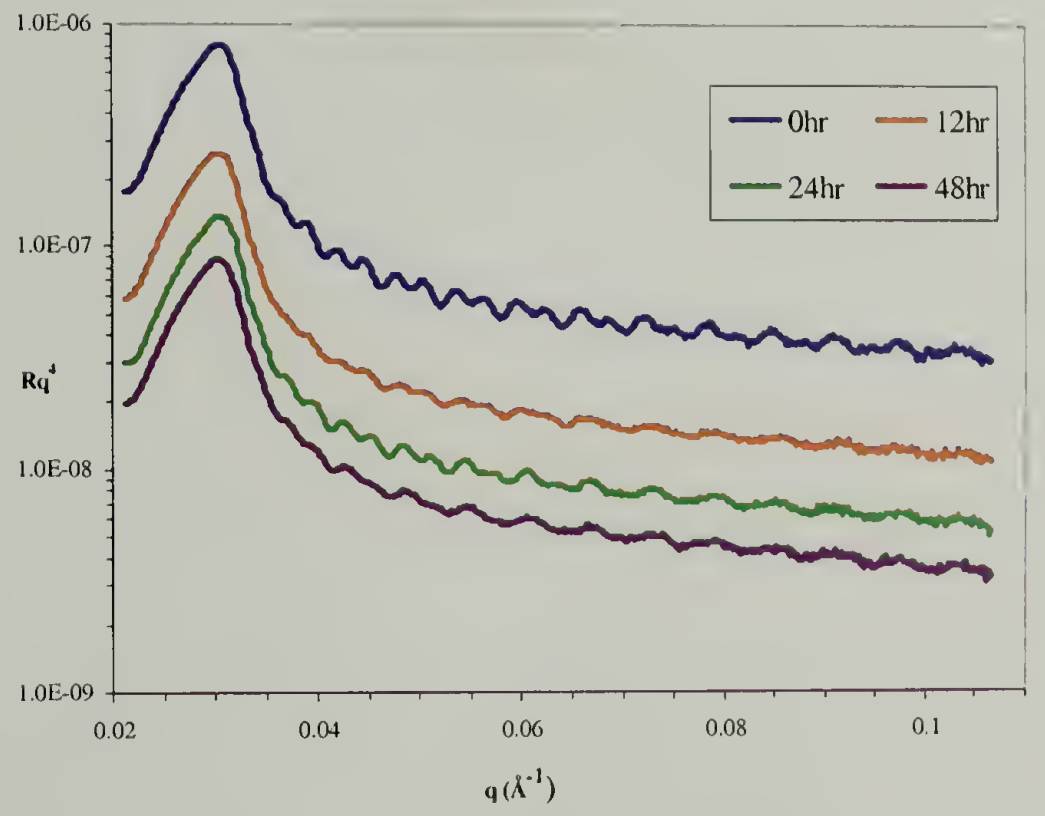

Figure 3.6 X-ray reflectivity profiles for bilayers annealed at 155C for varying times. Top: PS/PDMS; Bottom: (PS with 2 wt % PS-b-PDMS)/PDMS. The same sample was used for all annealing times.

3.3.5. Other Observations from Electric Field Experiments

When one component of the bilayer is much thicker than the other, holes in the thinner layer are generated rather than pillars, as shown in Figure 3.7 for Sample 2 and Figure 3.8 for Sample 3. However, the holes are not stable when they reach the substrate, as shown in Figure 3.9, also for Sample 3. Because dewetting of the silicon substrate is nucleated when the depression in the PS film grows deep enough, an expanding hole with a rim forms. This problem might be ameliorated by functionalizing the silicon wafer with covalently attached polystyrene in order to generate stable arrays of straight-sided holes in the polymer film.

3.4. Conclusions

The hypothesis that block copolymer could be added to a bilayer to reduce the wavelength of electrohydrodynamic instabilities was confirmed by adding PS-b-PDMS to the PS component of a PS/PDMS bilayer.The surface tension gradient was used to drive the copolymer to segregate at the PS/air surface. Significant reductions in the wavelength of PS/air electrohydrodynamic instabilities were not observed. However, a 20-fold reduction in the wavelength was observed for the PS/PDMS bilayer with just 2 wt % block copolymer added. This corresponds to an effective interfacial tension lowered from 6.1 mN/m to 0.025 mN/m. Although this interfacial tension reduction could not be measured independently, x-ray reflectivity on these bilayers qualitatively confirmed that the block copolymer significantly reduced the interfacial tension and broadened the interface between the polymers.

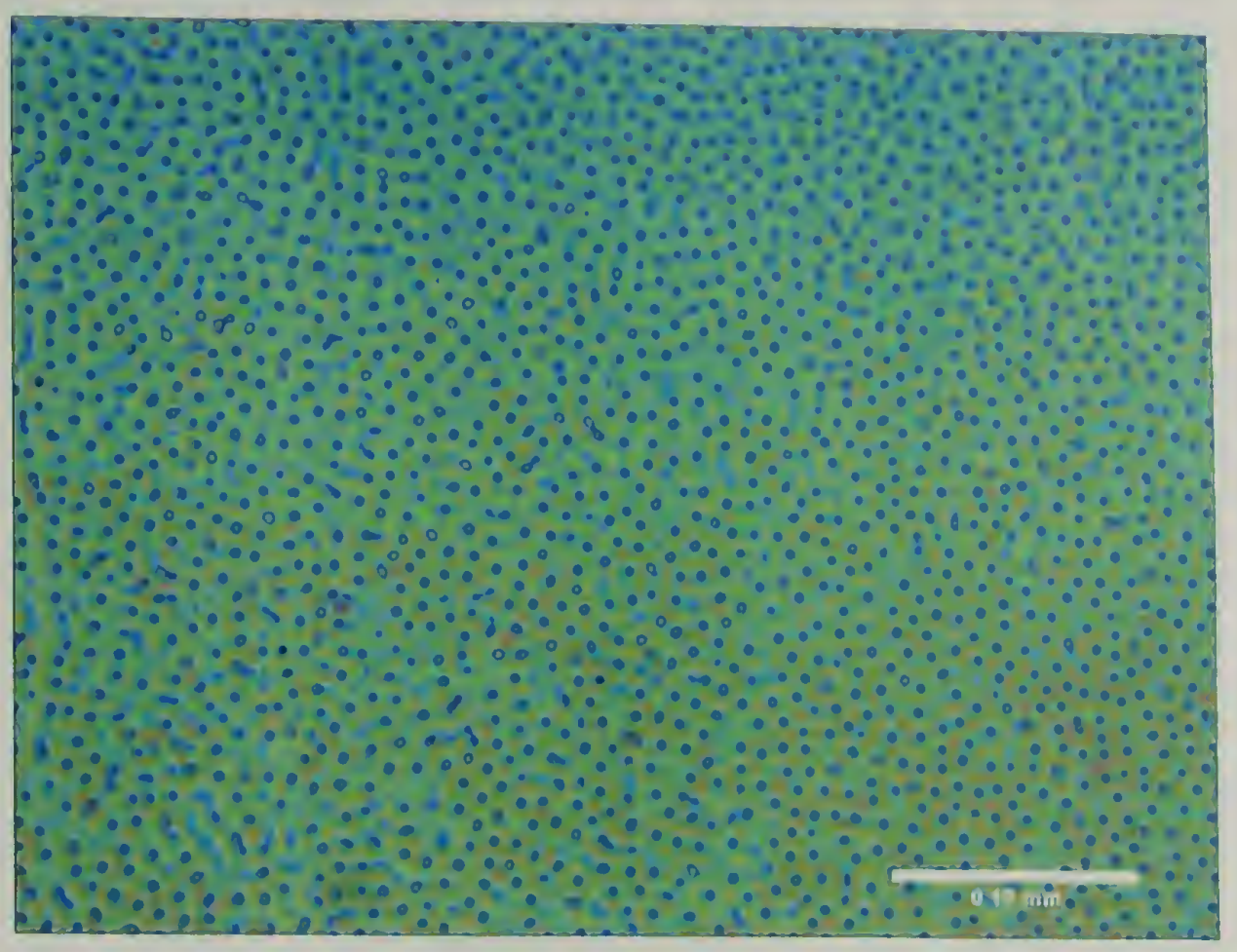

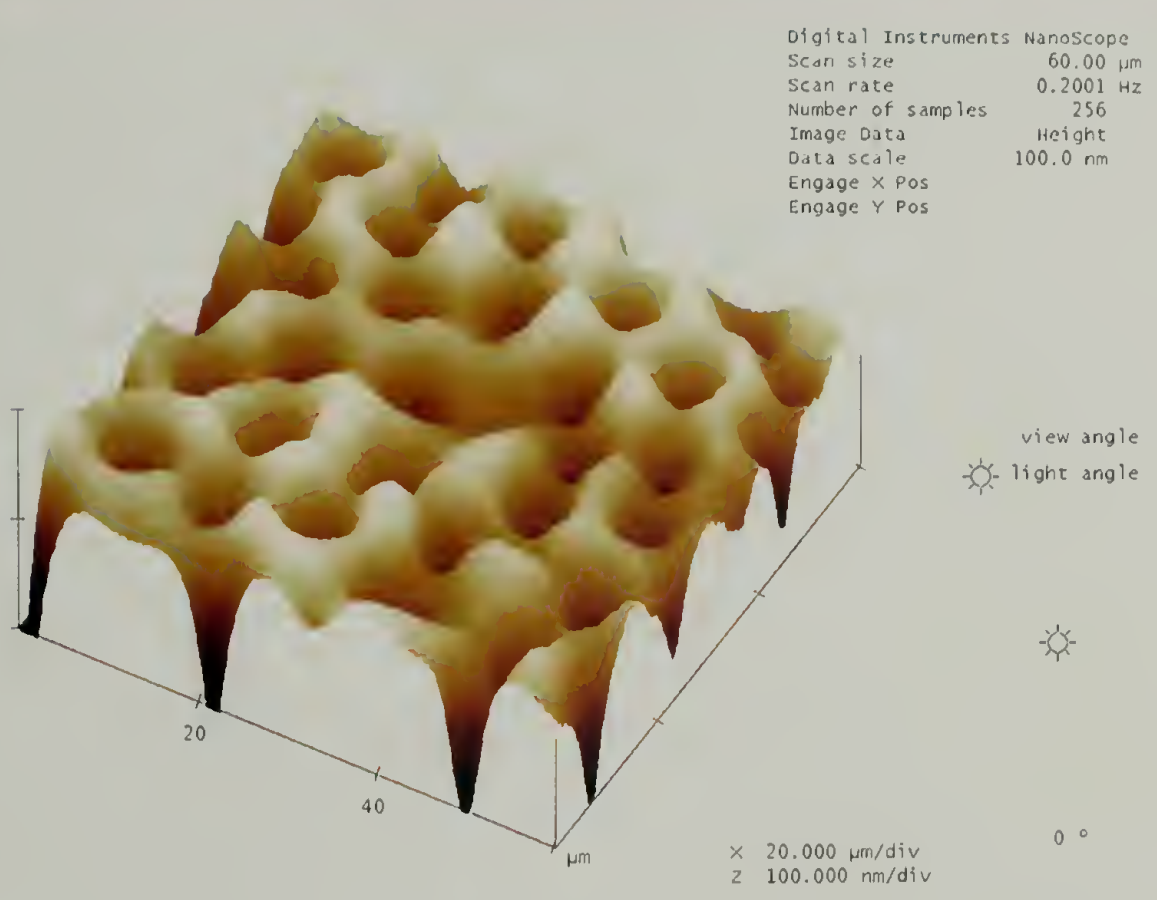

Figure 3.7. (a) Optical micrograph of 365 nm PS with 2 wt % block copolymer / 2300 nm PDMS under 22 V at 150°C for 24 hrs, after rinsing with heptane. Image dimension is 480 x 360 μm^2 (b) 3D projection of 60 x 60 μm^2 AFM height scan.

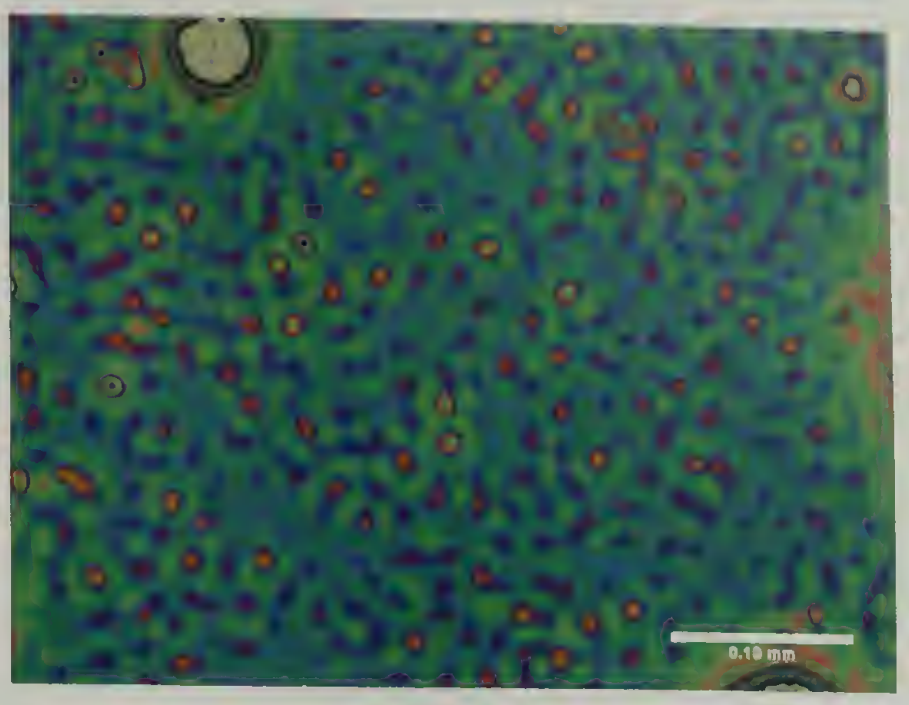

Figure 3.8. Optical micrograph of 463 nm PS with 2 wt % block copolymer / 4500 nm PDMS under 19 V at 150°C for 17 hrs, after rinsing with heptane. The fluctuations develop into depressions in the PS layer.

(a) (b)

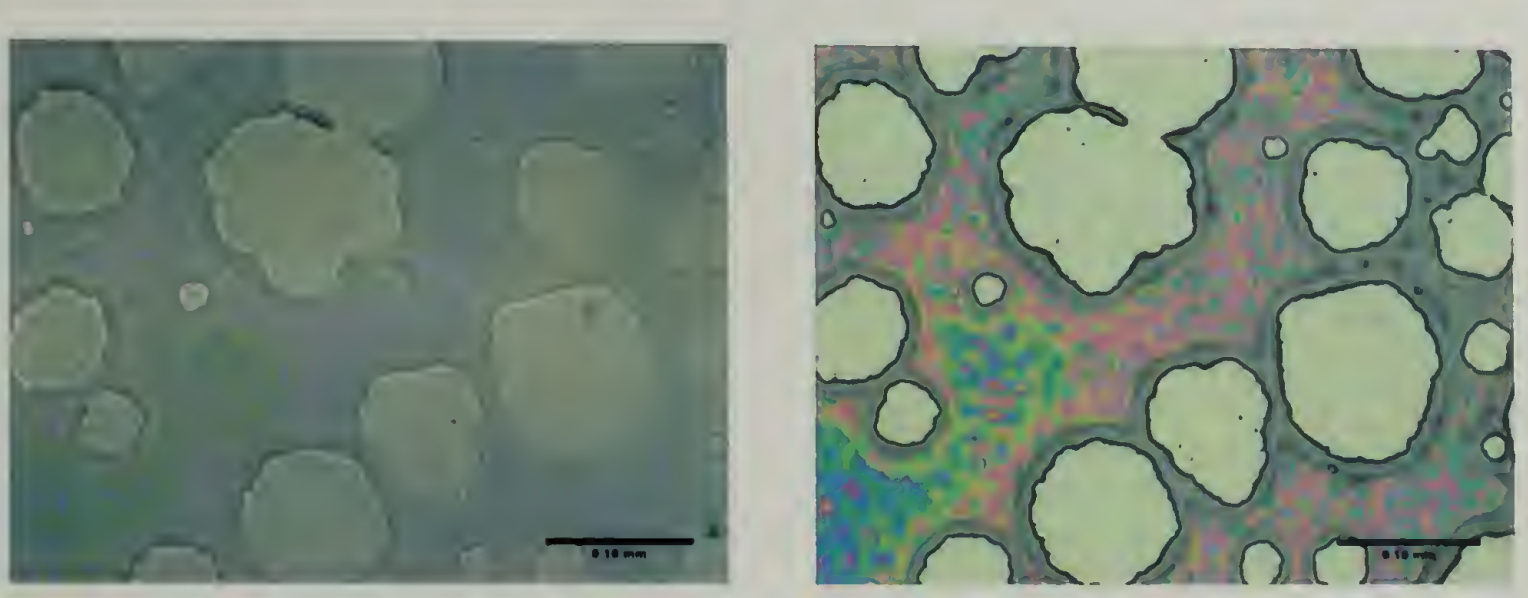

Figure 3.9. (a) Optical micrograph of 463 nm PS with 2 wt % block copolymer / 4500 nm PDMS under 19 V at 150°C C for 17 hrs, after rinsing with heptane. The fluctuations develop into depressions in the PS layer, which coalesce when they become holes in the PS layer. (b) The same area, after rinsing with heptane to remove PDMS. All three images are 480 x 360 μm^2, with 0.1 mm scale bars.

3.5. References

1. Ruzette, A.-V.; Leibler, L. Block Copolymers in Tomorrow's Plastics (Review) *Nature Materials* **2005**, *4*, 19-32.

2. Milner, S. T. How Do Copolymer Compatibilizers Really Work? Mater. Res. Soc. Bull. **1997**, *22*, 38-42.

3. Anastasiadis, S. H.; Gancarz, R.; Koberstein, J. T.; Compatibilizing Effect of Block Copolymers Added to the Polymer/Polymer Interface. *Macromolecules* **1989**, *22*, 1449-1454.

4. Shull, K.; Kramer, E.; Hadziioannou, G.; Tang, W. Segregation of Block Copolymers to Interfaces Between Immiscible Homopolymers. *Macromolecules* **1990**, *23*, 4780-4787.

5. Shull, K. R.; Kramer, E. J. Mean Field Theory of Polymer Interfaces in the Presence of Block Copolymers. *Macromolecules* **1990**, *23*, 4769-4779.

6. Leibler, L. Block Copolymers at Interfaces. Physica A 1991, 172, 258-268.

7. Noolandi, J.; Hong, K. M. Interfacial Properties of Immiscible Homopolymer Blends in the Presence of Block Copolymers. *Macromolecules* **1982**, *15*, 482-493.

8. Noolandi, J.; Hong, K. M. Effect of Block Copolymers at a Demixed Homopolymer Interface. *Macromolecules* **1984**, *17*, 4531-4538.

9. Wu, S. Polymer Interface and Adhesion. Marcel Dekker: New York, 1982.

10. Lee, H.; Archer, L. A. Functionalizing Polymer Surfaces by Field-Induced Migration of Copolymer Additives. I. Role of Surface Energy Gradients. Macromolecules 2001, 34, 4572-4579.

11. Hu., W.; Koberstein, J. T. Interfacial Tension Reduction in Polystyrene/Poly(dimethylsiloxane) Blends by the Addition of Poly(styrene-b-dimethylsiloxane). *Macromolecules* **1995**, *28*, 5209-5214.

12. Lin, Z.; Kerle, T.; Russell, T. P.; Schäffer, E.; Steiner, U. Structure Formation at the Interface of a Liquid/Liquid Bilayer in Electric Field. *Macromolecules* **2002**, *35*, 3971-3976.

CHAPTER 4

ELECTRIC-FIELD INDUCED DEWETTING AND HIERARCHICAL STRUCTURE FORMATION IN POLYMER/POLYMER/AIR TRILAYERS

4.1 Introduction

One promising approach to lithography in soft condensed matter is to harness and tune the pattern formation methods that are already found in nature, including self-assembly, phase separation, and dewetting processes, to induce controlled pattern formation in thin polymer films. The mechanism and length scale of the process of dewetting of a thin (micrometers in thickness) liquid film from a nonwettable substrate depend on the film's thickness, viscosity, and surface tension, and on van der Waals forces affecting the liquid-substrate interface.[1,2] Similarly, electric fields can be used to induce an instability which depends on the same parameters, plus the permittivity and conductivity of the liquid as well as the strength of the applied field. Several laboratories have recently used electric fields to pattern polymer films on the 100 nm length scale, with potential application to even smaller feature sizes, simply by tuning the properties of the material and the strength of the field.

Previous work by Lin et al.[3] and Morariu et al.[4] showed that when poly(methyl methacrylate) (PMMA) films are covered by polystyrene (PS) films of similar or lower molecular weight, an electric field applied to the PMMA/PS/air trilayer generates fluctuations, first at the polymer/air interface, with the PMMA film remaining relatively unperturbed. In those experiments, the wavelength of the fastest-growing fluctuation amplified by the electric field defined the characteristic spacing of a well-ordered array of PS columns, spanning the electrodes. This column formation process also induced dewetting of PS on PMMA and the formation of a dewetting rim around each column.

Patterning in the PS film was accompanied by a smaller deformation in the PMMA film, occurring primarily at the PS/PMMA contact line, where the PMMA component is drawn up along the PS surface, parallel to the overall electric field. Deformation was also observed in the part of the PMMA film under the dewetting rim. Under a planar electrode, flow of PMMA resulted in concentric pillars after several days, while under an electrode with a topographic pattern of lines, the topographic pattern was reproduced in the PS layer, with a surrounding outline of PMMA. This drawing-up approach to layered, hierarchically ordered structures has the advantage that it results in significantly reduced feature sizes in the pattern after the PS component is removed with a selective solvent. However, it appears that viscosity imposes a strong kinetic restriction on this patterning technique, since several days are required for the PMMA layer to be drawn up most of the way to the upper electrode.

In the experiments of Lin, et al. and Morariu, et al., the behavior of PMMA was nearly solid-like due to its high viscosity relative to the PS layer, and they attribute the lack of an electric field-induced fluctuation at the PS/PMMA interface to interfacial slip. Additionally, since PMMA wets silicon oxide but not PS, fluctuations that would increase the area of the PS/PMMA interface are not energetically favorable, except under the locally high electric field gradient around the contact line. Qu et al.[5] used measurements of dewetting velocities to confirm quantitatively the theoretical predictions of Brochard-Wyart and coworkers.[6] These results suggested that, for liquid/liquid dewetting where $\eta_A/\theta_E < \eta_B$ (η_A and η_B are the viscosities of the upper and lower layer respectively, and θ_E is the equilibrium contact angle between the two liquids), the upper layer dictates dewetting dynamics and morphology, while the lower layer displays solid-

like behavior, similar to the situation observed for the PMMA/PS/air trilayers. However, for $\eta_A/\theta_E > \eta_B$, Brochard Wyart et al. predict a crossover to a regime in which viscous dissipation occurs mostly in the lower layer, which therefore controls dewetting dynamics.

The inverted configuration, in which PS is initially spread on the silicon substrate and there is a PMMA/air interface subject to electric field-induced instability, was not shown or discussed. In that configuration, both PS/PMMA dewetting and PS/silicon oxide dewetting are energetically favorable and can be initiated by an electric-field induced fluctuation amplification. Understanding the concerted effects of dewetting at the substrate and polymer/polymer interface and electrostatic pressure at the polymer/polymer and polymer/air interfaces may lead to a better fundamental understanding of the liquid/liquid interface. In this work, results are shown for experiments that begin with a PS film sandwiched between a silicon substrate and a layer of PMMA. Also, it is shown that the degree to which the viscosity of the polymer film at the substrate is smaller than that of the upper layer has a strong effect on the morphology of structure formation. Several unique three-dimensional microstructures are made possible by tuning electric-field induced fluctuations in concert with dewetting. The combined effects of increasing polymer mobility by lowering viscosity and changing polymer-electrode surface interactions strongly enhance the kinetics of structure formation, resulting in much faster patterning than achieved in prior studies.

4.2 Experimental Methods

Films of PS and PMMA, having the molecular weights shown in Table 4.1, were spin coated onto polished silicon substrates from solutions in toluene or, when a selective solvent was required to deposit the upper layer, cyclohexane and acetic acid, respectively. Prior to spin coating, the silicon substrates were cleaned in concentrated sulfuric acid and inorganic oxidizers. All of the polymer films were uniformly smooth (±1 nm over the 1 x 1 cm^2 sample area) and measured by spectral interferometry to have thicknesses of 500 nm (±10nm). Trilayer systems were assembled using the silicon substrate as one electrode and a soda-lime glass slide coated with chromium for the other, as shown in Figure 4.1 . Using a polymer mask at the edges of the slide, a rectangular well was etched by immersing the glass slide in buffered hydrofluoric acid. The electrode spacing was varied between experiments by varying the etching time to control the depth of the well, which was measured using a contact probe profilometer (Veeco Dektak 3). Soda-lime glass contains mobile sodium ions, therefore preventing decay of the electric field over the thickness of the glass slide, so that the electric field gradient is entirely across the air gap and polymer films. Furthermore, flow of electrons, is prevented. The voltage was applied and the films heated to 170 °C, well above their glass transition temperatures, for 1.5 to 3 hours. Following each experiment, the upper electrode was removed and the film on the silicon substrate was broken into three sections for selective solvent washing. One section was rinsed with acetic acid to remove the PMMA component, another was rinsed with cyclohexane to remove the PS component, and the third was not rinsed. Finally, optical and electron microscopy of the films were performed and comparisons were made between each set of three images to determine the overall morphology.

Table 4.1 Characteristics of the Polymers Used In This Study

	M_w (g/mol)	M_w/M_n	Viscosity (Pa s) at 170C *	Dielectric Constant
PS	7,700	1.09	24	2.95
PS	157,000	1.04	7.3×10^4	2.95
PMMA	32,000	1.61	2.3×10^5	5.24
PMMA	99,000	1.04	9.2×10^5	5.24

* PS viscosities calculated from reference 7; PMMA viscosities measured using a TA Instruments AR2000 Rheometer.

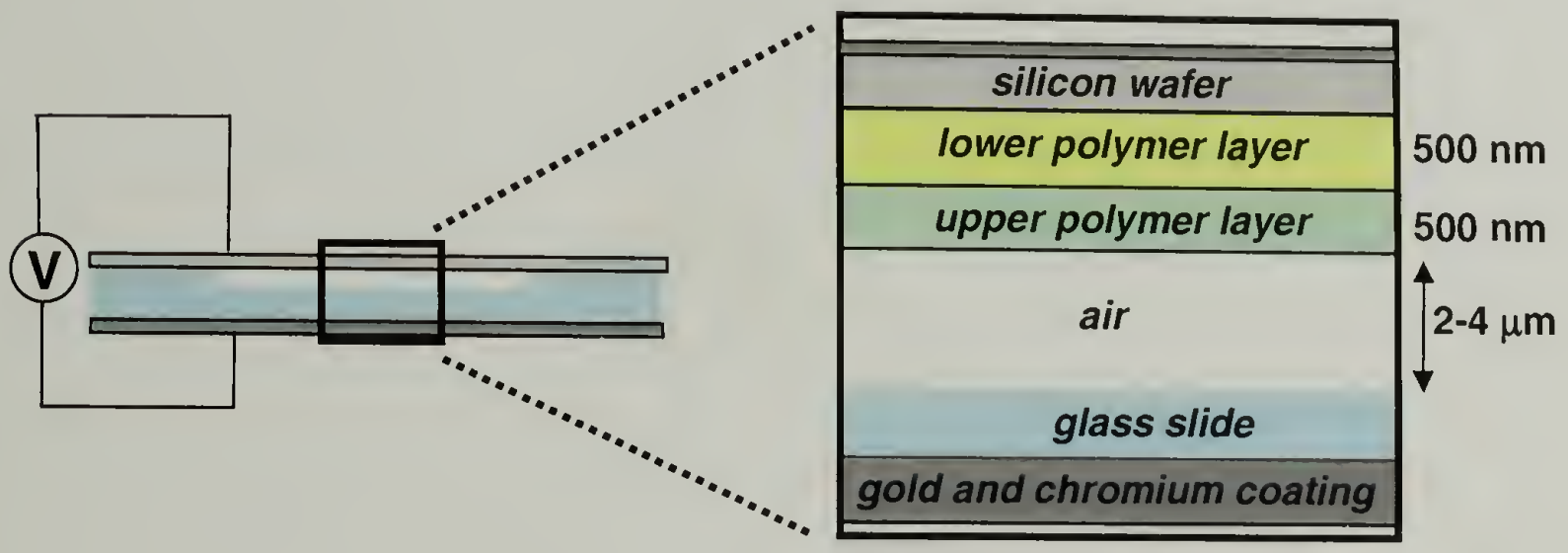

Figure 4.1 Experimental Schematic

4.3 Results and Discussion

For this study, the relative viscosity of the two layers was varied. Among the experiments discussed here, three viscosity ratios are represented: $\eta_A/\eta_B = 3$, $\eta_A/\eta_B = 1 \times 10^3$ and $\eta_A/\eta_B = 4 \times 10^5$, where η_A denotes the viscosity of the upper layer, and η_B that of the lower layer. For PS/PMMA/air trilayers, these viscosity ratios correspond to M_w

ratios of 0.2, 4.2, and 13, respectively. In contrast to previous work, in which the lower layer was nearly solid-like due to its higher viscosity relative to the upper layer, the lower layer behaves, to varying degrees, like a liquid relative to the upper layer.

First, we consider the dewetting process which occurs without the presence of an applied electric field. Film thicknesses were approximately 500 nm and, therefore, expected to be metastable without the application of an electric field. Without an applied external field, dewetting should proceed only by heterogeneous nucleation and growth of holes rather than spinodal dewetting[8]. Figures 4.2 (a) and (b) show optical microscopy of a 500 nm thick 32k PMMA film on top of a film of 157k PS which has been heated to 170C for 7 days under nitrogen. Figure 4.2 (c) shows an AFM scan of the dewetting rim before and after rinsing with acetic acid. For this pair of polymers, the viscosities of PS and PMMA are on the same order of magnitude: $\eta_A/\eta_B = 3$. The overall appearance of the bilayer is consistent with dewetting by nucleation of holes by heterogeneities followed by the expansion in radius of a dewetting rim. However, the upper PMMA layer displaces the PS component at the substrate, along the rims of the dewetting pattern. The upper film of PMMA appears to have penetrated into the lower film of PS along the contour of the dewetting pattern. A film of PS, annealed under the same conditions as the inverted bilayer, showed dewetting rims with a much smaller radius, while a PMMA film under the same conditions showed no evidence of dewetting.

Observation of layer inversion by dewetting liquid/liquid bilayers has been reported for PS/PMMA[9] and PS/PVP[10]. In both pairs, the polystyrene layer was initially placed at the silicon substrate while the more polar polymer was at the surface. The

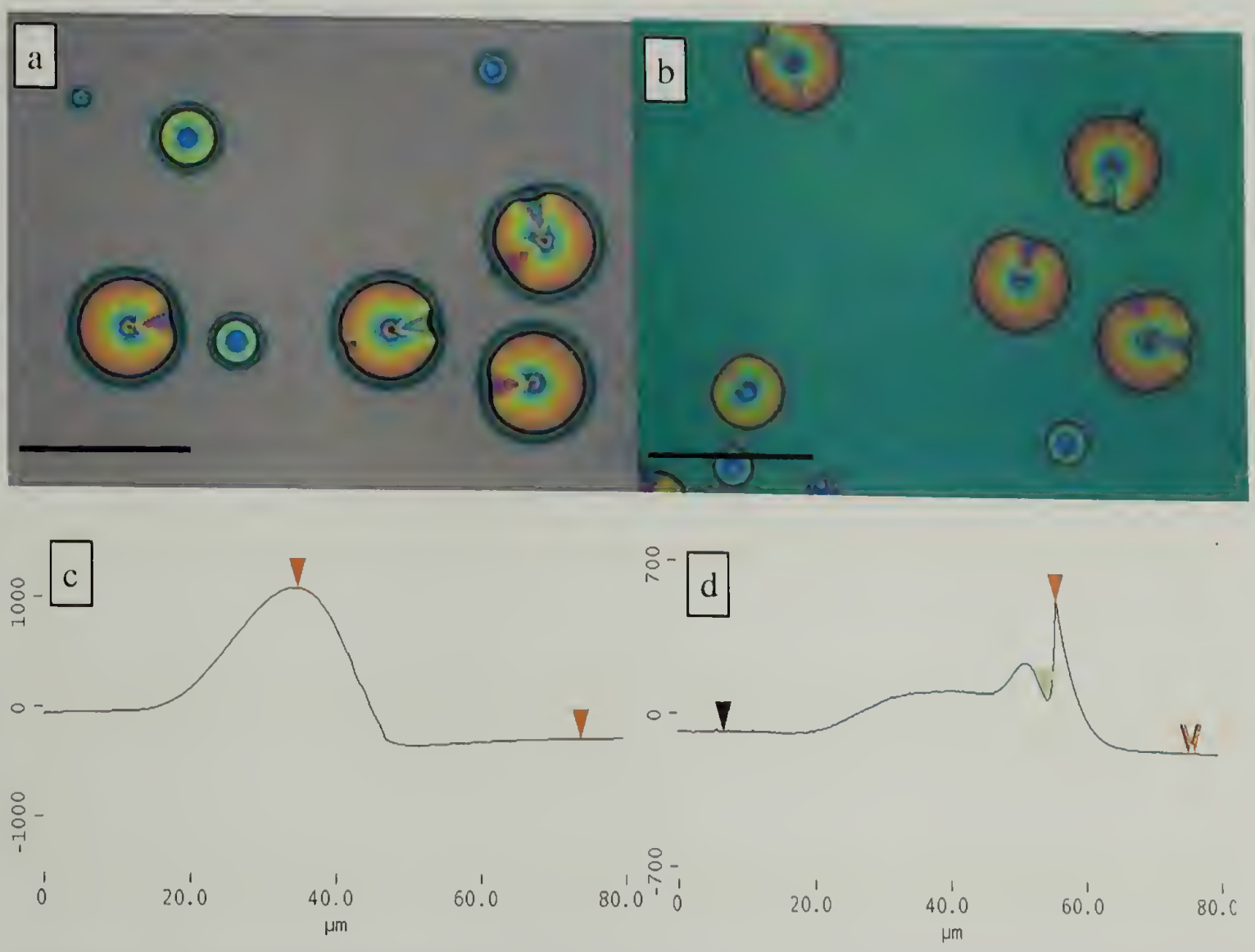

Figure 4.2 Micrographs of PS/PMMA bilayer films annealed without an applied electric field. Scale bars are 0.5 mm. (a) Bilayer after annealing (b) After washing with acetic acid (c) AFM profile of the dewetting rim of the bilayer after annealing (d) After washing with acetic acid

driving force for inversion when gravitational effects are negligible, as they are for films of these thicknesses, is Laplace pressure generated by wetting conditions for which either the upper layer preferentially wets the substrate or the lower layer is strongly preferred at the air surface. The effect of such conditions on polymer films has been studied for blends and films of block copolymers[11], as well as block copolymers in electric fields[12,13]. In particular, the latter studies have shown that preferential surface segregation is difficult to overcome even with strong external electric fields. However, the results of previous studies on bilayer films imply that the kinetics and morphologies of layer inversion depend significantly on the difference in the thicknesses and viscosities.

Electric field-induced instabilities provide a way to control the dewetting and inversion process and to incorporate surface-segregated structures into highly periodic arrays. When a voltage was applied to the inverted configuration of layers discussed above, the resulting morphology of the structures exhibited a significant dependence on the strength of the applied electric field. The electrostatic pressure significantly diminishes as the electrode spacing is increased, while the capillary pressure influencing dewetting does not. The amplitude of electric field-induced fluctuations has been shown to increase exponentially at early times, followed by acceleration at later times. [14] The characteristic time scale for the initial period of exponential growth is even more strongly nonlinear in its dependence on the electric field strength. As in the studies by Lin et al. and Morariu et al., the observed structures result from a competition between the kinetics of capillary and electrohydrodynamic instabilities.

We consider the case where the strength of the electric field is low, shown by Figure 4.3(a), for 157k PS/32k PMMA/air in a 5 μm gap and 136V applied voltage. In this case, PMMA dewetting is likely to be nucleated by a heterogeneity before electrohydrodynamic instabilities are significantly amplified at either the polymer/air or polymer/polymer interface. The propagation of the nucleated hole forms a dewetting rim at the hole's edge. In this case, electrohydrodynamic instabilities are strongly amplified at

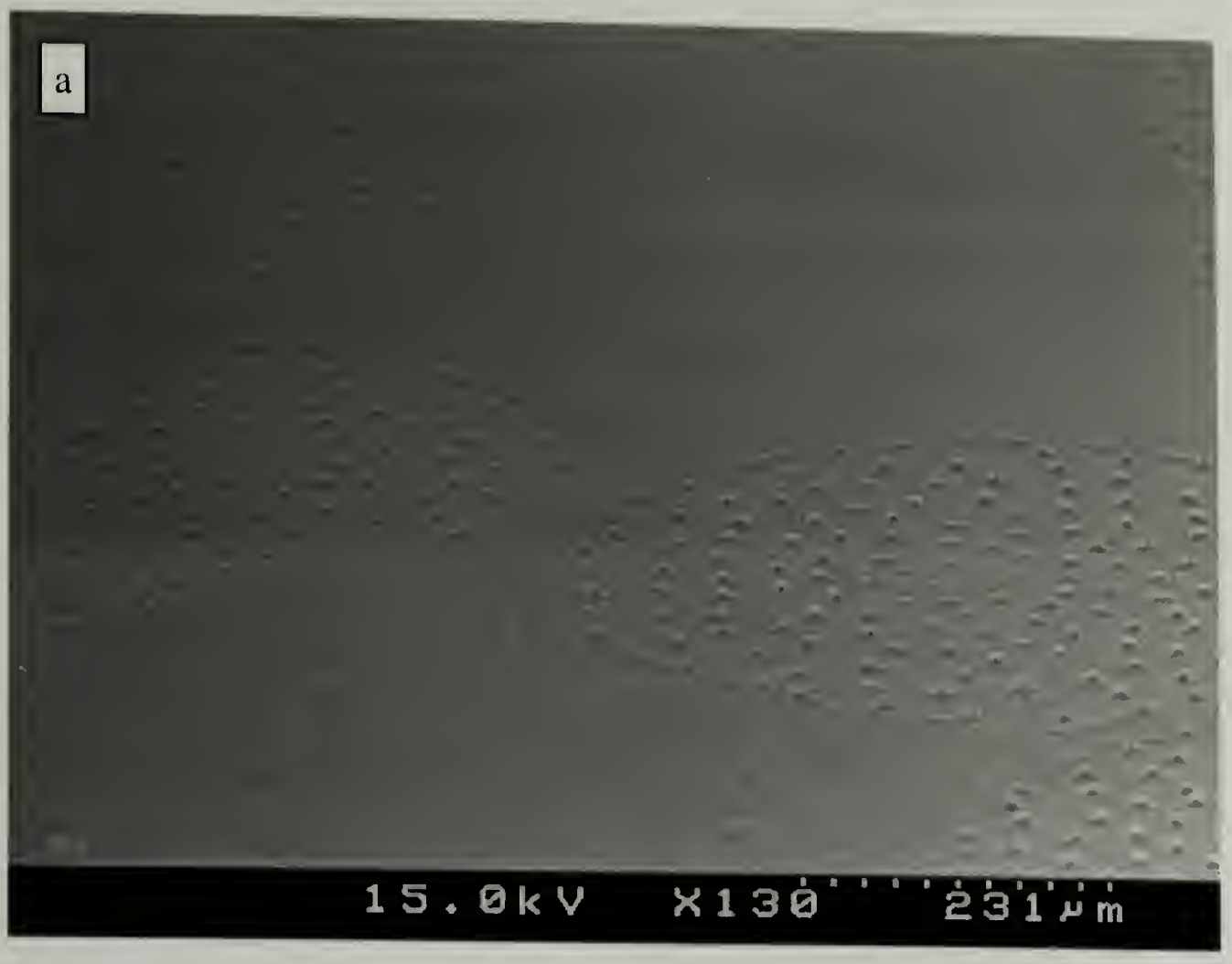
a
15.0kV X130 231µm

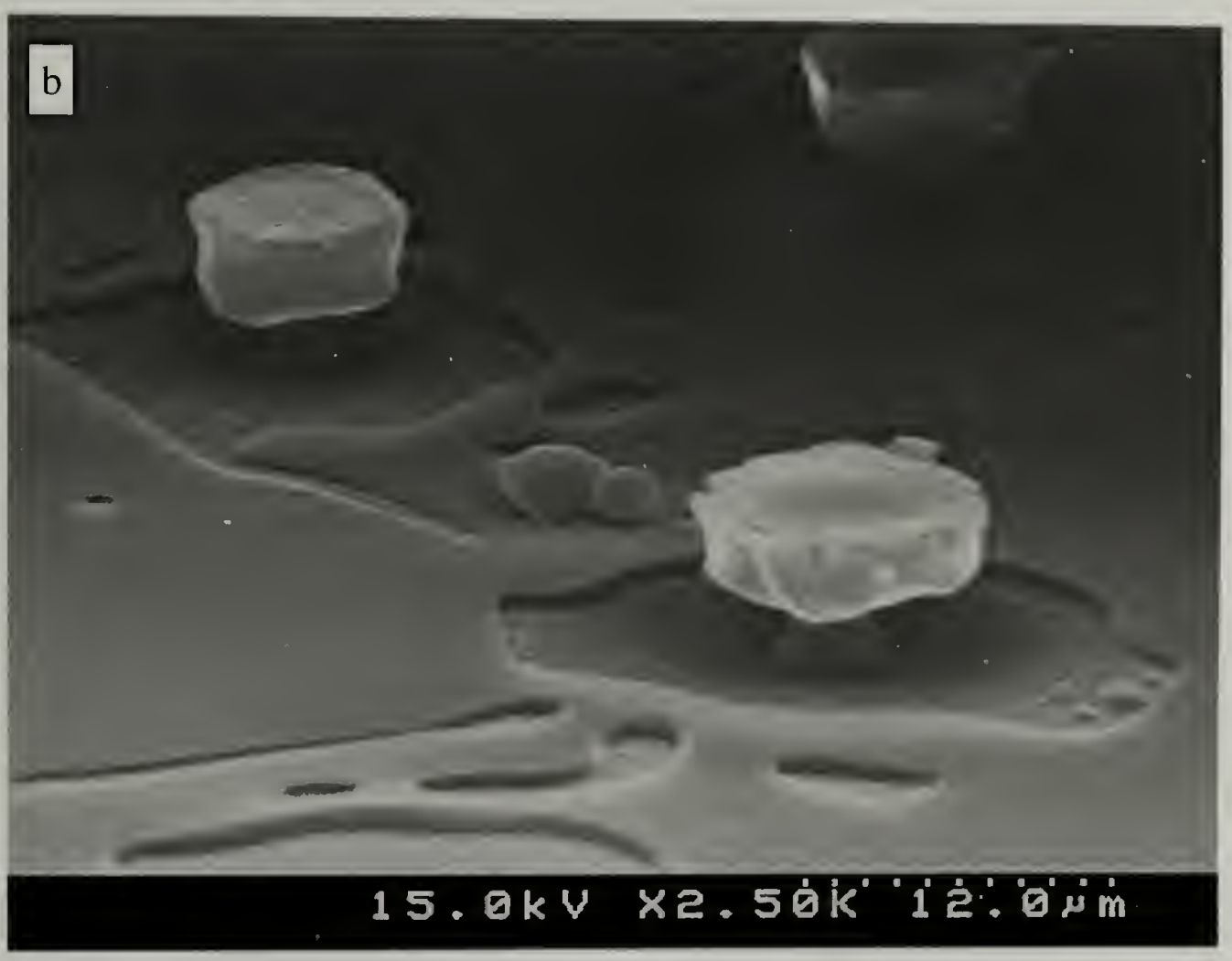
b
15.0kV X2.50K 12.0µm

(continued)

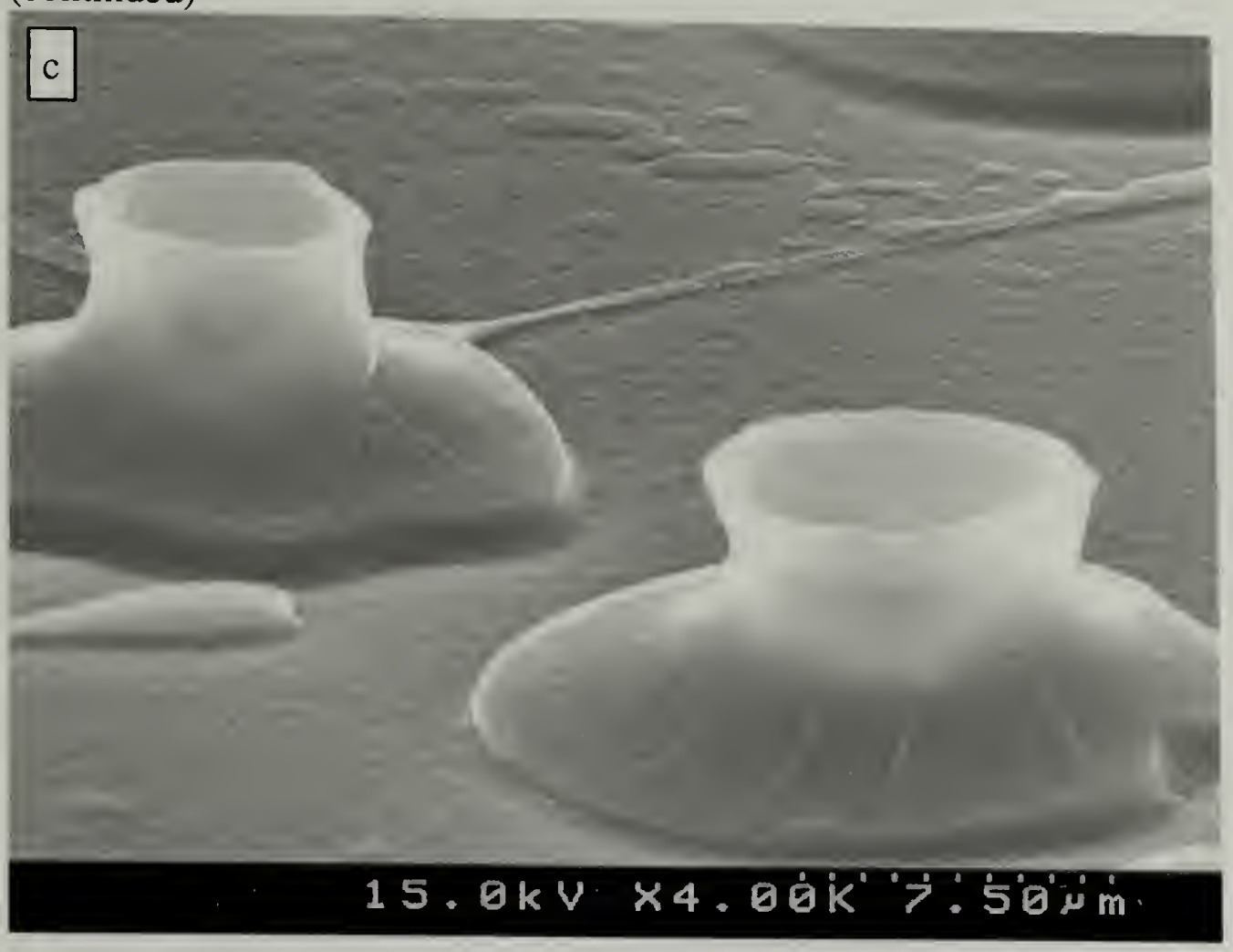

Figure 4.3 SEM of 170k PS/25k PMMA/air in a 5 µm electrode spacing, 136 V field (a) Prior to selective solvent treatment (b) After rinsing with acetic acid (c) after rinsing with cyclohexane.

the crest of the moving dewetting rim, where the PMMA film is thickest. As the rim moves outward from the nucleation center, circular rows of pillars form. The spacing of these pillars along the circumference of the rim is approximately 15-25 µm, compared to a theoretical value of 31 µm, predicted using the analysis of Schäffer et al.[15,16], as the wavelength of the fastest growing electrohydrodynamic fluctuation. The equation relating wavelength, λ, to the applied voltage, U, surface tension, γ, dielectric constant, ε_P, permittivity in a vacuum, ε_0, and the electric field at the polymer-air interface, E_P, is shown below.

When the PMMA component is removed by acetic acid washing, a different morphology is seen, as shown in Figure 4.3(b). The pillars of polystyrene are

disconnected from the continuous PS film, and resemble flattened mushrooms. In this morphology, the PS pillars are supported by small central 'stems' of PS. The complementary morphology of PMMA, shown in Figure 4.3c, is seen by washing with cyclohexane. The PMMA component surrounds the PS 'stems' and form mounds around the pillars, displacing PS from the area near the pillars. Like the PS component of the pillars, the PMMA parts of the pillars are mostly disconnected from other PMMA domains in the sample, although some thread-like connections are visible. The inversion of the layers of PS and PMMA within the columns produced by the electric field is expected from the preferential wetting of PMMA on the substrate. Furthermore, there is a stronger attraction of the PMMA layer for the substrate due to its significantly larger dielectric constant than PS. However, as in the case of no applied field, inversion requires initiation by a perturbation at the polymer/polymer interface. The early stages of liquid/liquid dewetting have been shown by Qu et al. and Kang et al. to cause fluctuation and thinning of the lower layer when it has a lower viscosity than the upper layer. It is reasonable, therefore, that dewetting of PS from the silicon substrate was induced by fluctuation-induced dewetting according to the lateral length scale of the electrohydrodynamic instability at the PMMA/air interface. Later, however, interfaces parallel to the electric field lines, such as the PMMA/air interface of the sides of the pillar and the PS/PMMA interface around the "stem" of PS are stabilized by the electric field.

In the second case of development of electrohydrodynamic instabilities in a 32k PMMA/157k PS/air trilayer, the electrode gap has been decreased to 3 μm and the applied voltage kept the same. Homogenous nucleation of fluctuations appears everywhere at the polymer-air interface, as shown in Figure 4.4(a). The wavelength of the

fastest growing fluctuation can be determined from the characteristic center-to-center spacing of the pillars shown in the film, found to be 12-15 μm, compared to the predicted wavelength of 11.9 μm. Removing the upper layer with acetic acid shows that, at early stages of development, fluctuations in the lower film have the same characteristic wavelength as those in the upper film.

An interesting feature is clearly shown in the troughs of the fluctuations in the PS film. Shallow holes have opened in the PS film (Figure 4.4(b)), that are not apparent in the PMMA film (Figure 4.4(d)). These holes must have been filled with PMMA before the bilayer was washed with acetic acid. In the troughs, one possibility is that the PS film may be thin enough to dewet from the substrate by fluctuations at the PS/PMMA interface and at the substrate, and then be replaced by PMMA, that, at the same time, dewets from the PS/PMMA interface. The important effects being shown here are the liquid-like behavior of the lower layer, the unfavorable interactions between the lower layer and the substrate, and the electrostatic attraction of PMMA to the silicon substrate. Compared to previous work, where fluctuations in the lower layer were not observed during the development of electrohydrodynamic instabilities in the upper layer, the switch of PS with PMMA for surface is not expected to have a large effect on the tendency for the upper film to dewet the lower film, since the two polymers have similar surface tensions (27.8 mN/m for PS vs 28.9 mN/m for PMMA, from reference 17.) Furthermore, the wavelength and characteristic growth constant predicted by the linearized models of electrohydrodynamic instability for PS/air and PMMA/air interfaces do not vary greatly for a change in dielectric constant from 2.95 for PS to 5.24 for PMMA (at 170C). Placing a lower dielectric constant material between PMMA and the

substrate does, however, yield a significant pressure on the PMMA/PS interface to deform.

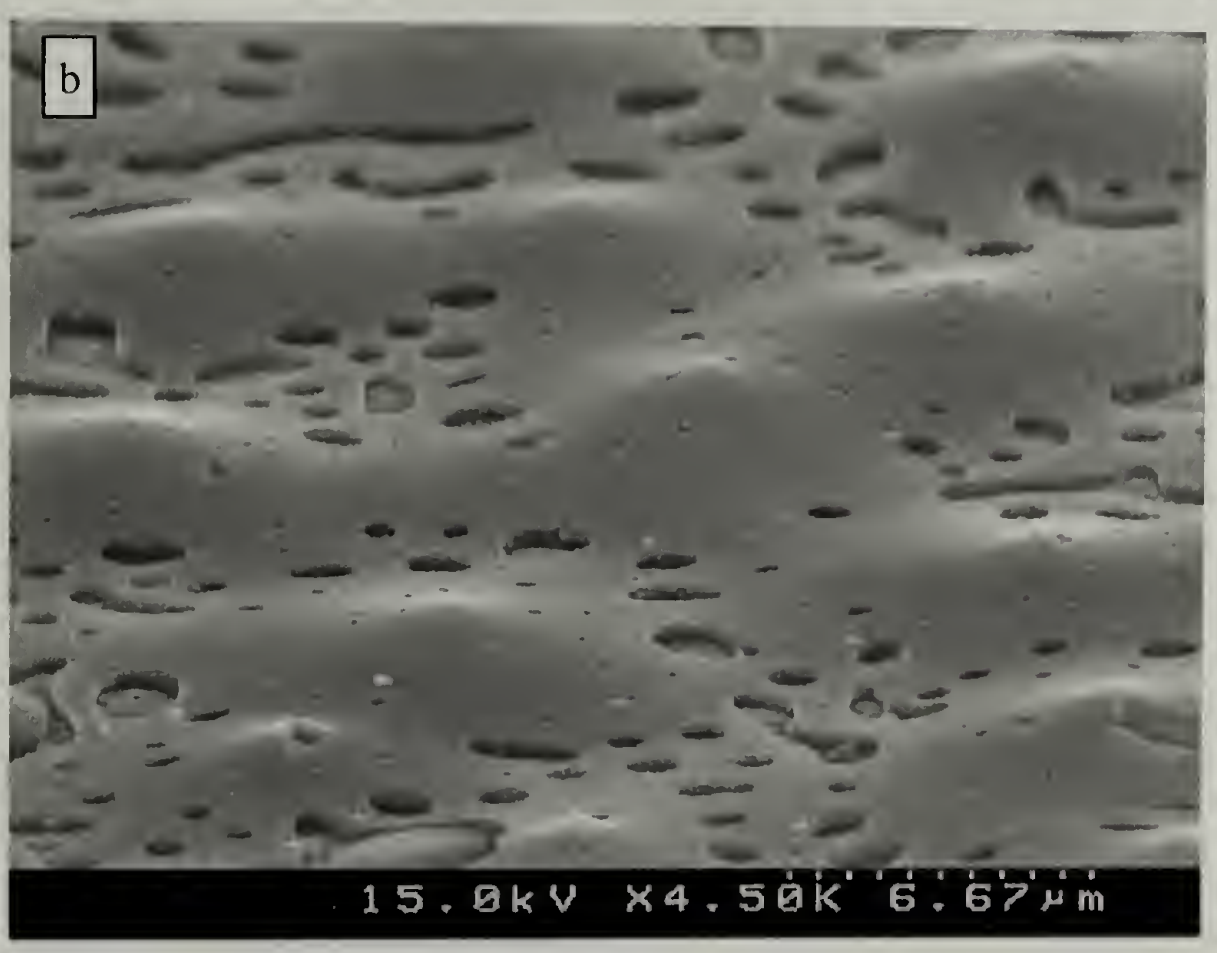

(continued)

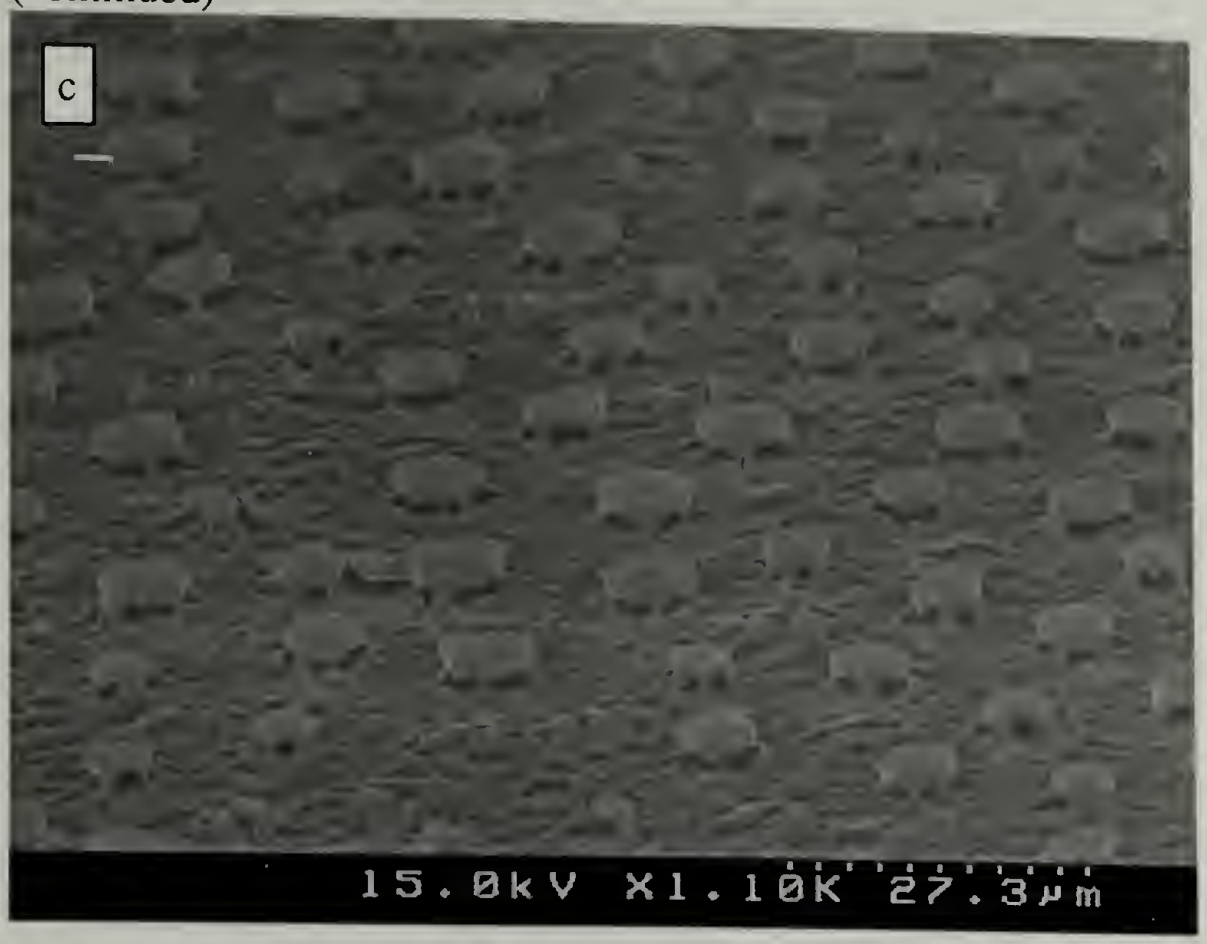

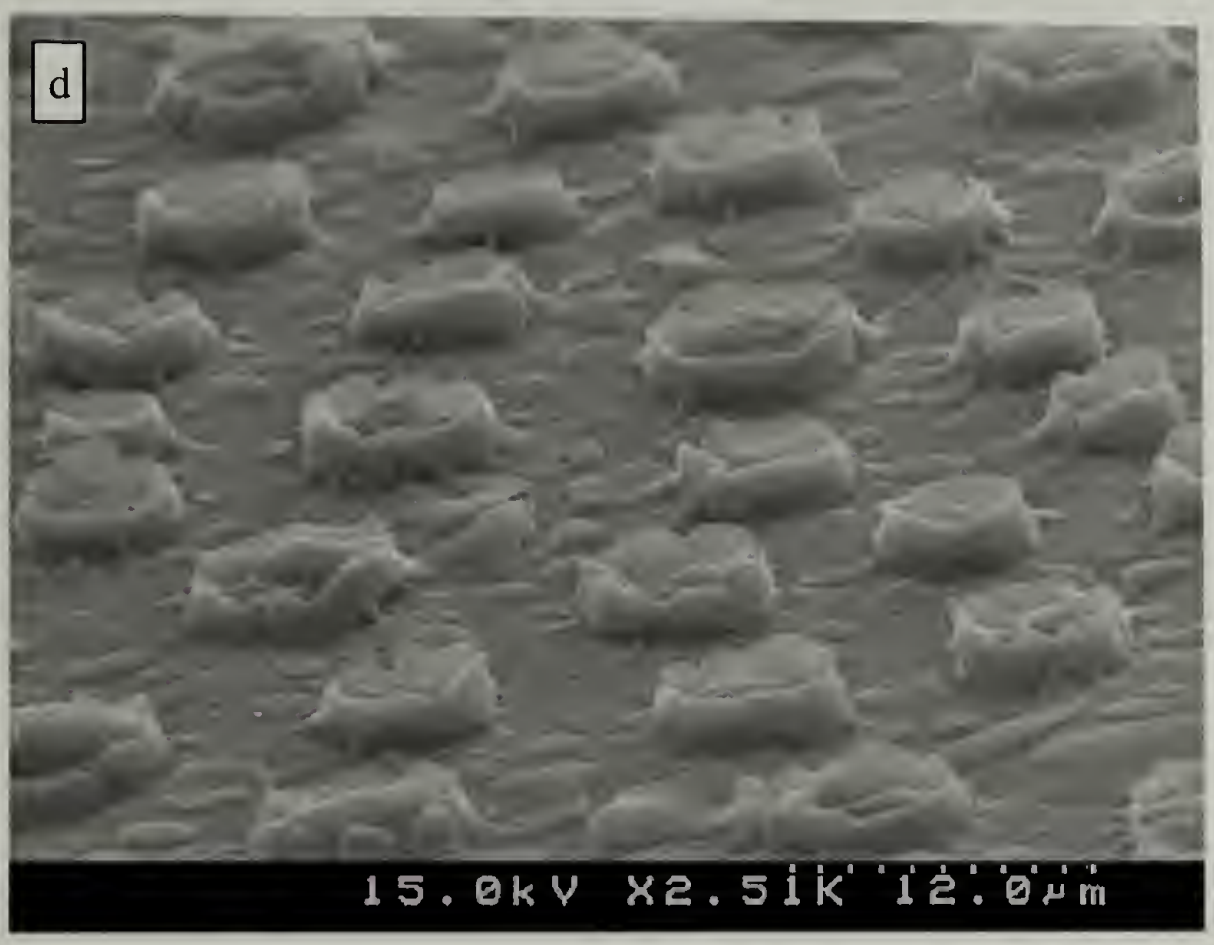

Figure 4.4 SEM of 170k PS/25k PMMA/air in a 3 µm electrode spacing, 136 V field (a) Prior to selective solvent treatment (b) After rinsing with acetic acid: early stages of fluctations (c) After rinsing with acetic acid: later stages of fluctations (d) After rinsing with cyclohexane.

If the evolution of fluctuations in the 157k PS/33k PMMA/air films continues, the peaks contact the upper electrode and spread on the upper electrode's surface (Figure 4.4(c)). At the same time fluctuations at the polymer-air interface are growing in amplitude, the holes in the PS film in the troughs of the fluctuation appear to coalesce (Figure 4.4(d)) allowing PMMA to spread further onto the substrate. Washing with cyclohexane (Figure 4.4(e)) shows that the upper PMMA film displaces the PS film especially underneath the growing peaks. The final morphology shows a PS pillar supported by a base of PMMA which has an irregular rim around the edges of the pillar. Some PS is left at the substrate, but most has been displaced by the PMMA component.

Next we consider a bilayer where the lower PS film has a much lower viscosity than the upper PMMA, with $\eta_A/\eta_B \sim 10^5$. For an air/99k PMMA/7.7k PS system in a 5 μm electrode gap and 136 V applied voltage, electric field-induced fluctuations at the air/PMMA interface, shown in Figure 4.5(a), have the same wavelength as the fluctuations at the PMMA/PS interface which are revealed by acetic acid washing. In these experiments, holes in the PS layer from dewetting of the substrate did not form. The final morphology of the pillars formed by amplification of the fluctuations showed an irregular disc of PMMA remaining at the upper electrode, on top of a PS pillar which is still connected to the underlying continuous PS film (Figure 4.5(c)). The PMMA disc is separated from the rest of the PMMA component, which remains as a continuous film, except for some small strands of PMMA extending from the upper PMMA disc to the substrate.

The disc and strand-like features originate from the break-up of the PMMA film surrounding the PS pillar. The amplification of electric field-induced fluctuations causes

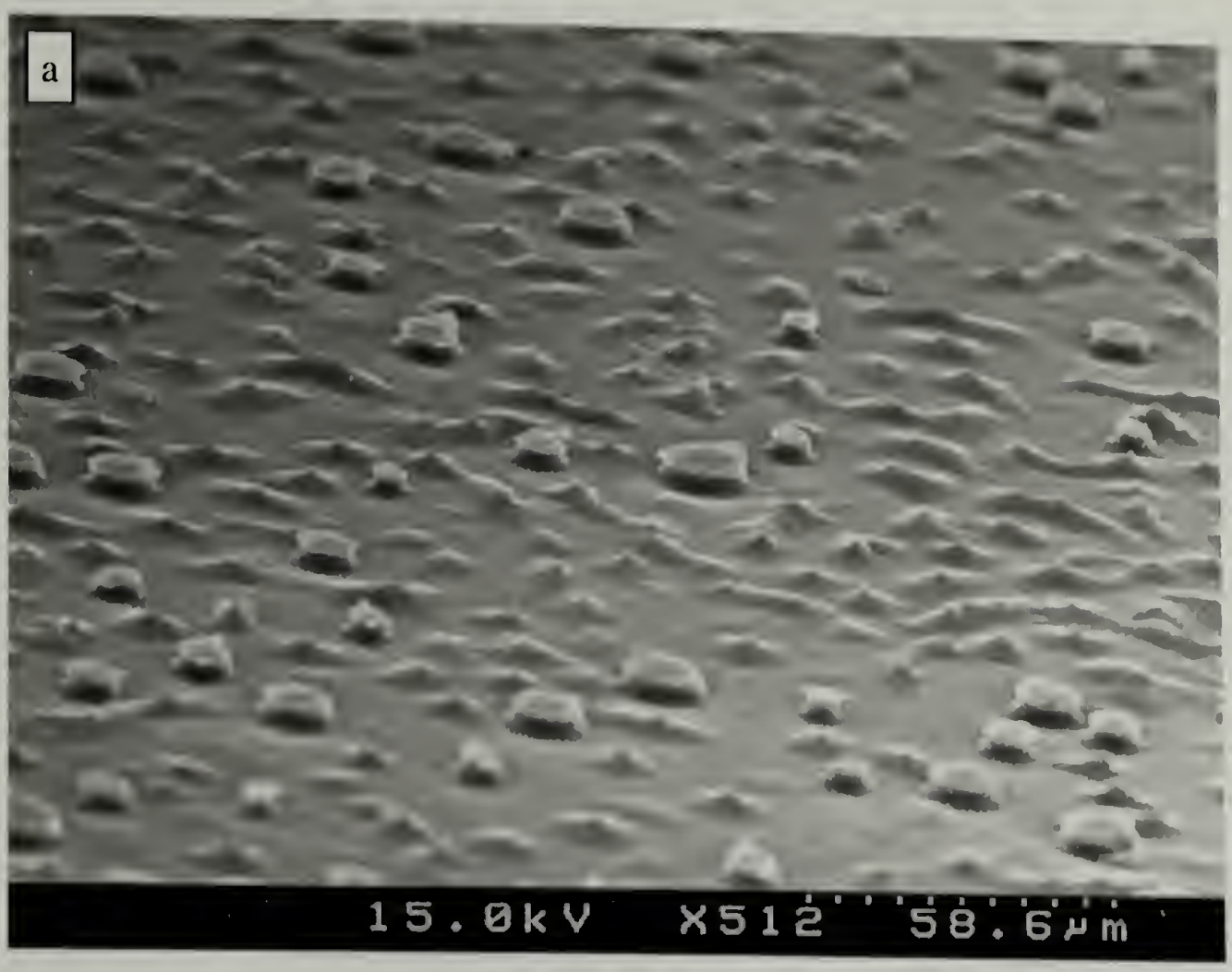
a
15.0kV X512 58.6µm

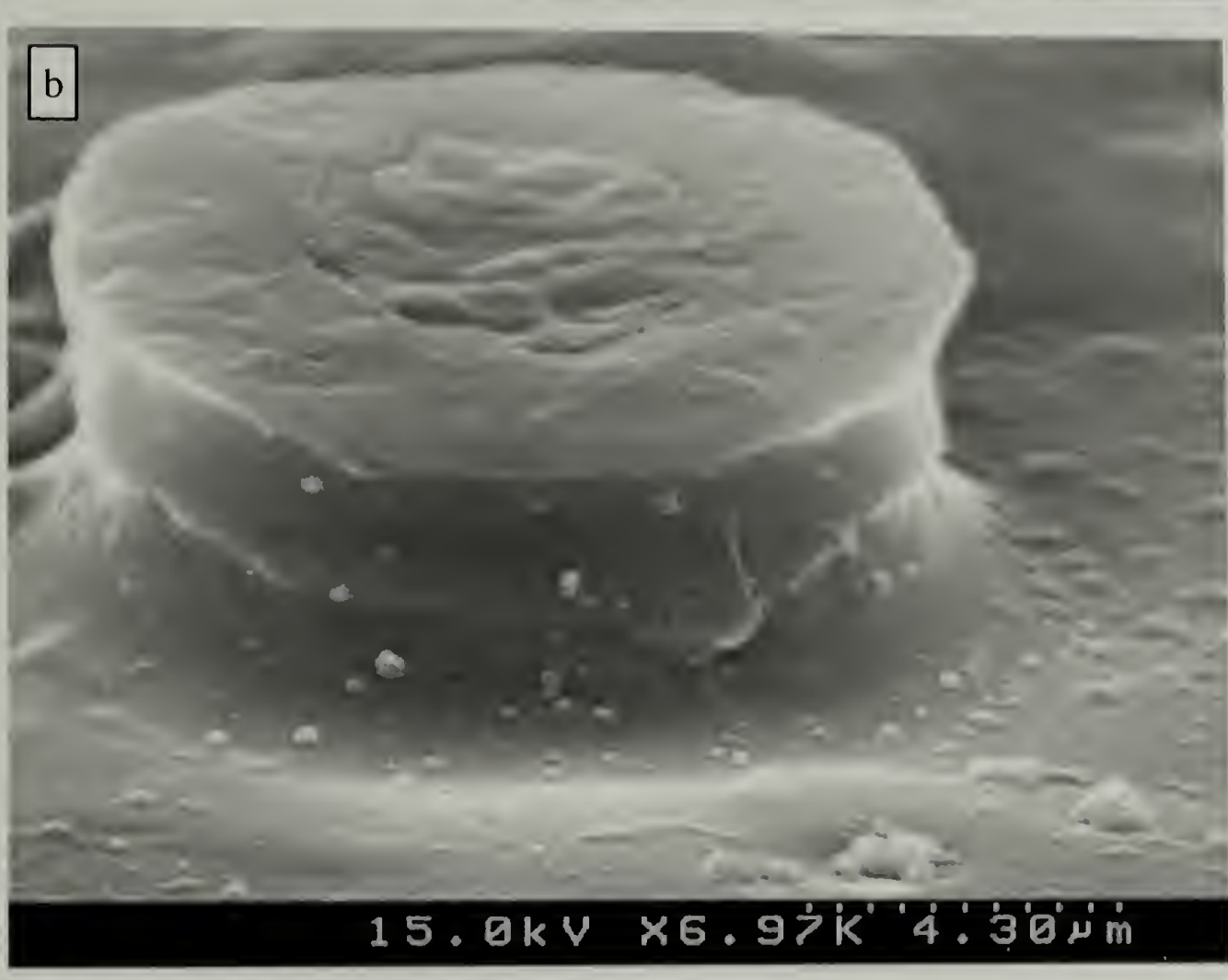
b
15.0kV X6.97K 4.30µm

Figure 4.5 SEM of air/100k PMMA/9k PS in a 5 µm electrode spacing, 136 V field (a) Prior to selective solvent treatment (b) After rinsing with acetic acid (c) After rinsing with cyclohexane.

the amplitude to increase exponentially with time at first and then accelerate towards the electrode. Although the PMMA film remains intact during the accelerating growth process, followed by spreading of pillar at the surface of the upper electrode, it finally dewets from PS around the edges of the pillar. The kinetics of dewetting, then are slow for this high molecular weight PMMA, especially relative to the low molecular weight PS. When PMMA dewets from the PS component at the edges of the pillar, it leaves behind a disc of PMMA due to preferential wetting on the upper electrode, even though electrostatic pressure does not promote the formation of interfaces perpendicular to the electric field lines. A residual layer of PMMA was also noted by Morariu et al. for the hierarchical structures formed in PMMA/PS/air trilayers, due to preferential wetting.

It was found that, when the electrode spacing for the 7.7k PS/99k PMMA/air system was decreased to 3 µm, shown in Figure 4.6(a), the isolated discs of PMMA were

no longer formed, and the PS component formed pillars that were completely detached from the substrate, as shown in Figure 4.6(a) and (b). The PMMA component, in Figure 4.6c, shows slightly elevated rims around the pillars and forms bowl-shaped bases under the the pillars. Apart from the pillars, the film appeared continuous and smooth, with some peaks where fluctuations had not yet spanned the electrodes. Where pillars formed, it appears that the film inverted, with PMMA covering the silicon oxide surface, from which PS was completely removed.

Since the characteristic time associated with the exponential growth in the electric field-induced fluctuations scales inversely with the sixth power of the gap distance[18], one might expect that, upon decreasing the electrode spacing from 5 μm to 3 μm, dewetting would occur more slowly than pillar formation. In fact, the more rapid growth of fluctuations appear to enhance dewetting, possibly due to increased slip between the layers. Due to the extreme viscosity mismatch between the polymers, slip at the fluctuating polymer/polymer interface is likely. The resulting morphology shows beautiful cylindrical symmetry, suggesting rupture of the PMMA film was initiated at the peak of the growing fluctuation, before contact with the upper electrode was made. If contact with the upper electrode is made before layer inversion, a more irregular boundary at the rim would be expected, similar to the result for larger spacings. Because the peak of fluctuations at the PS/PMMA interface are the locations of greatest curvature, these could be the nucleation points for PMMA dewetting PS. Propagation of the hole in the PMMA film away from the peak tip would result in exactly the rim shape which is shown in the Figure 4.6(c). Layer inversion must occur before pillar formation, since after the peak makes contact with the upper electrode, electrostatic

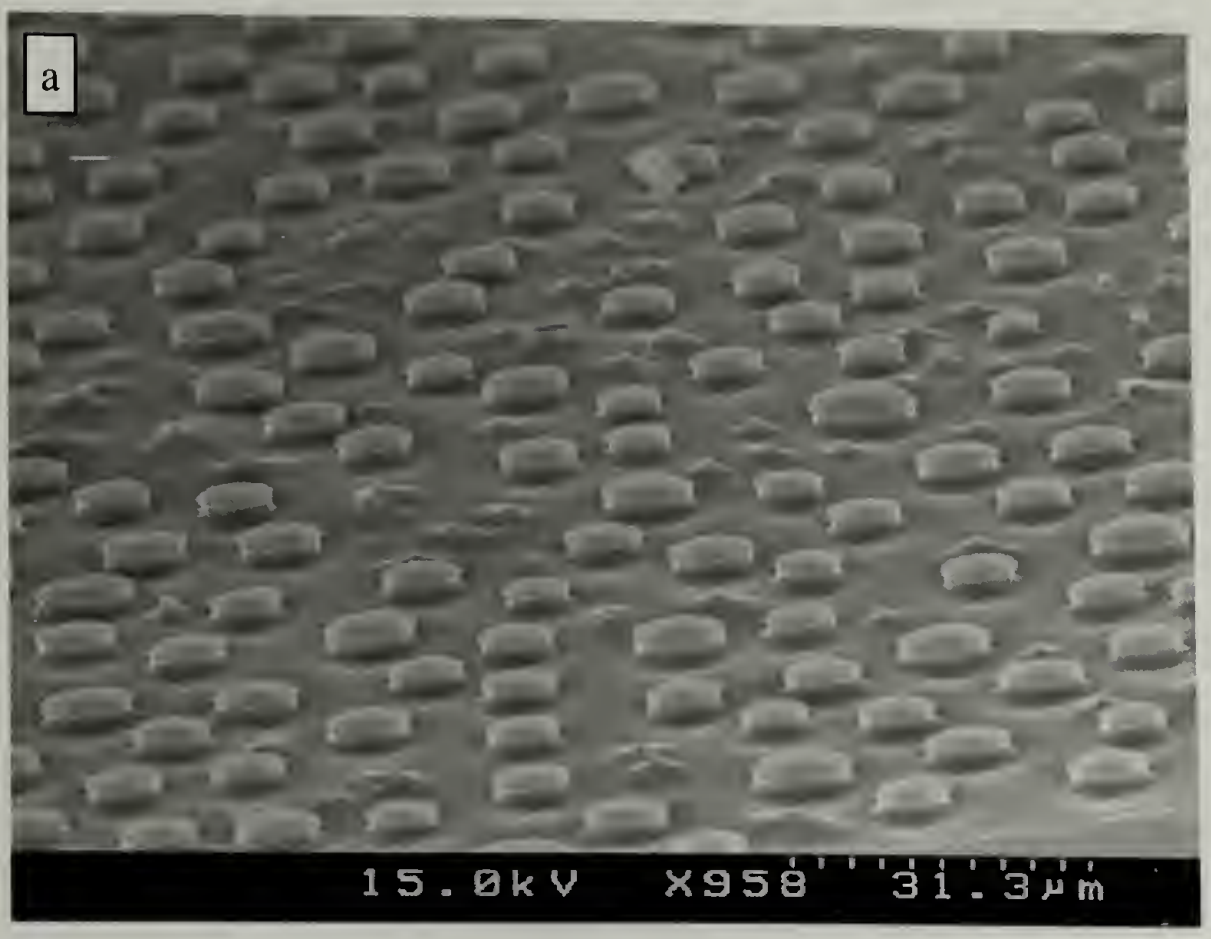
a
15.0kV X958 31.3µm


b
15.0kV X1.80K 16.6µm

(continued)

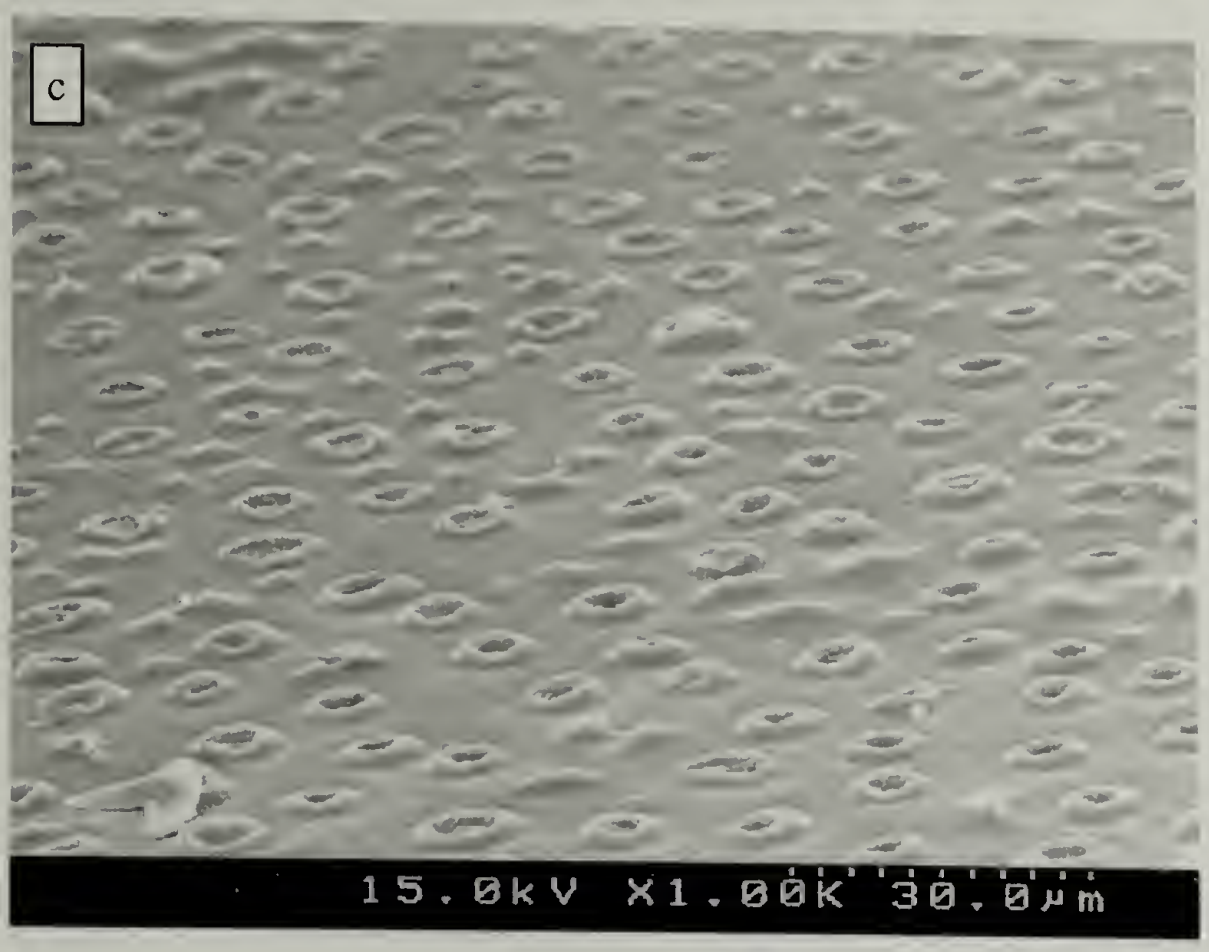

4.6 SEM of air/100k PMMA/9k PS in a 5 µm electrode spacing, 136 V field
(a) Prior to selective solvent treatment (b)After rinsing with acetic acid
(c) After rinsing with cyclohexane.

pressure would strongly oppose inversion, since this would require the creation of interfaces normal to the electric field gradient. At the lower electrode, dewetting of PS from the silicon substrate generates a three-phase contact line between PS, PMMA and the substrate. Since PMMA preferentially wets the substrate, it is energetically favorable for a thin layer of PMMA to replace PS at the substrate.

Finally, we examine a slightly lower molecular weight of PMMA on the same PS molecular weight, the 7.7k PS/32k PMMA/air system in a 3µm electrode spacing (Figure 4.7(a)-(c)), for which $\eta_A/\eta_B = 10^3$. The PS component again forms pillars which are isolated from each other, but in this case they are not displaced from the substrate. The PMMA component in this system spreads on the silicon substrate everywhere *except*

underneath the PS pillars. In further contrast to the behavior of the higher molecular weight of PMMA, the PMMA film remains continuous so that it now encapsulates the PS cylinder, except for the base. Unlike the system involving the higher molecular weight of PS, a smaller radius 'stem' does not support the PS pillar off the substrate The rapid rate of electric field induced fluctuation has stabilized the concentric PMMA/PS pillar before dewetting of PS from the substrate induced layer inversion. Thus, as with the other morphologies, the competition between kinetics of PS dewetting and electro-hydrodynamic instabilities govern the morphology.

This morphology results in a polymer/polymer interface very close to the upper electrode, similar to the situation in which the PMMA layer formed a cap on top of the PS pillar. In the sections rinsed with acetic acid to remove PMMA, holes in the the top of the PS pillars were sometimes observed (see Figure 4.8(a)), complemented by tapered columns of PMMA inside the PS pillar(see Figure 4.8(b)), extending down to the silicon wafer, visible in the sections where cyclohexane had been used to remove PS. Formation

(continued)

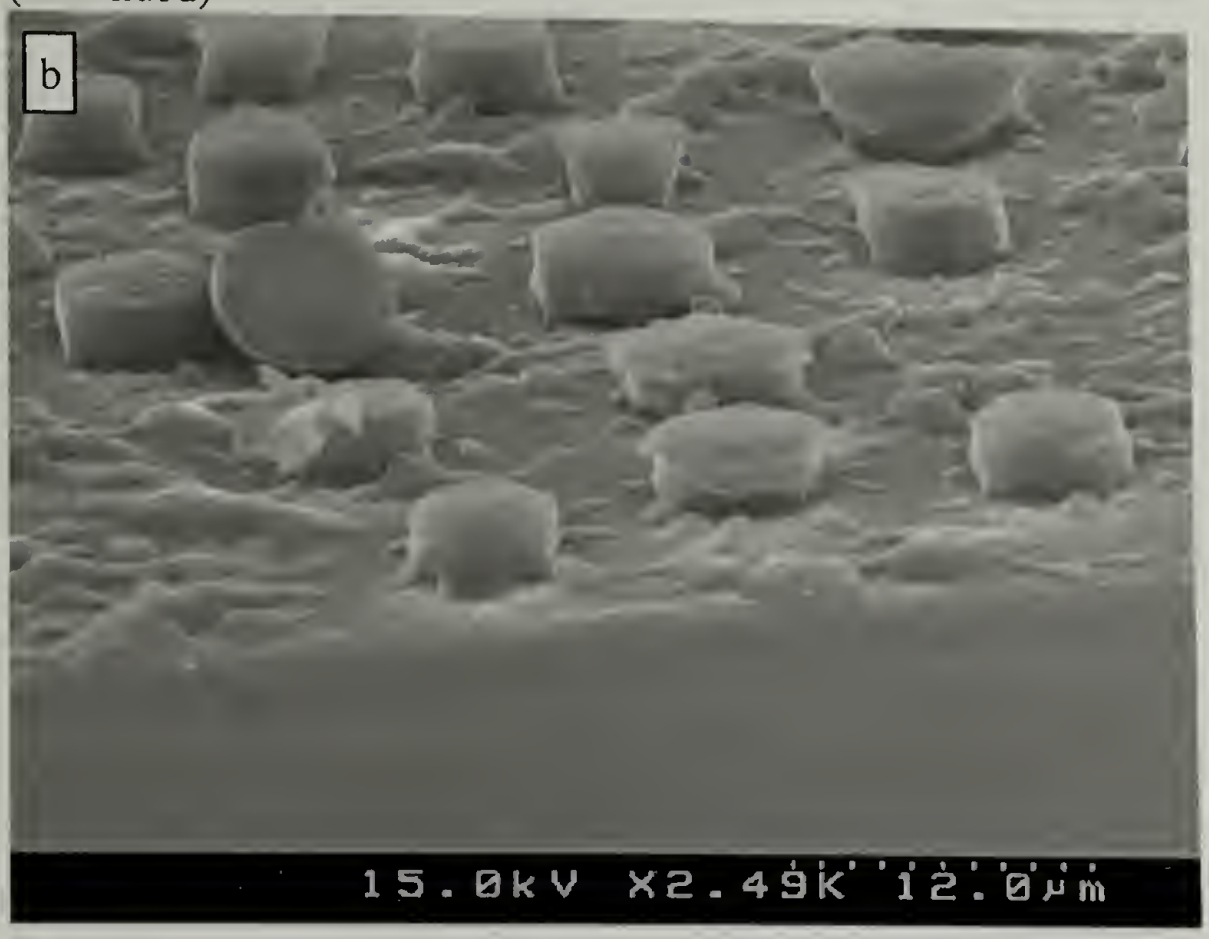

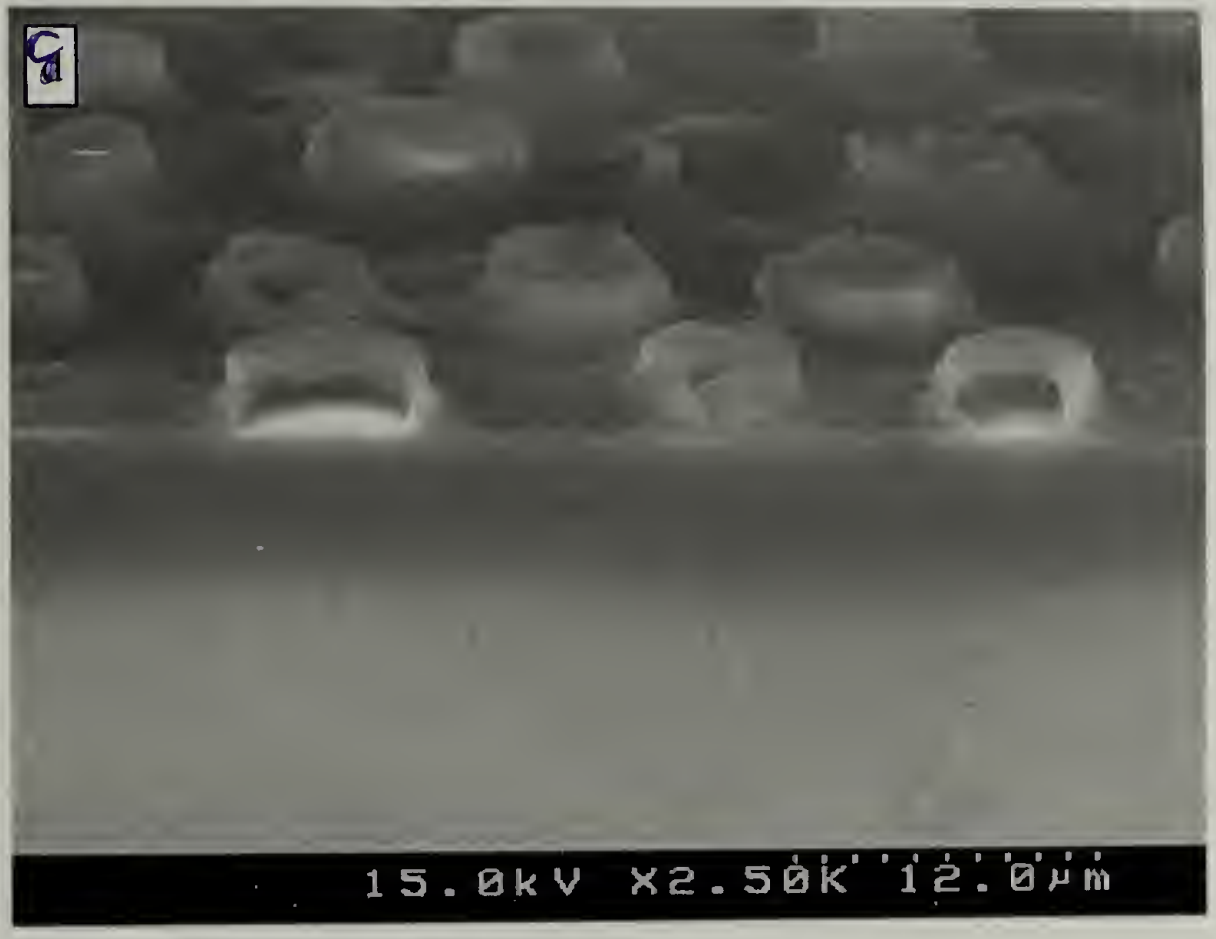

Figure 4.7 SEM of 9k PS/25k PMMA/air in a 3 µm electrode spacing, 136 V field
(a) Prior to selective solvent treatment (b) After rinsing with acetic acid
(c) After rinsing with cyclohexane

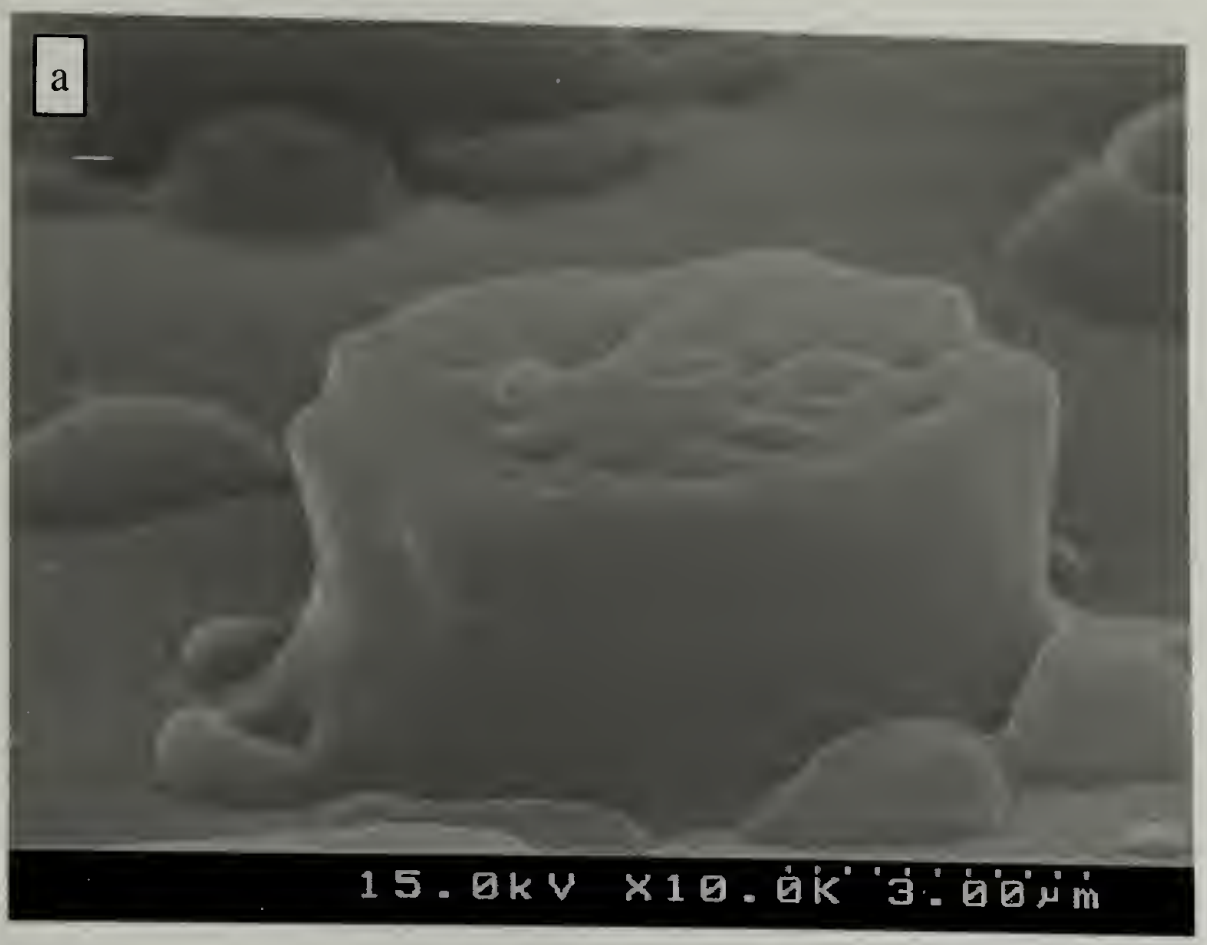

4.8 Examples of instabilities at the bilayer interface
(a) After acetic acid washing, showing the polystyrene pillar with holes.
(b) After cyclohexane washing, showing the strands of PMMA from inside the PS pillar

of these smaller columns is due to electrohydrodynamic instabilities at the PS/PMMA interface, which is very close to the electrode after pillar formation, and oriented perpendicular to the electric field lines. Since the electrostatic pressure is strongest for interfaces closest to the electrodes, it is not unexpected that electrohydrodynamic instabilities form at this interface. The characteristic wavelength at polymer/polymer interfaces is known to be much smaller than that at polymer/air interfaces, due to the reduction of Laplace pressure by the replacement of surface tension with the interfacial tension.[19] Using the linearized analysis of Lin et al. for a 3 μm PS layer (approximately the final height of the pillar) with a 0.5 μm layer of PMMA in a 136 V applied voltage, the characteristic spacing is expected to be 4.3 μm, comparing well to the 2-3 μm spacing which can be roughly estimated for the interior of the pillar.

4.4. Conclusions

The periodicities of all of the patterns observed were determined by the electric field-induced fluctuation at the polymer-air interface. Therefore, the patterning can be controlled by manipulating the applied field, and these microstructures can be reproduced on range of size scales. Unlike previous studies, fluctuations were observed in the lower layer, with the same periodicity as in the upper layer. By controlling the viscous properties and dewetting kinetics in the trilayers, we can vary the three-dimensional microstructural morphology. In this work, PS dewetting from the silicon substrate has been used to form encapsulated structures 100 times faster than PMMA/PS/air trilayers. Work is ongoing to replicate these three dimensional structures under patterned electrodes.

4.5. References

1. Lambooy, P., Phelan, K. C., Haugg, O., Krausch, G. Dewetting at the Liquid-Liquid Interface. *Physical Review Letters* **76**, 1110-1113 (1996).

2. Sferazza, M. Hepenstall-Butler, M., Cubitt, R., Bucknall, D. Webster, J., Jones, R. A. L. Interfacial Instability Driven by Dispersive Forces: The Early Stages of Spinodal Dewetting of a Thin Polymer Film on a Polymer Substrate. *Physical Review Letters* **81**, (1998).

3. Lin, Z., Kerle, T., Russell, T. P. Electric Field Induced Dewetting at Polymer/Polymer Interfaces. *Macromolecules* **35**, 6522-6262 (2002).

4. Morariu, M. D., Voicu, N. E., Schäffer, E., Lin, Z., Russell, T. P. Hierarchical Structure Formation and Pattern Replication Induced By An Electric Field. *Nature Materials* **2**, 48-53 (2003).

5. Qu, S., Clarke, C. J., Liu, Y, Rafailovich, M. H., Sokolov, J., Phelan, K.C., Krausch, G. Dewetting Dynamics at a Polymer-Polymer Interface. *Macromolecules* **30**, 3640-3645 (1997).

6. Brochard-Wyart, F., Martin, P., Redon, C. Liquid-Liquid Dewetting. *Langmuir* **9**, 3682-3690 (1993).

7. Fox, T. G. and Flory, P. J. Second-Order Transition Temperatures and Related Properties of Polystyrene. I. Influence of Molecular Weight. *Journal of Applied Physics* **21**, 581-592 (1950).

8. Seeman, R., Herminghaus, S., Jacobs, K. Gaining Control of Pattern Formation of Dewetting Liquid Films. *Journal of Physics: Condensed Matter* **13**. 4925-4938 (2001).

9. Harris, M., Appel, G., Ade, H. Surface Morphology of Annealed Polystyrene and Poly(methyl methacrylate) Thin Films and Bilayers. *Macromolecules* **36**, 3307-3317 (2003).

10. Kang, H., Lee, S.-H., Kim, S., Char, K. Dewetting and Layer Inversion of Inverted PVP/PS Bilayer Films. *Macromolecules* **36**, 8579-8583 (2003).

11. See, for example, Interfacial Interaction Dependence of Microdomain Orientation in Diblock Copolymer Thin Films. *Macromolecules* **38**, 2802-2805 (2005); Mansky, P., Liu, Y., Huang, E., Russell, T. P. Controlling Polymer-Surface Interactions with Random Copolymer Brushes. *Science* **275**, 1458-1460 (1997); G. Coulon, V. R. Deline, P. F. Green, T. P. Russell, *Macromolecules* **22**, 2581 (1989); S. H. Anastasiadis, T. P. Russell, S. K. Satija, C. F. Majkrzak, *Phys. Rev. Lett.* **62**, 1852 (1989).

12. Xiang, H., Lin, Y., Russell, T. P. Electrically Induced Patterning in Block Copolymer Films. *Macromolecules* **37**, 5358-5363 (2004).

13. Xu, T., Hawker, C. J., Russell, T. P. Interfacial Energy Effects on the Electric Field Alignment of Symmetric Diblock Copolymers. *Macromolecules* **36**, 6178-6182 (2005).

14. Leach, K. A., Lin, Z., Russell, T. P. Early Stages in the Growth of Electric Field Induced Fluctuations. *Macromolecules* 38, 4868-4873 (2005).

15. Schäffer, E., Thurn-Albrecht, T., Russell, T. P., Steiner, U. Electrically Induced Structure Formation and Pattern Transfer. *Nature* **403**, 874-878 (2000).

16. Schäffer, E., Thurn-Albrecht, T., Russell, T. P., Steiner, U. Electrohydrodynamic Instabilities in Polymer Films. *Europhysics Letters* **53**, 518-524 (2001).

17. Wu, S. *Polymer Interfaces and Adhesion* . (Marcel Dekker, 1982).

18. Schäffer, E.; Thurn-Albrecht, T.; Russell, T. P.; Steiner, U. Electrically Induced Structure Formation and Pattern Transfer. *Nature* **2000**, *403*, 874-877.

19. Lin, Z., Kerle, T., Baker, S. M., Schäffer, E. Steiner, U., Russell, T. P. Structure Formation at the Interface of a Liquid/Liquid Bilayer in Electric Field. *Macromolecules* **35**, 3971-3976 (2002)

CHAPTER 5

ELECTROHYDRODYNAMIC PATTERNING OF A PHOTOCURABLE MATERIAL

5.1 Introduction

The success of photolithography for submicron scale patterning has inspired research into alternative patterning techniques that overcome limitations inherent to light-based methods. Methods that can generate patterns in just a few steps and be extended to nanometer length scales, such as self-assembly of block copolymers[1,2] and imprinting tools, like step-and-flash imprint lithography (SFIL)[3,4] and nano-imprint lithography (NIL)[5,6], have been developed. Patterning via electrohydrodynamic (EHD) instabilities in homopolymer films has also recently shown promise as a simple, fast and reliable route to ordered nanostructures.[7,8,9,10]

Here, pattern formation by EHD instabilities has been applied to a photocurable mixture of multifunctional thiols and multifunctional alkenes. The thiol-ene reaction has the advantageous combination of properties, in comparison to other types of photo-induced curing, including self-initiation, adaptability to a wide variety of thiol and vinyl functional reagents, a rapid rate of reaction, and minimal sensitivity to oxygen.[11] The resulting material is optically clear and exhibits low shrinkage and good substrate adhesion.

The thiol-ene reaction is a radical chain reaction generally involving three steps, shown schematically in Figure 5.1(a). The first step, initiation, is the generation of a thiyl radical by photoinitiation or an added radical initiator. Second, the thiyl reacts by addition across the double bond of the ene functionality. The third step is a chain-transfer

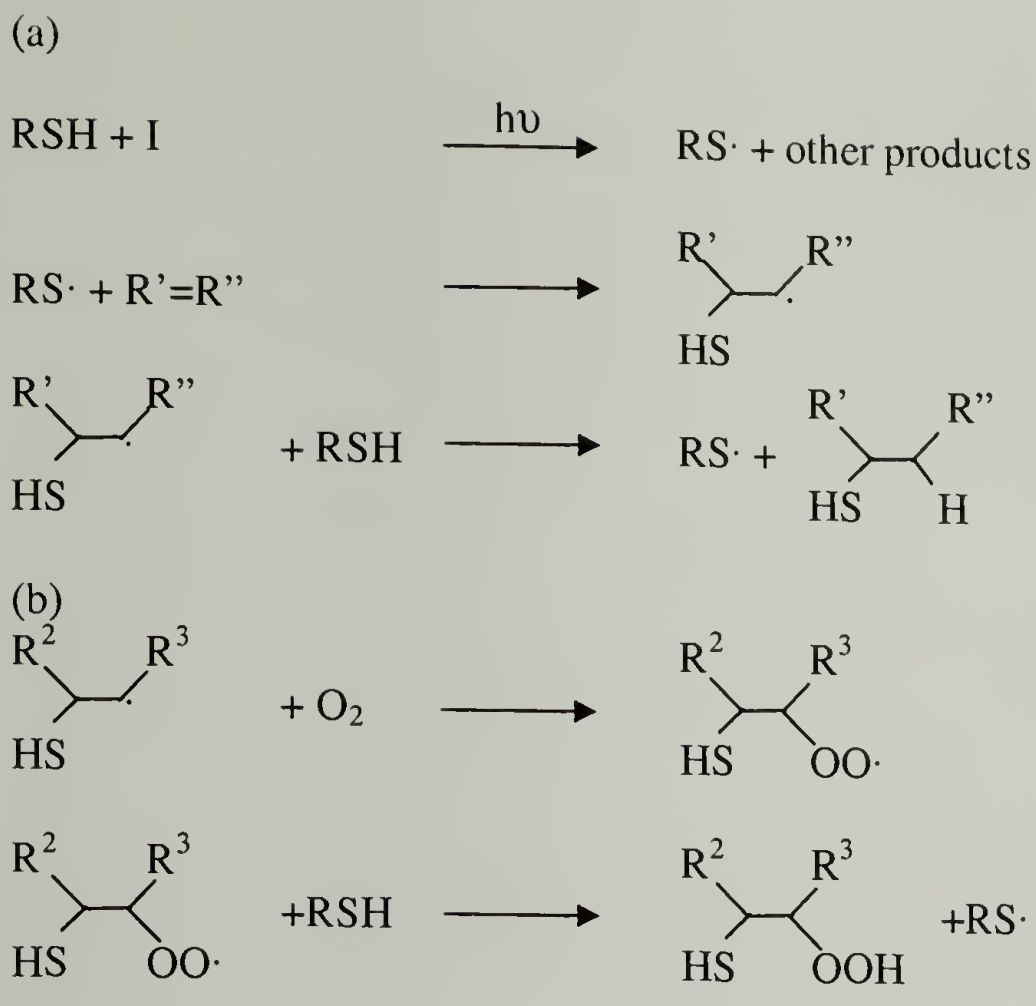

Figure 5.1 General Thiol-ene Reaction Steps. (a) initiation, propagation, and chain transfer; (b) reaction with oxygen to generate a new thiyl radical.

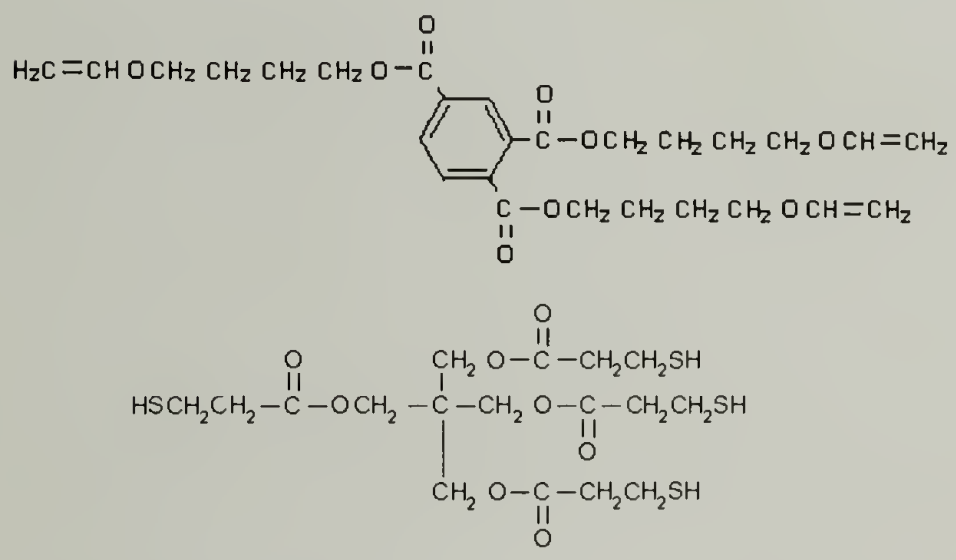

Figure 5.2 Chemical structures of the multifunctional thiol and ene monomers used.

propagation step in which the carbon-centered radical abstracts a proton from a thiol species, generating a new thiyl radical. Termination occurs by radical combination of the propagating species in the reaction mixture. The low sensitivity of this reaction to oxygen arises because thiols may react with peroxy radicals to yield additional thiyl radicals, as shown in Figure 5.1(b).

Multifunctional monomers are necessary to form a crosslinked material, and there is a great deal of flexibility in the choice of both thiol and ene. Reaction rates are reported to be higher for thiol compounds with ester functionalities than for alkanethiols, due to the weakened hydrogen-sulfur bond, arising from hydrogen bonding of the thiol hydrogen to the oxygen of the ester carbonyl.[11] For the ene species, the rate of reaction generally increases with increasing electron density of the double bond, with the exception that conjugated double bonds are less reactive.[12] Singly-substituted or terminal alkene bonds are more reactive than highly-substituted or internal double bonds, due to the reversibility of the propagation step for highly substituted alkenes, and, in the case of multifunctional monomers, steric hindrance.

The choice of thiol and ene is not only important for the reaction rate, but also for determining the final properties of the material. The hardness or elasticity of the final material can be finely tuned by adjusting the ratio of different degrees of functionality in the reaction mixture, so that materials ranging from glassy to rubbery can be produced. For a conformal coating, it is necessary to have low shrinkage during crosslinking, which depends on the reaction conversion at the gel point. Characteristic of radical chain additions, the thiol-ene reaction mixture consists of low molecular weight species until the gel point, which can be determined from the molar ratio of thiol to ene functional

groups in the mixture, r, and the degree of functionality of the thiol and ene, f_{thiol} and f_{ene}.[13] The conversion at the gel point, α, is given by $\alpha = [1/(r(f_{thiol}-1)(f_{ene}-1))]^{1/2}$. For systems where both the thiol and ene are trifunctional, the gel point occurs at about 50% conversion, which is much later than in typical acrylate photopolymerizations (~ 2-7%). Stresses arising from shrinkage while the coating is still liquid are released, and endpoint level of conversion is increased due to the diffusion of reactants.

For those reasons, thiol-ene chemistry is attractive for use in thin film coating and patterning. Here, experiments were conducted to determine the suitability of a photopolymerizable thiol-ene system for electrohydrodynamic patterning. The relative rates of photopolymerization and electric field-induced amplification of capillary waves determined whether the cured structures represented intermediate or final stages of the amplification process. Curing sometimes induced a decay in structure height before preservation of the patterned morphology. The advantages of this synergy of chemical and physical processes for solvent-free lithography are discussed.

5.2 Experimental Methods

The photocurable material used was a 50/50 (wt. %) mixture of pentaerythritol tetrakis(3-mercaptopropionate) and tris [4-(vinyloxy) butyl] mellitate. The chemical structures are shown in Figure 5.2. Thin films of the monomer mixture were spin coated from toluene solutions onto silicon wafers. Indium tin oxide-coated float glass slides (ITO-glass, Delta Technologies) were mounted opposite the films, with narrow strips of 4.4 μm thick Mictron (Toray Industries) as gap spacers between the edges of the two electrodes. The film and gap thickness were measured using spectral reflectance

interferometry (F-10, Filmetrics, Inc.). A power supply was used to apply a 10-100V DC potential between the electrodes.

The behavior of the polymer film was observed *in situ* by reflected-light imaging through the transparent ITO-glass using the 458 nm argon laser line of a Leica TCS-SP2 laser scanning confocal microscope (LSCM). For the *in situ* microscopy experiments, the films were cured using a UVA spot light with a power of 10 mW/cm^2, although the position and angle of the lamp and the absorption by the ITO coated glass slide signigficantly reduced the transmitted intensity to just 0.1 mW/cm^2, as measured using a UV radiometer. Other films were cured using a 5.7 mW/cm^2 UV flood lamp for one hour, prior to separation from the ITO glass. The patterns were also characterized by conventional reflected light microscopy.

5.3 Results and Discussion

The motivation for applying EHD patterning to a photopolymerizable system is to increase the rate at which patterns can be generated. The length and time scales for patterning depend on the growth of height fluctuations on the film surface. The film height, as a function of lateral position, x, and time, t, can be modeled as sinusoidal waves: $h(x,t)=h_0+ue^{iqx+t/\tau}$, where the τ is a characteristic time, h_0 is the initial film thickness, u is the amplitude of the fluctuation, and q is the wavenumber of the fluctuation. As shown by Shäffer et al.[7], the characteristic time associated with the initial rate of amplification is proportional to the viscosity of the liquid, according to eqn 5.1.

$$\tau = \frac{3\gamma\eta}{\varepsilon_0{}^2 h_0{}^3 V^4}\left(\frac{\varepsilon}{\varepsilon-1}d-h_0\right)^6\left(1-\frac{1}{\varepsilon}\right)^2 \qquad (5.1)$$

In the above expression, γ is surface tension, V is the applied voltage, η is the viscosity, d is the separation distance between the two electrodes, ε_0 is the permittivity in a vacuum, and ε is dielectric constant.

With high temperatures, it is possible to increase growth rate by lowering the viscosity of the polymers used in EHD patterning, limited by the degradation temperature of the polymer. Low viscosity materials that can be quickly cured at room temperature are more convenient, and avoid possible temperature gradient-induced instabilities during heating and cooling. Figure 5.3 shows the formation of an ordered array of pillars in a pentaerythritol tetrakis(3-mercaptopropionate) and tri[4-(vinyloxy) butyl] mellitate thiol-ene film with subsequent photocuring. The array formed within 5 seconds of the application of an electric field. Furthermore, no signs of shrinkage or other deformation were observed during photocuring of the film. This can be compared to the experiments with polystyrene and polymethylmethacrylate[7-10], for example, in which structure formation required 24 – 48 hours at 170 C.

When a relatively weak electric field is applied, EHD instabilities in the liquid surface grow slowly enough to be measured in detail. Figure 5.4 shows a sequence of images representing the growth of an electric field induced fluctuation in a thiol-ene film. Peaks are characterized by circular interference fringes, arising from changes in film thickness. The spacing of minima and maxima in the interference pattern can be used to determine the slope of the film topography and the height of the amplified fluctuation. By calculation of peak height for each frame, the growth rate can be measured.

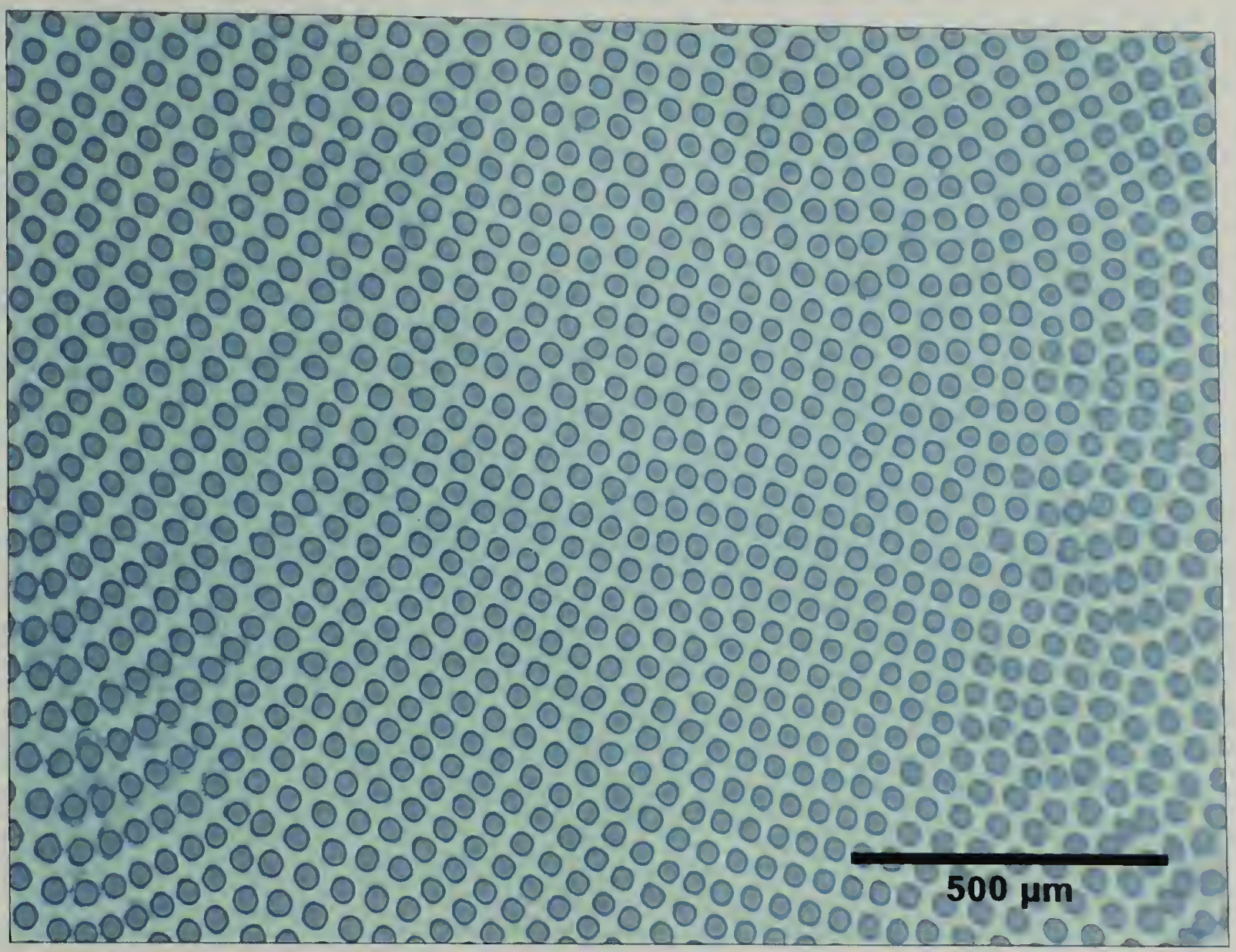

Figure 5.3 Photocured electric field-induced pattern in a thin film, consisting of a photocrosslinkable mixture of 50/50 wt % pentaerythritol tetrakis(3-mercaptopropionate) and tris [4-(vinyloxy) butyl] mellitate. The film was initially 1.47 µm thick with a 6.0 µm air gap; 38 V was applied for 10 s.

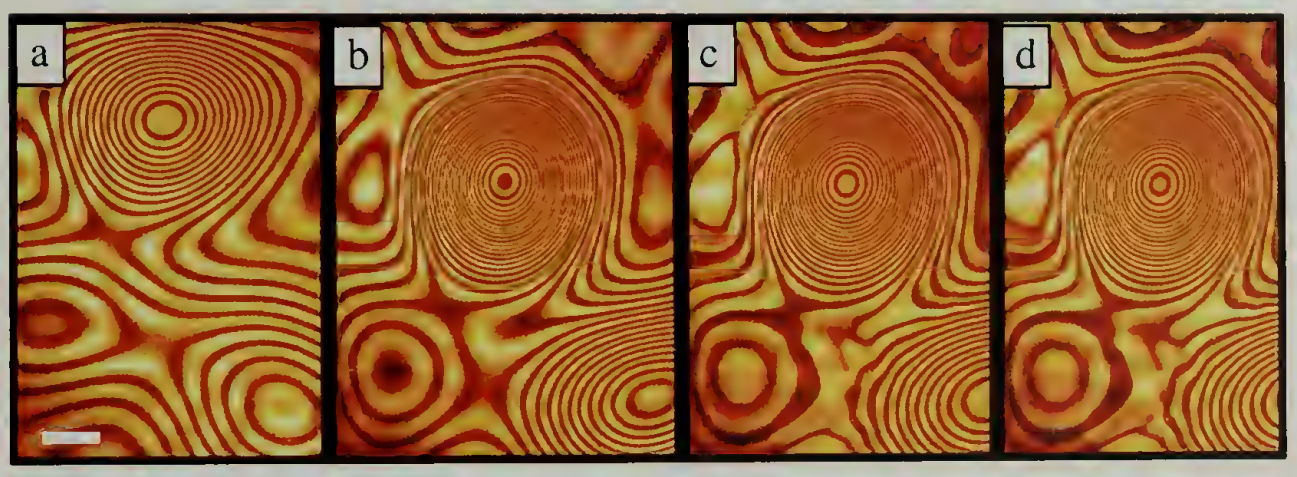

scale bar = 100 µm

Figure5.4 Confocal image series showing peak height development with time. (a) peaks encircled by interference fringes, 45 minutes after 25 V was applied. (b) 38 minutes later, just before irradiation with UV, the number of fringes has increased with peak height (c) after 5 minutes of photocuring, the peak has slightly decreased in height. After 37 minutes of curing, the peak height is stable when the applied electric field is removed.

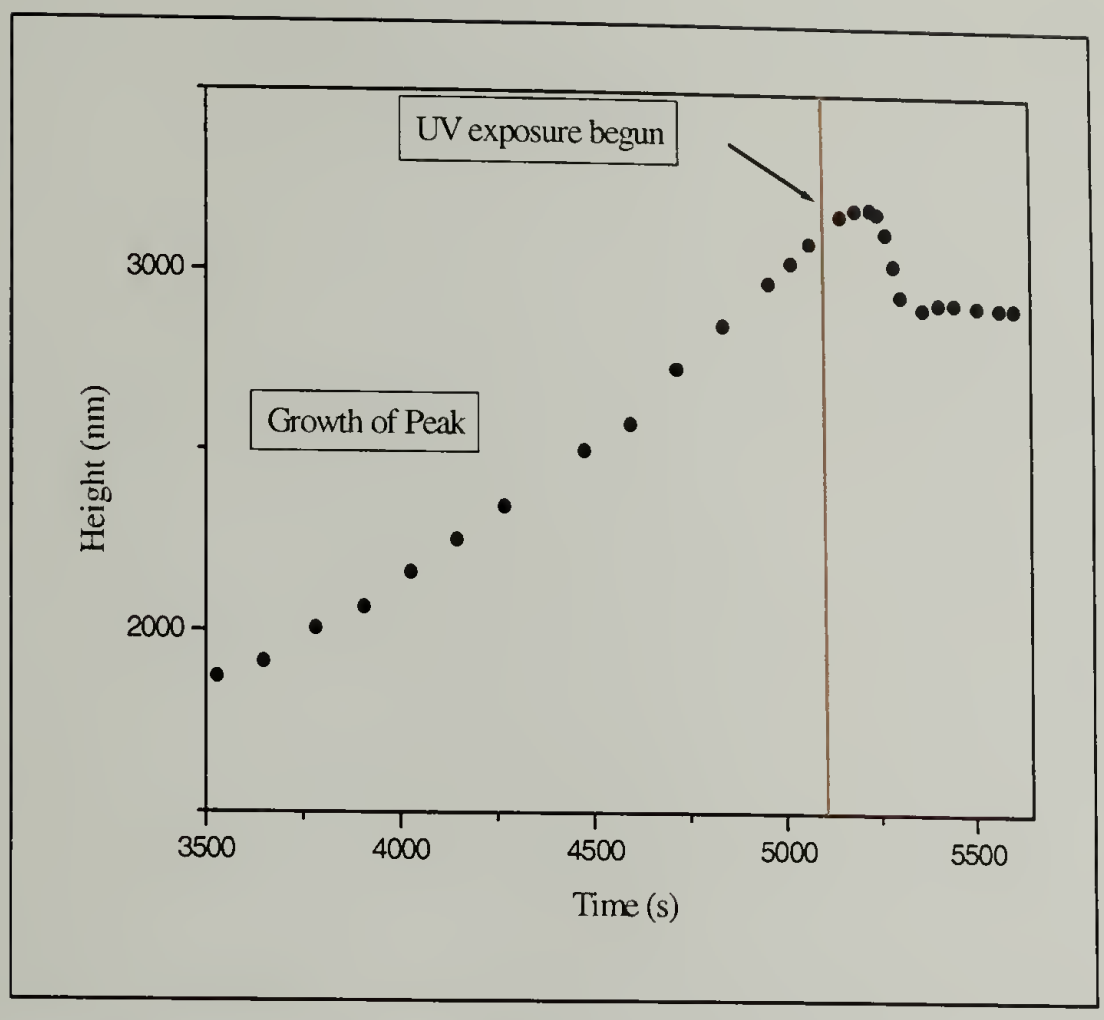

Figure 5.5. Plot of peak height as a function of time during EHD patterning with photocuring. The x axis gives the elapsed time after application of the electric field.

As shown in Figure 5.5, peak growth follows an exponential change in height with time. When curing begins during the intermediate growth stage, before the peak contacts the upper electrode, the growth rate slows and reverses. Upon further crosslinking, the peak structure is preserved at a constant height.

According to the linearized instability models, changes in viscosity during photocrosslinking are not expected to cause peak decay. However, shrinking is possible during the reaction, and the gel point for this system of thiol and ene, in the 50/50 weight percent mixture, is calculated to be at 35% conversion. After the gel point, little or no change in the morphology of the height of the peaks formed in the film is expected. The dose of UV during the *in situ* experiment was apparently enough for the material to reach

the gel point, causing a change in the elastic properties of the film, but not enough to reach full conversion before decay of peak height occurred. Increasing the power of the UV irradiation should enable preservation of peaks without such a change in morphology.

Alternatively, increasing the applied voltage during crosslinking could counterbalance the effects of crosslinking causing the observed decay. We have also observed that, when crosslinking is incomplete, an increase in the applied electric field can cause the decaying peak to again grow toward the upper electrode. The pillar thus formed from partially crosslinked material had a smaller diameter than the pillars formed from the uncrosslinked material. The theoretical arguments presented by Schäffer et al regarding EHD instabilities in thin liquid films do not predict any relationship between viscosity and the critical electrostatic pressure for amplification of capillary waves. However, the peaks which decay during intermediate stages of structure formation experience positionally varying electric field distributions, with lateral components in the electric field gradient, and significant deviations from the linear instability regime are expected.

If the photocurable mixture behaves as a perfect dielectric, the wavelength of the fastest growing fluctuation is expected have the same relationship with electrostatic pressure as the polymer films, as discussed by Schäffer et al.[14,15]

$$\lambda = 2\pi\sqrt{\frac{\gamma W}{\varepsilon_0 \varepsilon \left(\varepsilon - 1\right)^2}} E_P^{-\frac{3}{2}} \tag{5.2}$$

$$E_P = \frac{V}{\left(\varepsilon d - \left(\varepsilon - 1\right) h_0\right)} \tag{5.3}$$

Here, E_P is the electric field at the liquid/air interface and λ is the wavelength of fastest growing fluctuation. For a 1.70 μm thick thiol-ene film with a 11.1 μm air gap after application of 90 V, the characteristic spacing between the pillars was 94 +/- 5 μm, and for a 1.47 μm thick thiol-ene film with a 6.0 μm air gap and 38 V applied, the characteristic spacing was 55 +/- 5 μm. The dielectric constant of the photocurable mixture was measured for several frequencies, as shown in Figure 5.6, and found to be 9.0 at 25°C. The surface tension of these liquids is not well-known, but can be estimated as 20 mN/m from the surface tensions of similar small molecules. This surface tension estimate is very conservative, and yet the predicted characteristic spacings are much larger than those observed: 173 μm and 164 μm for the films with 90 V and 38 V applied, respectively. An investigation of the feature sizes formed in these materials is ongoing for thinner films and under patterned electrodes,[16] from which more will be understood about their behavior in electric fields.

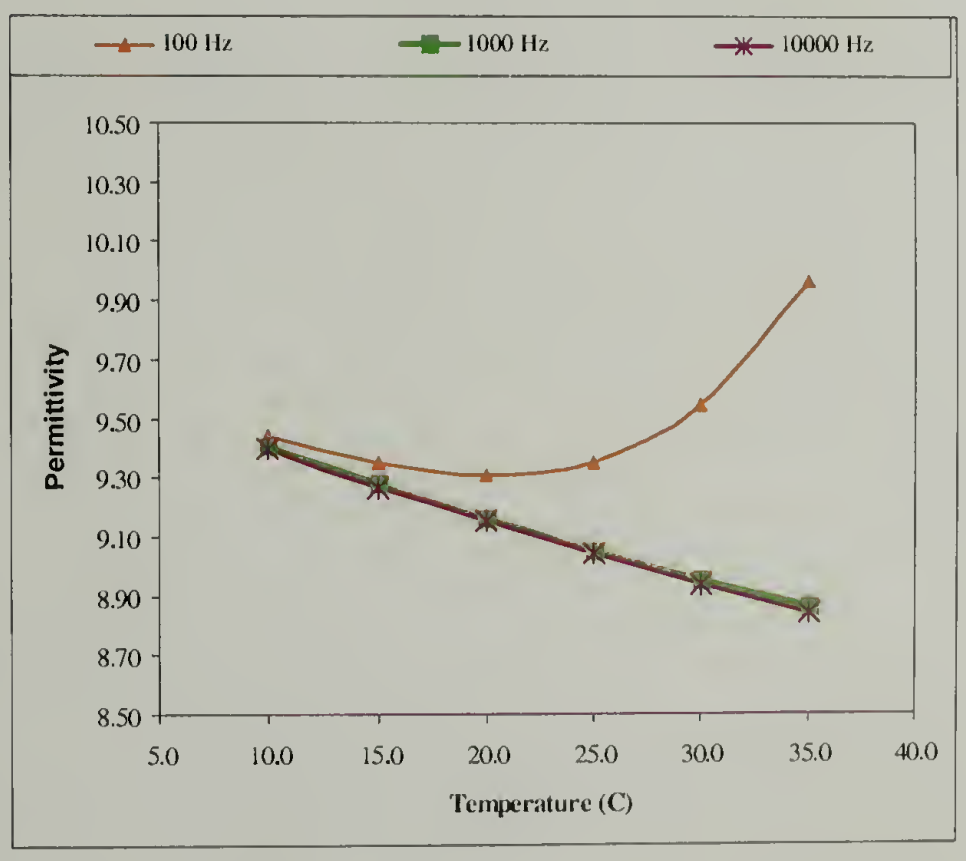

Figure 5.6 Dielectric Constant Measurement of 50/50 Mixture of pentaerythritol tetrakis(3-mercaptopropionate) and tris [4-(vinyloxy) butyl] mellitate.

While the electric-field induced fluctuation may be initially modelled by lateral Poiseuille flow along the surface of the film, the later stages of structure formation are accompanied by a nonlinear acceleration in amplitude growth where the patterning material is forced to flow parallel to the applied electric field. Upon contact with the opposite electrode, electrostatic and surface forces combine to generate liquid surfaces parallel to electric fields lines and a circular interfacial area between the patterning liquid and the electrode surface. The arrays of columns formed by amplification of the electric field-induced fluctuation are energetically metastable, and may evolve into pillars of larger diameter by coalescence or by incorporation of additional material from the underlying reservoir. In numerical simulations by Verma, et al.[17], it was shown that coalescence is most limited when the ratio of the gap size to the film thickness is large, as it is in the experiments discussed here.

However, in some experiments on thiol/ene films, another factor contributing to the stability of the liquid pillars was depletion of the reservoir. During the growth process, a circular area of the film surrounding the growing structure is depleted with respect to the overall film thickness. For the thiol/ene films, we find that dewetting can be initiated at the minimum in film thickness produced by depletion when the peak forms a pillar. This process results in the formation of a circular dewetting rim around the pillar. The radius of the depleted area and the dewetting rim around each pillar varied between experiments. Figure 5.7 (a) shows an array with only a small amount of material depleted around the pillars. Figure 5.7 (b) shows pillars which were nucleated by the rim formed around another pillar, which has also been observed in polystyrene, and which have depleted areas with radii twice as large as the radii of the pillars. In Figure 5.8(a),

similarly proportioned dewetting rims are found for pillars formed without nucleation by a disturbance in the film.

When the distance between structures is small, it is possible for very little liquid to be left on the substrate between them, due to draining into the columns. In some cases, as in Figure 5.8(b) and Figure 5.9(a), the array of pillars incorporates nearly all of the patterning material. If some pillars adhere to the upper electrode when the electrodes are separated, there are holes in the film from which they were removed. At the location of these holes, the residual layer thickness can be measured. The thickness of the residual layer was measured by atomic force microscopy to be as small as 13 nm for arrays in which the initial film thickness was 1.3 μm, the pillar wavelength was 120 μm, pillar radius of 40 μm and height of 11.6 μm, in Figure 5.9. Thus, more than 99% of the patterning material was incorporated into the features of the pattern. This behavior, which is probably due to the low viscosity of the prepolymer, could be very useful as a way to improve the fidelity of patterning by reduction of the so-called "scum layer" which must be etched away before a pattern can be transferred to the underlying substrate. In order for the film between pillars to be very thin, the pillars should have a larger radius and a smaller wavelength. Unfortunately, no existing model allows prediction of the radius of the pillars from the initial conditions of the experiment. For the cases we studied, in which $h_0/d \sim 0.1$, very thin residual layers were observed for $\lambda/h_0 < 0.12$.

(a)

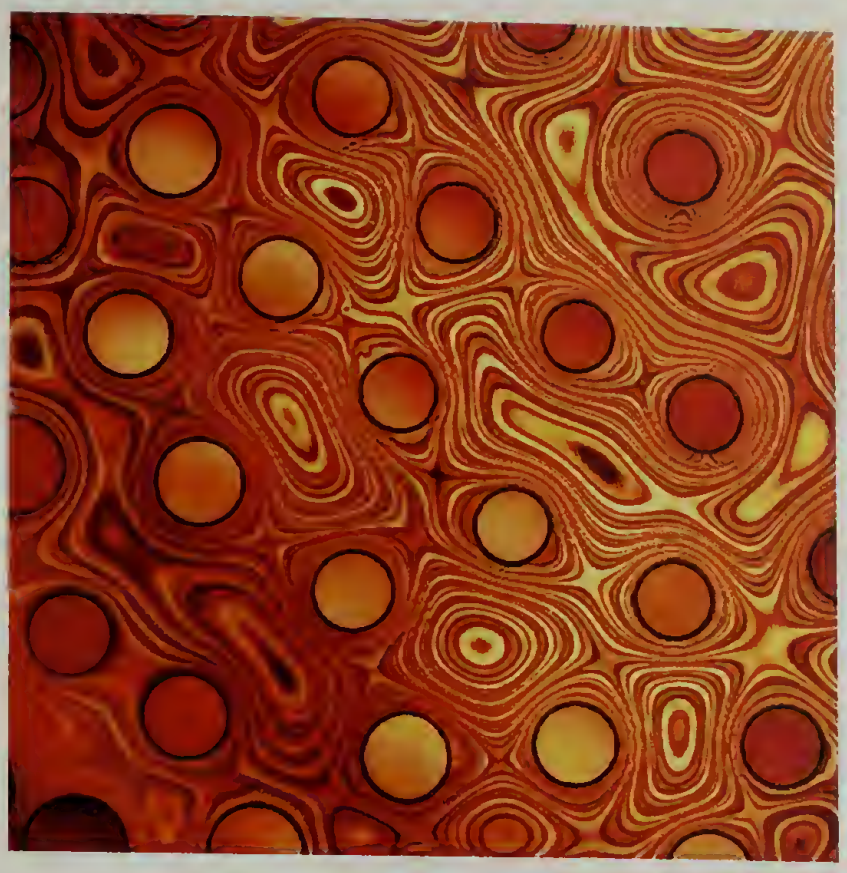

(b)

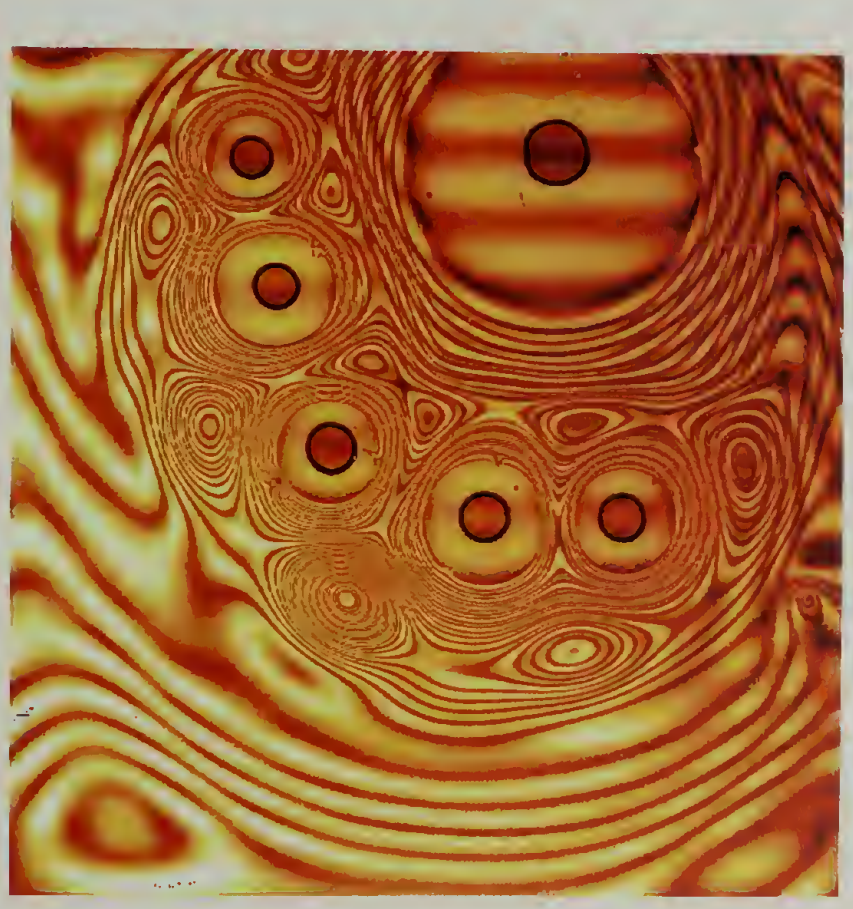

Figure 5.7 Confocal microscope images of pillars formed as (a) an array and (b) at the peak of a rim. Image dimensions are 1.0 x 1.0 mm^2

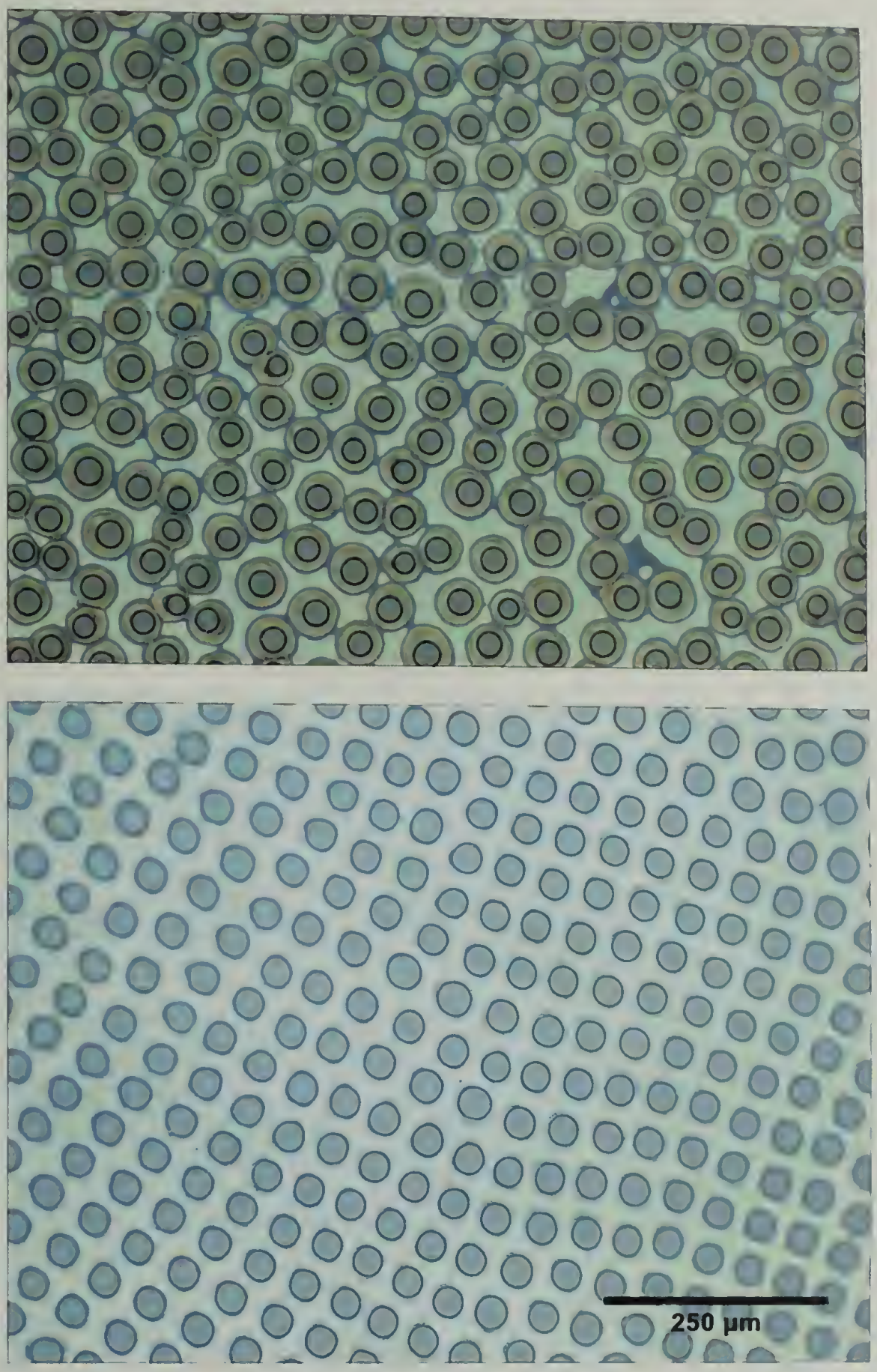

Figure 5.8 Electric field-induced patterns in photocrosslinked films. Top: 1.70 µm thick thiol-ene film with a 11.1 µm air gap after application of 90 V, showing gray depletion zones and blue dewetting rims around each pillar. Image size is 1.92 x 1.44 mm^2. Bottom: 1.47 µm thick thiol-ene film with a 6.0 µm air gap after application of 38 V, showing nearly complete incorporation of patterning material into the pattern. Image size is 960 x 720 μm^2.

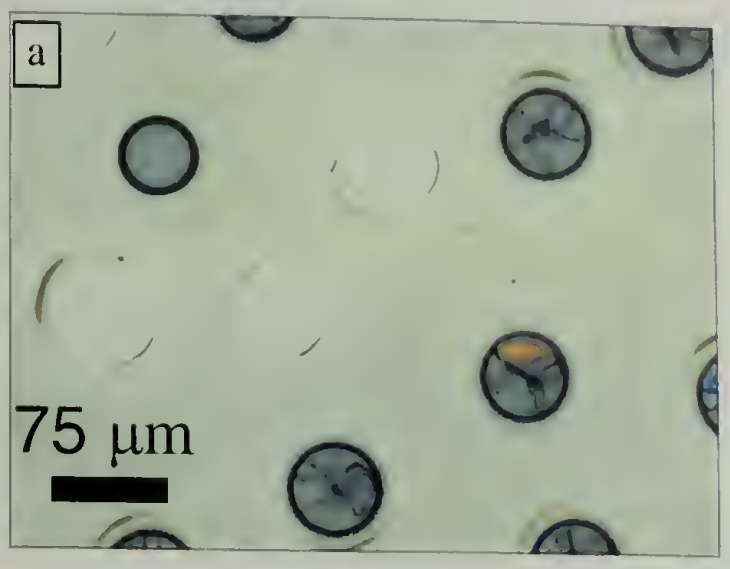

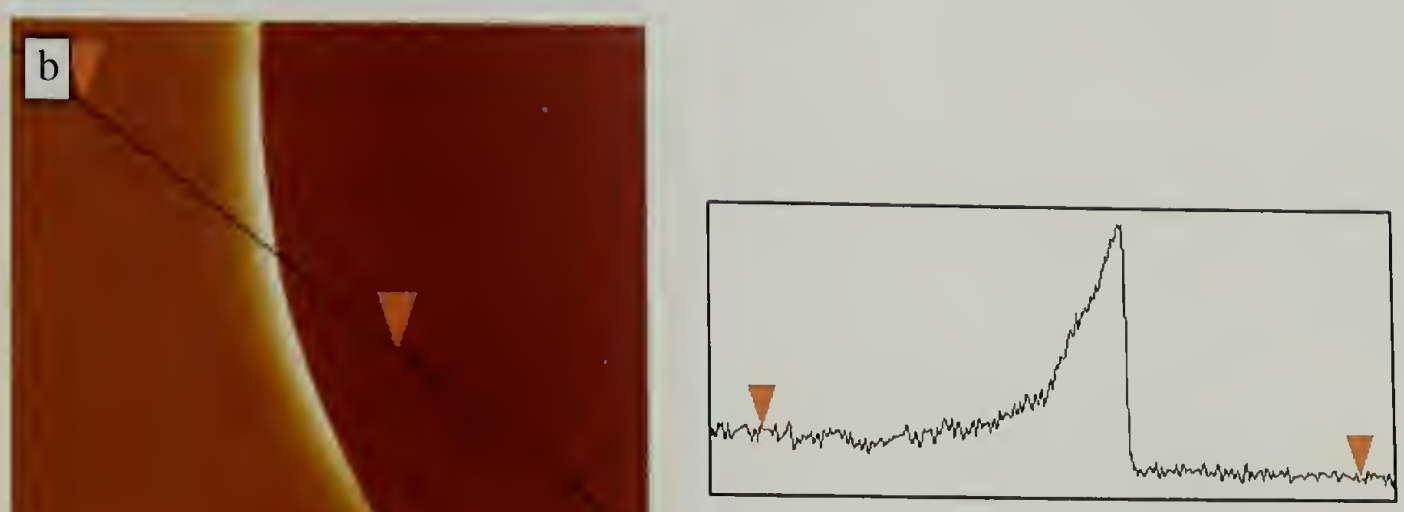

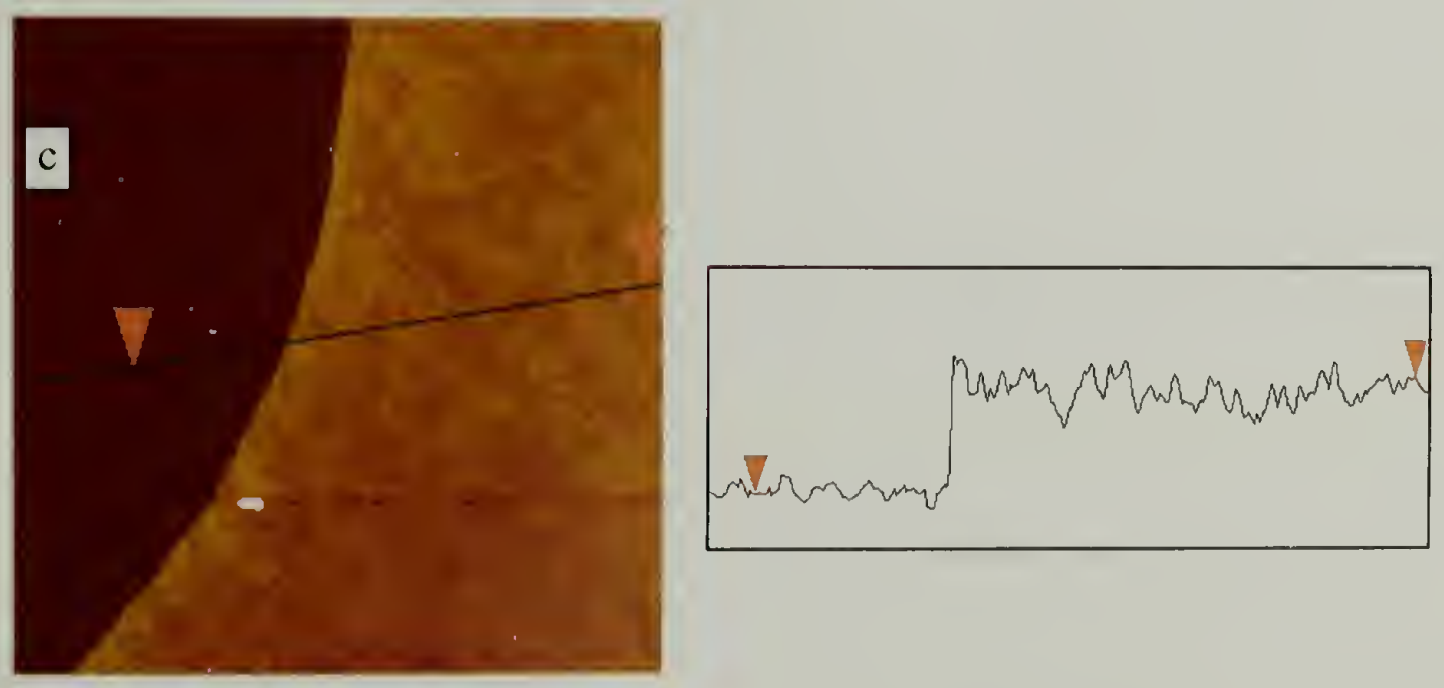

Figure 5.9 Measurement of residual film thickness by AFM. (a) Optical image of holes left from pillars which adhered to the top electrode. (b) and (c) AFM height image and cross-section scan with AFM height scales of 150 nm and film thickness differences between the arrows measured to be 13 nm.

5.4 Conclusions

Patterning by electric field-induced instabilities in thin liquid films was shown to occur over very short times for a photocurable mixture of multifunctional thiol and multifunctional ene. The photopolymerization occurred without inducing defects in the final arrays of pillars, but some decay in structure height occurred when photocrosslinking began before the peaks spanned the electrodes. Due to the low viscosity of the patterning material, the formation of pillars induced dewetting around each feature. Uniform depletion of the reservoir was observed for arrays in which the pillars are close together. The reduction of the residual layer could be useful in limiting the coalescence of closely spaced features produced or replicated by this patterning method. This reduction may also be beneficial in applications requiring pattern transfer to an underlying layer, since the amount of sacrificial etching of the pattern would be reduced.

5.5 References

1. Morkved, T. L.; Lu, M.; Urbas, A. M.; Ehrichs, E. E.; Jaeger, H. M.; Mansky, P.; Russell, T. P. Local Control of Microdomain Orientation in Diblock Copolymer Thin Films with Electric Fields. *Science* 1996, *273*, 931-933.

2. Park, M.; Harrison, C.; Chaikin, P. M.; Register, R. A.; Adamson, D. H. Block Copolymer Lithography: Periodic Arrays of ~1011 Holes in 1 Square Centimeter. *Science* 1997, *276*, 1401-1405.

3. Colburn, M.; Johnson, S. C.; Stewart, M. D.; Damle, S.; Bailey, T. C.; Choi, B.; Wedlake, M.; Michaelson, T. B.; Sreenivasan, S. V.; Ekerdt, J. G.; Willson, C. G. Step and Flash Imprint Lithography: A New Approach to High-Resolution Patterning. *Proc. SPIE-Int. Soc. Opt. Eng.* 1999, *3676*, 379-389.

4. Willson, C. G.; Colburn, M. Step and Flash Imprint Lithography.U.S. Patent Ser. No. 09/266,663.

5. Chou, S. Y.; Krauss, P. R.; Renstrom, P. J. Imprint of Sub-25 nm Vias and Trenches in Polymers. *Appl. Phys. Lett.* 1995, *67*, 3114-3116.

6. Chou, S. Y. Nanoimprint Lithography. U. S. Patent No. 5,772,905. June 30, 1998

7. Schäffer, E.; Thurn-Albrecht, T.; Russell, T. P.; Steiner, U. Electrically Induced Structure Formation and Pattern Transfer. *Nature* **2000**, *403*, 874-877.

8. Schäffer, E.; Thurn-Albrecht, T.; Russell, T. P.; Steiner, U. Electrohydrodynamic Instabilities in Polymer Films. *Europhys. Lett.* **2001**, *53*, 518-524.

9. Lin, Z.; Kerle, T.; Baker, S. M.; Hoagland, D. A.; Schäffer, E.; Steiner, U. Russell, T. P. Electric Field Induced Instabilities at Liquid/Liquid Interfaces. *J. Chem. Phys.* **2001**, *114*, 2377-2381.

10. Lin, Z.; Kerle, T.; Russell, T. P.; Schäffer, E.; Steiner, U. Structure Formation at the Interface of a Liquid/Liquid Bilayer in Electric Field. *Macromolecules* **2002**, *35*, 3971-3976.

11. Hoyle, C. E.; Lee, T. Y.; Roper, T. Thiol-Enes: Chemistry of the Past with Promise for the Future. *J. Polym. Sci., Part A: Polym. Chem.* **2004**, *42*, 5304-5338.

12. Morgan, C. R.; Magnotta, F.; Ketley, A. D. Thiol/Ene Photocurable Polymers. *J. Polym. Sci. Polym. Chem. Ed.* **1977**, 15, 627-645.

13. Jacobine, A. F.; Glase, D. M.; Grabek, P. J.; Masterson, M.; Nakos, S. T.; Rakas, M. A.; Woods, J. G. Photocrosslinked Norbornene-Thiol Copolymers: Synthesis, Mechanical Properties, and Cure Studies. *J. Appl. Polym Sci.* **1992**, *45*, 471-485.

14. Schäffer, E.; Thurn-Albrecht, T.; Russell, T. P.; Steiner, U. Electrically Induced Structure Formation and Pattern Transfer. *Nature* **2000**, *403*, 874-877.

15. Schäffer, E.; Thurn-Albrecht, T.; Russell, T. P.; Steiner, U. Electrohydrodynamic Instabilities in Polymer Films. *Europhys. Lett.* **2001**, *53*, 518-524.

16. Dickey, M.; Willson, C. G. Manuscript in Preparation.

17. Verma, R.; Sharma, A.; Kargupta, K.; Bhaumic, J. Electric Field Induced Instability an Pattern Formation in Thin Liquid Films. *Langmuir* **2004**, *212*, 3710-3721.

CHAPTER 6

DECAY AND REVERSIBILITY OF FLUCTUATIONS IN VARYING ELECTRIC FIELDS

6.1 Introduction

Investigation of electrohydrodynamic instabilities has successfully enabled prediction and control over the dimensions of patterns formed and the kinetics of their formation. However, there is still only a limited description of the structure development process during the intermediate stages, although some theoretical and experimental observations predict the formation of cusps at the peaks of the fluctuations before contact with the electrodes, similar to the Taylor cone formed during the initiation of electrospinning.

Here, the intermediate stages of the growth of electrohydrodynamic instabilities in PDMS thin films is discussed. *In situ* laser scanning confocal microscopy is used to study the effect of removing the applied electric field before columns are formed between the electrodes. Then, cycles of growth and decay of fluctuations in varying electric fields are shown. The effect of adding crosslinking agents on growth and decay, as well as the preservation of the patterns in thermally crosslinked rubber films, was observed. Finally, the results of increasing the electrode separation distance to detach the columns after electrode contact are shown. Quantitative information on the growth and decay rates of fluctuations in fluid and partially crosslinked materials was obtained that suggests applications in microfluidics.

6.2 Experimental Methods

The polymer liquid, Dow Corning Sylgard 184, was spin coated from the bulk or solutions in toluene. Sylgard 184 is a 2-part silicone elastomer kit which cures thermally to yield silicone rubber. One part ("Sylgard I") consists of linear methyl- and dimethyl siloxanes bearing dimethyl vinyl endgroups, dimethyl vinylated and trimethylated silica, and tetratrimethylsiloxy silane, with a viscosity of 5.5 Pa s at 25 C. The second part contains dimethyl silane, dimethyl vinyl-terminated dimethylsiloxane, dimethyl vinylated and trimethylated silica, and tetramethyl tetravinyl cyclotetrasiloxane, and has a viscosity of 4.0 Pa s at 25 C. When mixed in a ratio of 10:1 by weight and cured, the silicone rubber produced is transparent and colorless, with a specific gravity of 1.05, and has an elastic modulus of 9.2 MPa. [1]

Indium tin oxide (ITO) coated glass slides (Delta Technologies, Ltd) were mounted opposite the films, with a spacer of ultrasmooth polyimide film (Mictron, Toray Industries) separating the silicon substrate and glass slide, ensuring precise air gaps of three to ten microns. The fill fraction, i.e. the ratio of film thickness to distance between silicon and glass, was varied from 0.1 to 0.5. Voltages ranging from 40 to 120V were applied from a DC power supply to the silicon wafer and ITO glass. A Filmetrics spectral reflectance instrument was used to measure film thickness. A confocal laser scanning microscope (Leica TCS-SP2) was used to record reflection images of the film at a wavelength of 633 nm.

Differences in gap size over the area of the film may create lateral gradients in electrostatic pressure, so careful attention was paid to the mounting of the ITO glass to make the electrodes as parallel as possible. Even without a wedge-shaped gap, structure

development may be affected by curvature of the electric field lines at the film's edge, so only regions near the center of the film were investigated. Perturbations arising from heterogeneities, such as dust particles in the film, also produce significant effects on structure formation. Sample preparation was therefore performed to minimize contaminants. Glass electrodes were cleaned by ultrasonication in aqueous ethanolamine, silicon wafers were cleaned in sulfuric acid bath containing inorganic oxidizers.

6.3 Results and Discussion

6.3.1 Growth and Decay Without Crosslinking

Films of Sylgard I, the polysiloxane films without crossliking agent, show fluctuations in electric field similar to those observed in the case of linear poly-dimethylsiloxanes. The height of these fluctuations can also be characterized by measurement of the number and spacing of interference fringes around individual peaks. Fig. 6.1 shows an example of a 1.5 μm thick film of Sylgard 184 with 75 V applied. In Fig. 6.1 (a) each fluctuation peak is surrounded by two or three dark rings. The number of rings increased to five or six over the next 70 seconds, shown in Fig. 6.2 (b), after which the applied voltage was removed. The peaks then decayed back to their original height over a period of time similar to the time required for the height increase (Fig. 6.2 (c) and 6.2 (d)).

A plot of the height of one of the peaks as a function of time during this process is shown in Fig. 2. In this case, the growth and decay process of the fluctuations were quite reversible in time. When the electrostatic pressure driving the growth of fluctuations is removed, the most significant driving force for peak decay is the Laplace pressure. It is

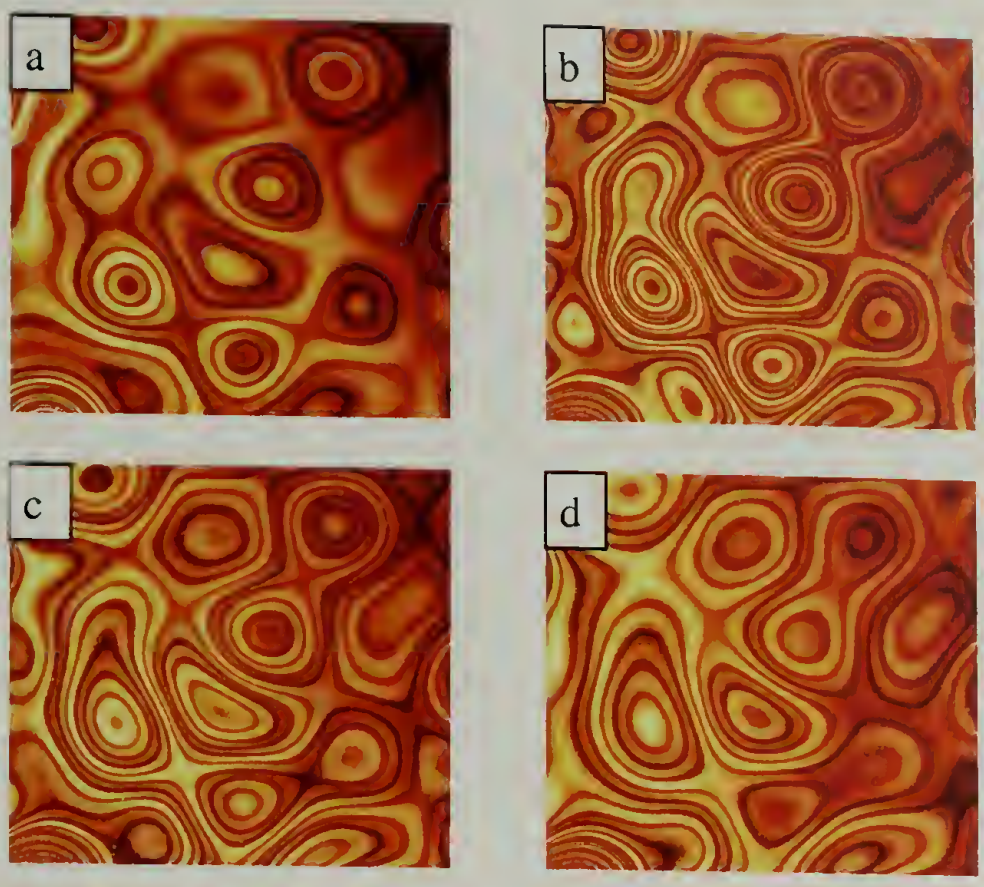

Figure 6.1 Amplification of electric field-induced fluctuations, followed by decay when the field is removed. (a) 94.4 s (b) 164 s (c) 189 s (d) 234 s.

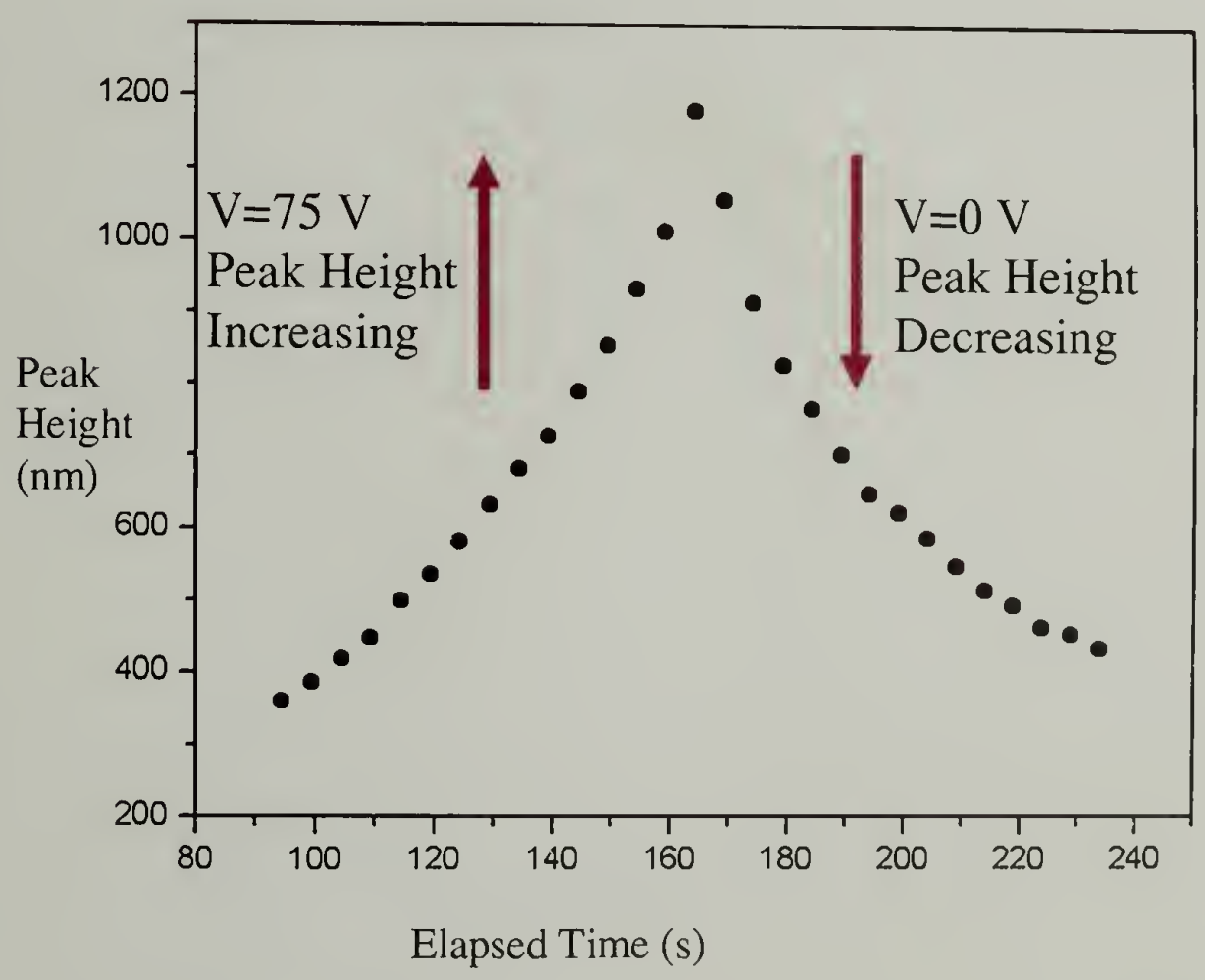

Figure 6.2 Plot of peak height during amplification of electric field-induced fluctuations, followed by decay when the field is removed. The maximum peak height corresponds to the image shown in Fig. 6.1 (b).

apparent that both growth and decay rates are nonlinear. Exponential growth is expected for incipient electrohydrodynamic instabilities, as described in Chapter 2. This form of decay is also expected from the nature of the Laplace pressure, which varies with the curvature of the surface. The pressure decreases as the height of the peak decreases. The evolution over time is then given by eq. 6.1, below. In that equation, Δh is the difference between the height of the peak and the average film thickness, and λ is the wavelength of the fluctuation, approximated as a sine wave.[2]

$$\frac{d(\Delta h)}{dt} = -\frac{\Delta h}{\tau} \qquad (6.1)$$

The time constant, τ, of such a decay is given by eq. 6.2, also from reference 2. In that expression, □is the viscosity, γ is the surface tension, h_0 is the average film thickness, and q is the wave number of the fluctuation.

$$\tau = \frac{3\eta}{\gamma h_0^3 q^4} \qquad (6.2)$$

For a viscosity of 5.0 Pa s, h_0=1.7 μm, and q = 2π/(100 μm), τ □10 s, similar to the time scale observed for the experiment.

In the case of the film shown in Figure 6.3, the voltage was varied but not removed, resulting in a growth and decay process with unequal rates. In this experiment, 60 V was applied to induce the electrohydrodynamic instability, then the voltage was raised to 120 V and alternated with a lower voltage of 40 V. Figure 6.3 (a) shows the film in the first period of 120 V applied, while film thickness was increasing. When the applied voltage was reduced to 40 V in Figure 6.3 (b), the peak height was at a maximum, and decayed more slowly than it had grown in the electric field. Restoring the voltage to

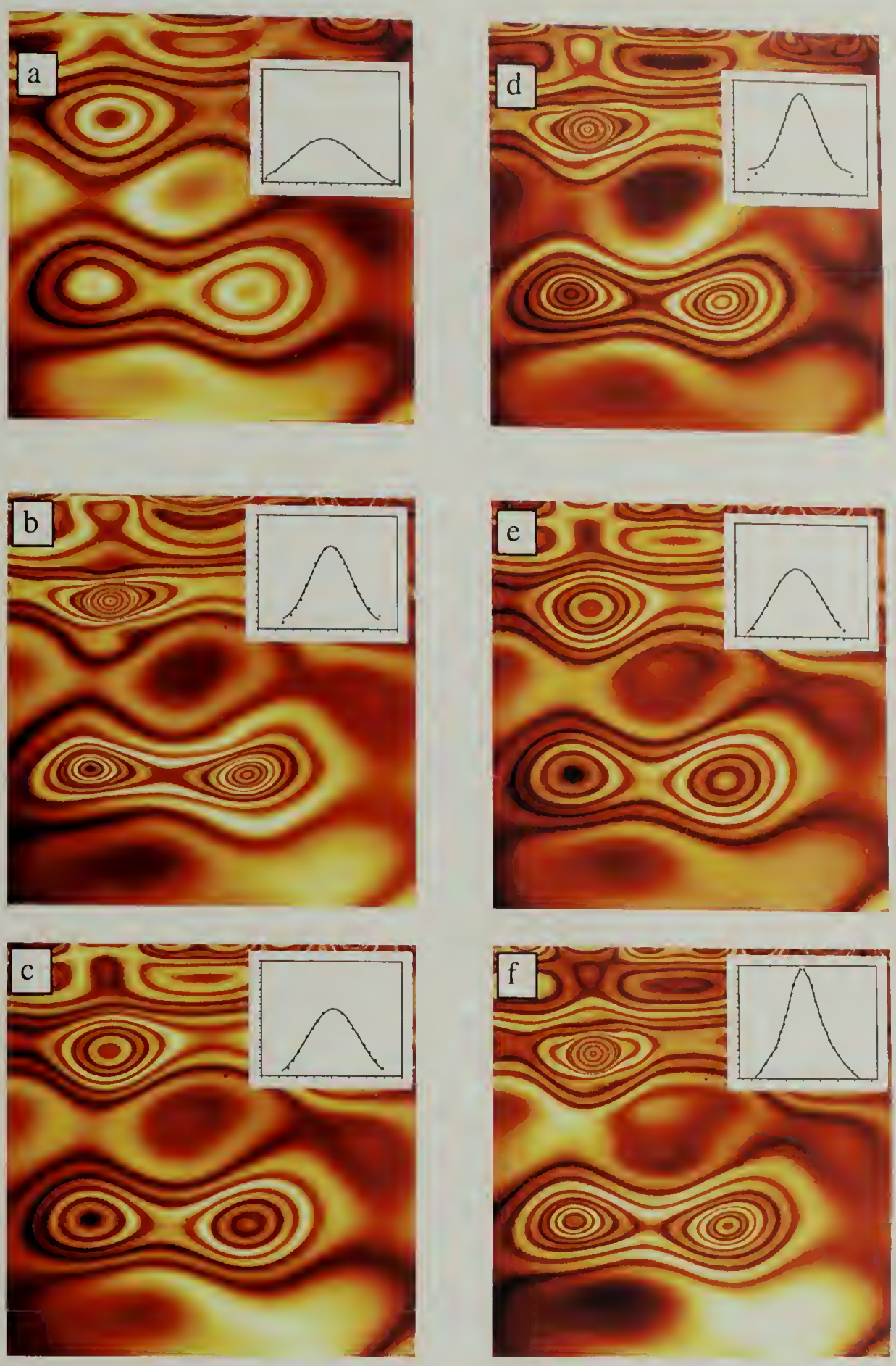

Figure 6.3 Amplification of electric field-induced fluctuations in a field cycling between 120V and 40 V. (a) 4 s (b) 70 s (c) 118 s (d) 140 s (e) 204 s (f) 228 s.

120 V, caused the peak to grow again, and reducing the voltage caused it to decay again. In each cycle, the rates of growth and decay are approximately the same as in previous cycles, which are plotted in Fig, 6.5. This process is shown in its entirety as an animation

in Figure 6.4. However, from the images it is apparent that the morphology of the film may change slightly when the peaks are repetitively amplified and allowed to relax. Due to slight lateral electrostatic pressure or variations in film thickness, some peaks merge and shift in the electric field, limiting the reproducibility of the process.

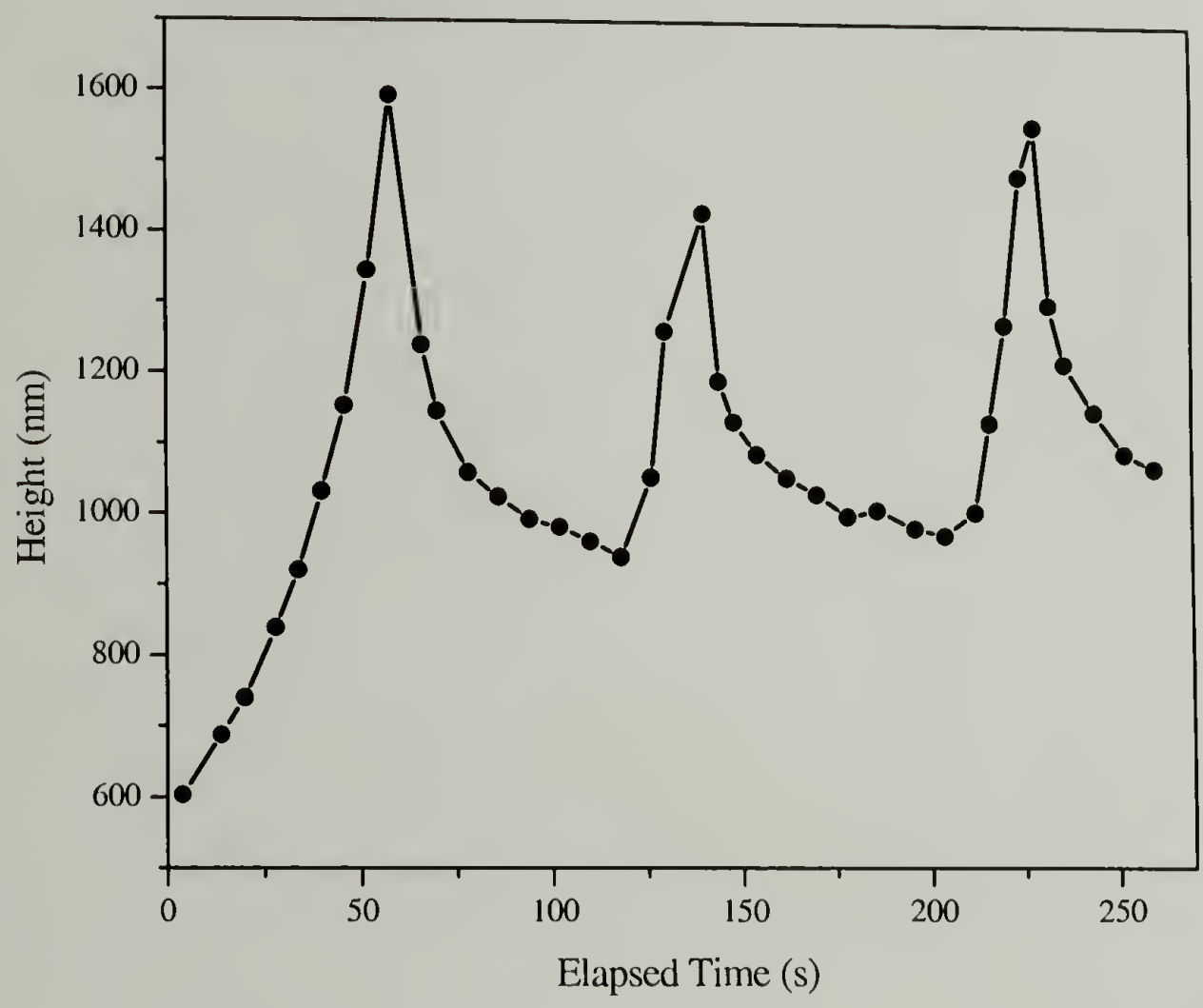

Figure 6.5 Plot of peak height vs. time showing the effect of varying field strength between 120V and 40V.

6.3.2 Growth and Decay With Crosslinking

The introduction of a crosslinking agent causes the viscosity to change over time and therefore one expects that the growth and decay of the fluctuations would become slower. Fig. 6.6 shows an experiment in which 120V was applied to a 1.7 μm film of Sylgard 184 that was mixed and then spin coated from bulk. The interference fringes

visible in Fig 6.6 (a), when no voltage had been applied, are from two effects. The lines running diagonally are from the misaligment of the sample in the optical path, i.e. the sample is tilted with respect the the plane perpendicular to the beam. The curved lines, however are slight variations in height that commonly arose during spin coating such a viscous fluid, and are difficult to avoid.

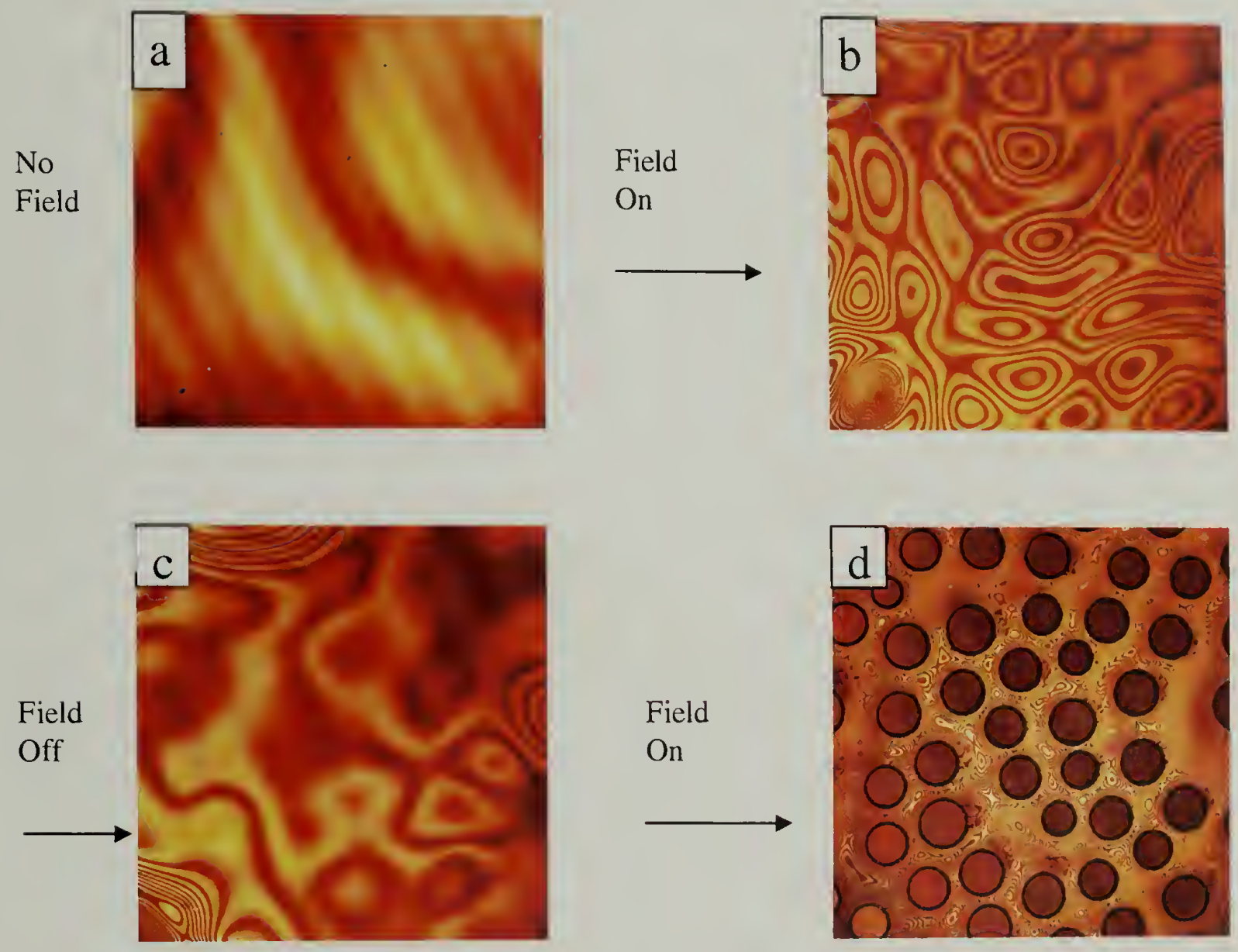

Figure 6.6 The effect of turning the field off and on for a thermally crosslinking film. (a) 0 s (b) 57 s (c) 98 s (d) 326 s

The initial growth period for the fluctuations was 57 seconds, shown in Fig. 6.6 (b) followed by a decay period of 41 seconds, after which the fluctuations were still visible, and one peak had touched the upper electrode (lower left corner of Fig. 6.6 (b).)

After the voltage was applied again for 228 seconds, pillars had formed, as shown in Figure 6.6 (d). After the peaks touched the upper electrode, they did not decay when the applied field was removed.

6.3.3 Separation of Final Structures from Upper Electrode

So far, no one has shown that structures, once formed, can be released from the upper electrode without application of mechanical force. Even when the applied field is removed, the polymer does not revert back to its original thin film configuration. The problem, in this case, is kinetic. Although the film would achieve its lowest free energy by forming a flat surface, the affinity of the polymer for the upper electrode creates a surface energy-related kinetic barrier to achieving this energy state. If the upper electrode is coated with a thin layer of a release agent, the affinity of the liquid for the electrode can be modified. This principle is used in consumer products such as Rain-X® and Shower Shield® to coat glass windows and doors to prevent wetting by soil-bearing droplets and keep surfaces clean. In terms of generating hydrophobic surfaces, Shower Shield® shows performance similar to flourinated coatings, for a much lower cost, as shown in Figure 6.7, by the results of a test of the behavior a drop of water on glass slides with the two different treatments.

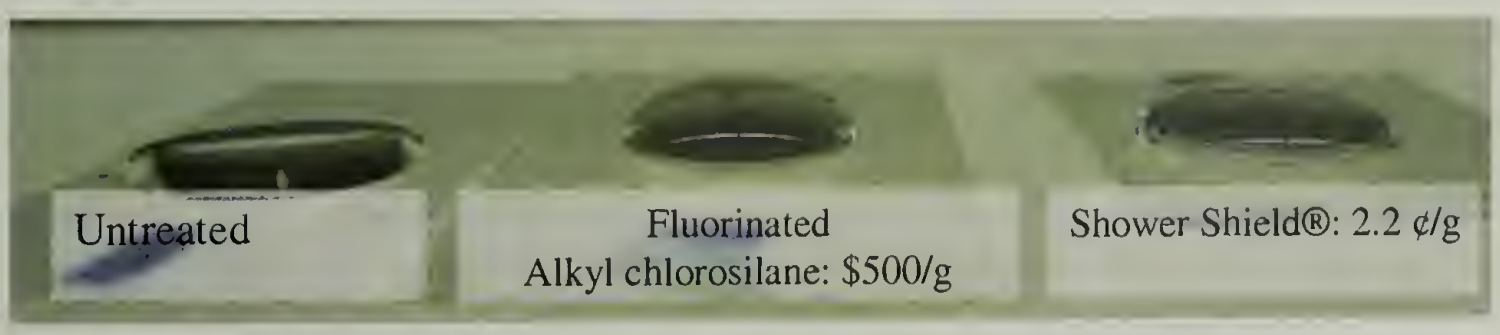

Figure 6.7 Surface treatments for rendering glass slides more hydrophobic.

Liquid pillars from which the applied electric field has been removed usually do not show detachment from the upper electrode over time. When the upper electrode was coated with Shower Shield®, the pillars were also stable. However, when the upper electrode was coated with Shower Shield®, and electrode separation distance was increased slightly after pillar formation, the pillars separated into two droplets, one on each of the electrodes, a process shown in Figure 6.8. Although the complete reversibility of pillar formation was not possible, the droplets on the upper electrode might be able to serve as points where fluctuations in the film could attach to the upper electrode upon increasing the electric field, since, as in a capacitor, the electric field is higher in a layer of dielectric material. In Figure 6.9, all of the frames corresponding to this experiment can be seen as an animation.

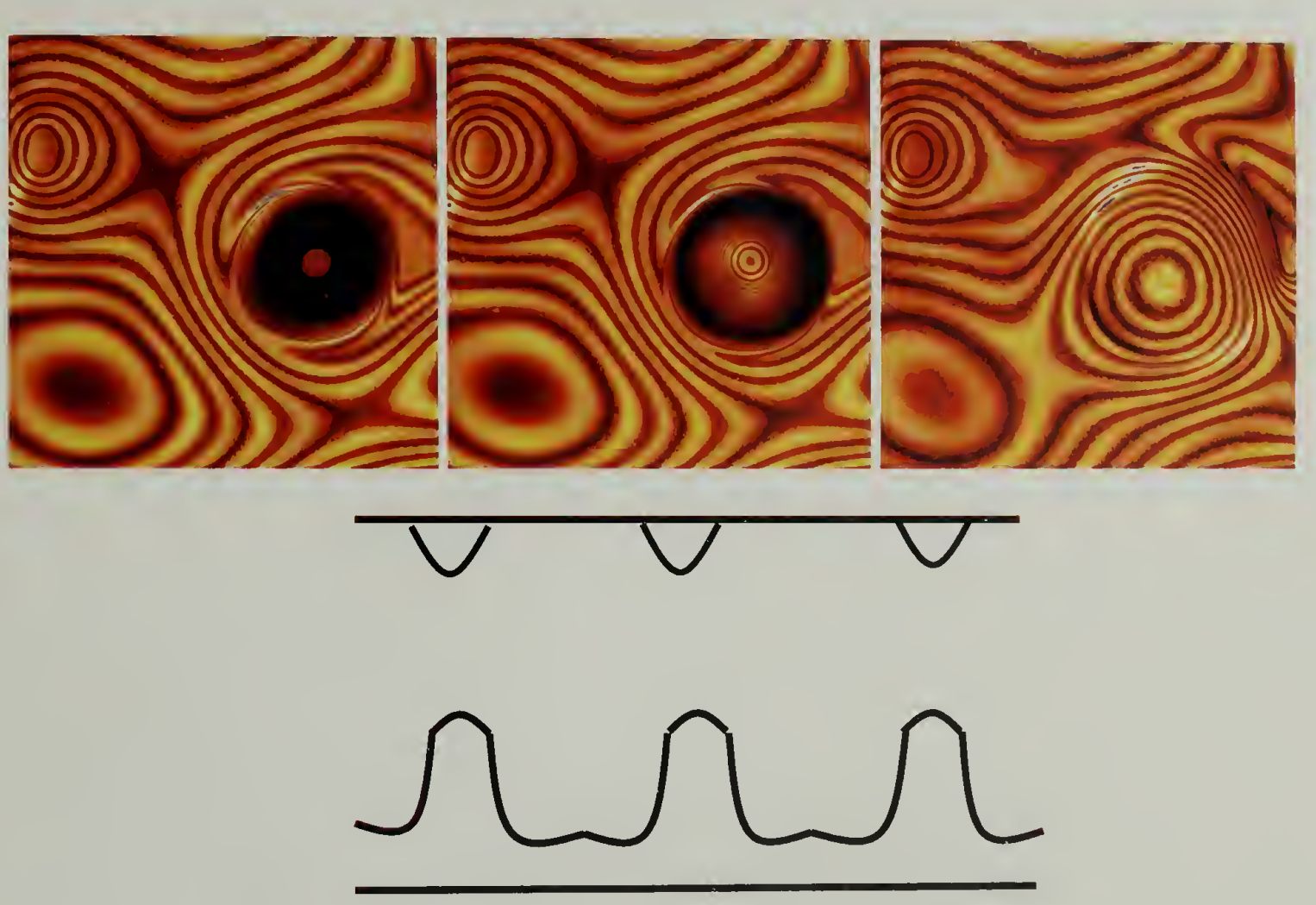

Figure 6.8 Process of detachment of a liquid pillar from an electrode coated with Shower Shield®. Top: sequence of confocal images. Bottom: cross sectional diagram of the end result.

6.4. Conclusions

In situ observation of the growth and decay of electrohydrodynamic instabilities in varying electric fields showed that the time scales are predictable and that they can be manipulated by varying the electric field. This effect could be used in microfluidic applications where the undulations of a PDMS film could be used as a means to drive fluid motion, as a micro-peristaltic pump. Furthermore, controlled variation of the topography of a microfluidic channel using electric fields could be used to disrupt laminar flow and promote mixing. Although the process could not be completely reversed once pillars formed, the pillars could be separated into two complementary patterns by adjusting the electrode spacing.

6.5 References

1. Dow Corning, Sylgard 184 Specifications.

2. de Gennes, P.G.; Brochard-Wyart, F.; Quéré, D. Capillarity and Wetting Phenomena: Drops, Bubbles, Pearls, Waves. Springer, New York, 2004.

CHAPTER 7

SUGGESTIONS FOR FUTURE WORK

7.1 Bilayer Kinetics

The puzzle of the growth kinetics of electrohydrodynamic instabilities at a polymer-polymer interface still remains a challenging one for future exploration. The experiment is challenging outside a clean room environment since two clean polymer films must be coated onto the silicon wafer. Also, measurement of the instability using reflectance microscopy is difficult because of the low contrast. Placing a fluorescent tag at the interface may allow imaging, but also may perturb the dielectric properties of the materials. The best way may be to use off-specular neutron reflectivity to measure in-plane correlations in the buried interface. Not only will this necessitate an intense neutron source, but also the development of a technique to keep the electrodes aligned over a larger area, such as the span of a 5 cm diameter silicon wafer.

7.2 Patterned Electrodes

Recently published theoretical work suggests several experiments which would provide useful insight into the application of electrohydrodynamic instabilities to nanometer scale lithography. Experiments under varying line widths with varying film thicknesses could verify that there is a minimum fill fraction for replication of lines on a topographically patterned electrode. Another interesting avenue is to study the ordering of electric-field induced instabilities in the polymer film along the edges of a line pattern.

Improvements in the regularity of the array of pillars formed by electric field-induced patterning would enhance the viability of this technique.

7.3 New Materials

New materials which might be useful for electric field-induced patterning include polymers with inorganic functional groups and polymer dispersions of inorganic nanoparticles. Those materials might add functionality such as luminescence, or might affect the size scale of the electrohydrodynamic instability, making it possible to reduce the feature size of the patterned materials. Preliminary data from experiments with cadmium selenide, silicon oxide, and gold nanoparticles has shown this area to very promising for reducing characteristic time and length scales for amplification of fluctuations

7.4 Incorporation Into Devices

As shown in Chapter 6, the electric field induced amplification of fluctuations can be controlled in a variable way. Applications such as microfluidic mixing and pumping are promising ones that have already been mentioned. Furthermore, amplification of fluctuations increases the surface area of the film, which could be used to enhance the diffusion of a small molecule out of the film, possibly leading to applications in sensing or drug delivery.

BIBLIOGRAPHY

Anastasiadis, S. H.; Gancarz, R.; Koberstein, J. T.; Compatibilizing Effect of Block Copolymers Added to the Polymer/Polymer Interface. *Macromolecules* **1989**, *22*, 1449-1454.

Anastasiadis, S. H.; Russell, T. P.; Satija, S. K.; Majkrzak, C. F.; *Phys. Rev. Lett.* **1989**, *62*, 1852.

Brochard-Wyart, F., Martin, P., Redon, C. Liquid-Liquid Dewetting. *Langmuir* **1993**, 3682-3690.

Chou, S. Y. Nanoimprint Lithography. U. S. Patent No. 5,772,905. June 30, 1998

Chou, S. Y.; Krauss, P. R.; Renstrom, P. J. Imprint of Sub-25 nm Vias and Trenches in Polymers. *Appl. Phys. Lett.* **1995**, *67*, 3114-3116.

Chou, S. Y.; Zhuang, L. Lithographically Induced Self-Assembly of Periodic Polymer Micropillar Arrays. *J. Vac. Sci. Technol., B* **1999**, *17*, 3197-3202.

Chou, S. Y.; Zhuang, L.; Guo, L. Lithographically Induced Self-Construction of Polymer Microstructures for Resistless Patterning. *Appl. Phys. Lett.* **1999**, *75*, 1004-1006.

Colburn, M.; Johnson, S. C.; Stewart, M. D.; Damle, S.; Bailey, T. C.; Choi, B.; Wedlake, M.; Michaelson, T. B.; Sreenivasan, S. V.; Ekerdt, J. G.; Willson, C. G. Step and Flash Imprint Lithography: A New Approach to High-Resolution Patterning. *Proc. SPIE-Int. Soc. Opt. Eng.* **1999**, *3676*, 379-389.

Coulon, G.; Deline, V. R.; Green, P. F.; Russell, T. P., *Macromolecules* **1989**, 22, 2581.

Daillant, F., Brochard-Wyart, F. Drying of Solids Wetted by Thin Liquid Films. *Can. J. Phys.* **1990**, 68, 1084-1088.

de Gennes, P. G. Wetting: Statics and Dynamics. *Rev. Mod. Phys.* **1985**, 57, 827.

de Gennes, P.G.; Brochard-Wyart, F.; Quéré. D. *Capillarity and Wetting Phenomena: Drops, Bubbles, Pearls, Waves*. Springer: New York, 2004.

Deshpande, P.; Sun, X.; Chou, S. Y. Observation of Dynamic Behavior of Lithographically Induced Self-Assembly of Supramolecular Periodic Pillar Arrays in a Homopolymer Film. *Appl. Phys. Lett.* **2001**, *79*, 1688-1690.

Doshi, J.; Reneker, D. H. Electrospinning Process and Applications of Electrospun Fibers. *J. Electrostat.* **1995**, *35*, 151-160.

Fox, T. G. and Flory, P. J. Second-Order Transition Temperatures and Related Properties of Polystyrene. I. Influence of Molecular Weight. *Journal of Applied Physics* **21**, 581-592 (1950).

Harris, M., Appel, G., Ade, H. Surface Morphology of Annealed Polystyrene and Poly(methyl methacrylate) Thin Films and Bilayers. *Macromolecules* **2003**,36, 3307-3317.

Hoyle, C. E.; Lee, T. Y.; Roper, T. Thiol-Enes: Chemistry of the Past with Promise for the Future. *J. Polym. Sci., Part A: Polym. Chem.* **2004**, *42*, 5304-5338.

Hu., W.; Koberstein, J. T. Interfacial Tension Reduction in Polystyrene/ Poly(dimethylsiloxane) Blends by the Addition of Poly(styrene-b-dimethylsiloxane). *Macromolecules* **1995**, *28*, 5209-5214.

Jacobine, A. F.; Glase, D. M.; Grabek, P. J.; Masterson, M.; Nakos, S. T.; Rakas, M. A.; Woods, J. G. Photocrosslinked Norbornene-Thiol Copolymers: Synthesis, Mechanical Properties, and Cure Studies. *J. Appl. Polym Sci.* **1992**, *45*, 471-485.

Jacobs, K; Herminghaus, S.; Mecke, K. Thin Liquid Polymer Films Rupture via Defects. *Langmuir* **1998**, *14*, 965-969.

Kang, H., Lee, S.-H., Kim, S., Char, K. Dewetting and Layer Inversion of Inverted PVP/PS Bilayer Films. *Macromolecules* **2003**, *36*, 8579-8583.

Kerle, T.; Yerushalmi-Rozen, R.; Klein, J.; Fetters, L.J. van der Waals Stable Thin Liquid Films: Correlated Undulations and Ultimate Dewetting. *Europhys. Lett.* **1998**, *44*, 484-490.

Lambooy, P., Phelan, K. C., Haugg, O., Krausch, G. Dewetting at the Liquid-Liquid Interface. *Physical Review Letters* **76**, 1110-1113 (1996).

Leach, K. A., Lin, Z., Russell, T. P. Early Stages in the Growth of Electric Field Induced Fluctuations. *Macromolecules* 38, 4868-4873 (2005).

Lee, H.; Archer, L. A. Functionalizing Polymer Surfaces by Field-Induced Migration of Copolymer Additives. I. Role of Surface Energy Gradients. *Macromolecules* **2001**, *34*, 4572-4579.

Leibler, L. Block Copolymers at Interfaces. *Physica A* **1991**, *172*, 258-268.

Lin, Z. Surface and Interfacial Structures Induced By Electrohydrodynamic Instabilities. Ph.D. Dissertation, University of Massachusetts, Amherst, MA, 2003.

Lin, Z.; Kerle, T.; Baker, S. M.; Hoagland, D. A.; Schäffer, E.; Steiner, U. Russell, T. P. Electric Field Induced Instabilities at Liquid/Liquid Interfaces. *J. Chem. Phys.* **2001**, *114*, 2377-2381.

Lin, Z.; Kerle, T.; Russell, T. P.; Schäffer, E.; Steiner, U. Structure Formation at the Interface of a Liquid/Liquid Bilayer in Electric Field. *Macromolecules* **2002**, *35*, 3971-3976.

Lin, Z., Kerle, T., Russell, T. P. Electric Field Induced Dewetting at Polymer/Polymer Interfaces. *Macromolecules* **2002**, *35*, 6522-6262.

Mansky, P., Liu, Y., Huang, E., Russell, T. P. Controlling Polymer-Surface Interactions with Random Copolymer Brushes. *Science* **1997**, *275*, 1458-1460.

Milner, S. T. How Do Copolymer Compatibilizers Really Work? *Mater. Res. Soc. Bull.* **1997**, *22*, 38-42.

Morariu, M. D., Voicu, N. E., Schäffer, E., Lin, Z., Russell, T. P. Hierarchical Structure Formation and Pattern Replication Induced By An Electric Field. *Nature Materials* **2**, 48-53 (2003).

Morgan, C. R.; Magnotta, F.; Ketley, A. D. Thiol/Ene Photocurable Polymers. *J. Polym. Sci. Polym. Chem. Ed.* **1977**, *15*, 627-645.

Morkved, T. L.; Lu, M.; Urbas, A. M.; Ehrichs, E. E.; Jaeger, H. M.; Mansky, P.; Russell, T. P. Local Control of Microdomain Orientation in Diblock Copolymer Thin Films with Electric Fields. *Science* 1996, *273*, 931-933.

Noolandi, J.; Hong, K. M. Interfacial Properties of Immiscible Homopolymer Blends in the Presence of Block Copolymers. *Macromolecules* **1982**, *15*, 482-493.

Noolandi, J.; Hong, K. M. Effect of Block Copolymers at a Demixed Homopolymer Interface. *Macromolecules* **1984**, *17*, 4531-4538.

Oddershede, L.; Nagel, S. Singularity During the Onset of an Electrohydrodynamic Spout. *Phys. Rev. Lett.* **2000**, *85*, 6, 1234-1237

Park, M.; Harrison, C.; Chaikin, P. M.; Register, R. A.; Adamson, D. H. Block Copolymer Lithography: Periodic Arrays of ~1011 Holes in 1 Square Centimeter. *Science* 1997, *276*, 1401-1405.

Pease, L. F., III; Russell, W. B. Limitations on Length Scales for Electrostaically Induced Submicron Pillars and Holes. *Langmuir* **2004,** *20*, 795-804.

Qu, S., Clarke, C. J., Liu, Y, Rafailovich, M. H., Sokolov, J., Phelan, K.C., Krausch, G. Dewetting Dynamics at a Polymer-Polymer Interface. *Macromolecules* **1997**, *30* 3640-3645.

Reiter, G. Dewetting of Thin Polymer Films. *Phys. Rev. Lett.* **1992**, *68*, 75-78.

Ruzette, A.-V.; Leibler, L. Block Copolymers in Tomorrow's Plastics (Review) *Nature Materials* **2005**, *4*, 19-32.

Schäffer, E.; Harkema, S.; Blossey, R.; Steiner, U. Temperature-Gradient-Induced Instability in Polymer Films *Europhys. Lett.* **2002**, *60*, 255-261.

Schäffer, E.; Thurn-Albrecht, T.; Russell, T. P.; Steiner, U. Electrically Induced Structure Formation and Pattern Transfer. *Nature* **2000**, *403*, 874-877.

Schäffer, E.; Thurn-Albrecht, T.; Russell, T. P.; Steiner, U. Electrohydrodynamic Instabilities in Polymer Films. *Europhys. Lett.* **2001**, *53*, 518-524.

Seeman, R., Herminghaus, S., Jacobs, K. Gaining Control of Pattern Formation of Dewetting Liquid Films. *Journal of Physics: Condensed Matter* **2001**, 13, 4925-4938.

Sferazza, M. Hepenstall-Butler, M., Cubitt, R., Bucknall, D. Webster, J., Jones, R. A. L. Interfacial Instability Driven by Dispersive Forces: The Early Stages of Spinodal Dewetting of a Thin Polymer Film on a Polymer Substrate. *Physical Review Letters* **81**, (1998).

Sharma, A.; Khanna, R. Pattern Formation in Unstable Liquid Films. *Phys. Rev. Lett.* **1998**, *81*, 3463-3466.

Shin Y. M.; Hohman, M. M.; Brenner, M. P.; Rutledge, G. C. Electrospinning: A Whipping Fluid Jet Generates Submicron Polymer Fibers. *Appl. Phys. Lett.* **2001**, *78*, 1149-1151.

Shin Y. M.; Hohman, M. M.; Brenner, M. P.; Rutledge, G. C. Experimental Characterization of Electrospinning. *Polymer* **2001**, *42*, 9955-9967.

Shull, K. R.; Kramer, E. J. Mean Field Theory of Polymer Interfaces in the Presence of Block Copolymers. *Macromolecules* **1990**, *23*, 4769-4779.

Shull, K.; Kramer, E.; Hadziioannou, G.; Tang, W. Segregation of Block Copolymers to Interfaces Between Immiscible Homopolymers. *Macromolecules* **1990**, *23*, 4780-4787.

Swan, J. W. Stress and Other Effects Produced in Resin and in a Viscid Compound of Resin and Oil by Electrification. *Proc. R. Soc. London* **1897**, *62*, 38-46.

Verma, R.; Sharma, A.; Kargupta, K.; Bhaumic, J. Electric Field Induced Instability an Pattern Formation in Thin Liquid Films. *Langmuir* **2004**, *212*, 3710-3721.

Vrij, A. Possible Mechanism for the Spontaneous Rutpture of Thin, Free Liquid Films. *Discuss. Farad. Soc.* **1966,** *42*, 23.

Willson, C. G.; Colburn, M. Step and Flash Imprint Lithography.U.S. Patent Ser. No. 09/266,663.

Wu, S. *Polymer Interface and Adhesion*. Marcel Dekker: New York. 1982.

Xiang, H., Lin, Y., Russell, T. P. Electrically Induced Patterning in Block Copolymer Films. *Macromolecules* **37**, 5358-5363 (2004).

Xu, T., Hawker, C. J., Russell, T. P. Interfacial Energy Effects on the Electric Field Alignment of Symmetric Diblock Copolymers. *Macromolecules* **36**, 6178-6182 (2005).

Yarin, A.L., Koombhongse, S.; Reneker, D.H. Taylor Cone and Jetting From Liquid Droplets in Electrospinning of Nanofibers. *J. Appl. Phys.* **2001**, *90*, 4836-4846.